Low Cost, High Performance Solar Air-Heating Systems Using Perforated Absorbers

INTERNATIONAL ENERGY AGENCY
Solar Heating & Cooling Programme

IEA Solar Heating and Cooling Report No. SHC.T14.Air.1
Final Report of Task 14 Air Systems Working Group
September 1999

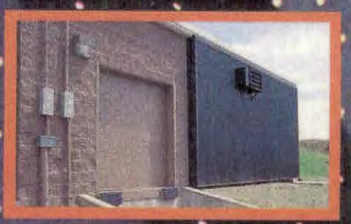

Low Cost, High Performance Solar Air-Heating Systems Using Perforated Absorbers

INTERNATIONAL ENERGY AGENCY
Solar Heating & Cooling Programme

IEA Solar Heating and Cooling Report No. SHC.T14.Air.1
Final Report of Task 14 Air Systems Working Group
September 1999

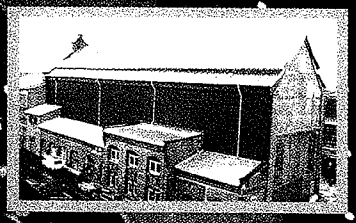

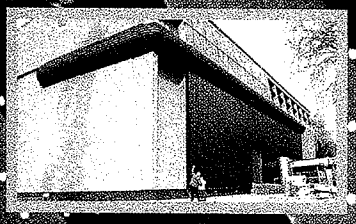

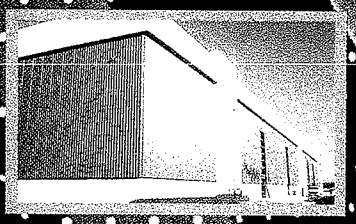

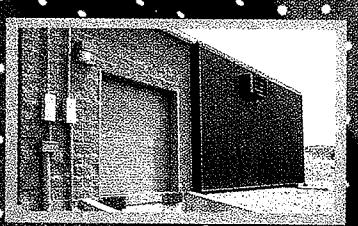

International Energy Agency

The International Energy Agency, headquartered in Paris, was founded in November 1974 as an autonomous body within the framework of the Organization for Economic Cooperation and Development (OECD) to coordinate the energy policies of its members. The twenty-three member countries seek to create the conditions in which the energy sectors of their economies can make the fullest possible contribution to sustainable economic development and the well-being of their people and the environment.

The policy goals of the IEA include diversity, efficiency and flexibility within the energy sector, the ability to respond promptly and flexibly to energy emergencies, the environmentally sustainable provision and use of energy, more environmentally-acceptable energy sources, improved energy efficiency, research, development and market deployment of new and improved energy technologies, and cooperation among all energy market participants.

These goals are addressed in part through a program of collaboration in the research, development and demonstration of new energy technologies consisting of about 40 Implementing Agreements. The IEA's R&D activities are headed by the Committee on Energy Research and Technology (CERT) which is supported by a small Secretariat staff in Paris. In addition, four Working Parties (in Conservation, Fossil Fuels, Renewable Energy and Fusion) are charged with monitoring the various collaborative agreements, identifying new areas for cooperation and advising the CERT on policy matters.

IEA Solar Heating and Cooling Program

The Solar Heating and Cooling Program was one of the first collaborative R&D agreements to be established within the IEA, and, since 1977, its Participants have been conducting a variety of joint projects in active solar, passive solar and photovoltaic technologies, primarily for building applications. The twenty members are:

Australia	France	Norway
Austria	Germany	Spain
Belgium	Italy	Sweden
Canada	Japan	Switzerland
Denmark	Mexico	United Kingdom
European Commission	The Netherlands	United States
Finland	New Zealand	

A total of 26 projects or "Tasks" have been undertaken since the beginning of the Solar Heating and Cooling Program. The overall program is monitored by an Executive Committee consisting of one representative from each of the member countries. The leadership and management of the individual Tasks are the responsibility of Operating Agents. These Tasks and their respective Operating Agents are:

Task 1* : Investigation of the Performance of Solar Heating and Cooling Systems - Denmark

Task 2* : Coordination of Research and Development on Solar Heating and Cooling - Japan

Task 3* : Performance Testing of Solar Collectors - Germany/United Kingdom

Task 4* : Development of an Insolation Handbook and Instrumentation Package - United States

Task 5* : Use of Existing Meteorological Information for Solar Energy Application - Sweden

Task 6* : Solar Systems Using Evacuated Collectors - United States

Task 7* : Central Solar Heating Plants with Seasonal Storage - Sweden

Task 8* : Passive and Hybrid Solar Low Energy Buildings - United States

Task 9* : Solar Radiation and Pyranometry Studies - Canada/Germany

Task 10*: Material Research and Development - Japan

Task 11*: Passive and Hybrid Solar Commercial Buildings - Switzerland

Task 12*: Building Energy Analysis and Design Tools for Solar Applications - United States

Task 13*: Advanced Solar Low Energy Buildings - Norway

Task 14*: Advanced Active Solar Systems - Canada

Task 15 : Not initiated

Task 16*: Photovoltaics in Buildings - Germany

Task 17*: Measuring and Modeling Spectral Radiation - Germany

Task 18*: Advanced Glazing Materials - United Kingdom

Task 19*: Solar Air Systems - Switzerland

Task 20*: Solar Energy in Building Renovation - Sweden

Task 21 : Daylight in Buildings - Denmark

Task 22 : Solar Building Energy Analysis Tools - USA

Task 23 : Optimization of Solar Energy Use in Large Buildings - Norway

Task 24 : Active Solar Procurement - Sweden

Task 25 : Solar Assisted Air Conditioning of Buildings - Germany

Task 26 : Solar Combisystems - Austria

* Completed

Contributing Authors

Alfred P. Brunger
Bodycote ORTECH Inc.
2395 Speakman Drive
Mississauga, ON
CANADA
L5K 1B3

Charles F. Kutscher
Christopher S. Dymond
National Renewable Energy Laboratory
1617 Cole Blvd.,
Golden, CO
U.S.A. 80401-3393

John Kokko
Enermodal Engineering Ltd.
650 Riverbend Drive
Kitchener, ON
CANADA
N2K 3S2

Angiolo Cali
Metec Engineering s.r.l.
Corso Quintino Sella
20-10131 TORINO
ITALY

John Hollick
Conserval Engineering Inc.
200 Wildcat Road
Downsview, ON
CANADA
M3J 2N5

Doug McClenahan
Natural Resources Canada
580 Booth Street
Ottawa, ON
CANADA
K1A 0E4

Rainer Pfluger
Institut für Thermodynamik und
Wärmetechnik
Universität Stuttgart
Pfaffenwaldring 6
70550 Stuttgart
GERMANY

Low Cost, High Performance Solar Air-Heating Systems Using Perforated Absorbers

A Report of Task 14

Air Systems Working Group

Angiolo Cali
Charles F. Kutscher
Christopher S. Dymond
Rainer Pfluger
John Hollick
John Kokko
Doug McClenahan

Alfred P. Brunger
(Editor)

September 1999

This report documents work performed within the IEA Solar Heating and Cooling Program Task 14: Advanced Active Solar Systems Working Group: Air Systems

IEA Report No. SHC.T14.Air.1

Additional Copies may be ordered from:

IEA Solar Heating and Cooling Program
Executive Secretary
Morse Associates, Inc.
1808 Corcoran Street, NW
Washington, DC
20009, USA

Tel: 1-202-483-2393, Fax: 1-202-265-2248

Table of Contents

Foreword

IEA Solar Heating and Cooling Task 14 was initiated to advance the state-of-the-art in active solar energy systems. Four working groups were part of the Task 14: Domestic Hot Water Systems, Air Systems, Large Systems and Dynamic System Testing. This report describes the results of the Air Systems Working Group. The work of the Air Systems Working Group of the Solar Heating and Cooling (SHC) Task 14, Advanced Active Solar Air Systems, focused on improving the scientific understanding and the practical implementation of solar air heating systems for industrial and commercial buildings. At the start of Task 14 in 1989, the unglazed perforated-absorber collector concept was new. Previously, both glazed and unglazed solar air-heating collectors had been built. Conventional glazed collectors had either solid sheet metal absorbers, with air flowing in the either the front pass or back pass configuration, or fibre matrix type absorbers, with the air traversing the absorber matrix (usually from front to back). Unglazed collectors were built with a solid metal or plastic absorber, behind which the air flowed in the back pass configuration. In these conventional collector systems, outdoor ventilation air required by the building was drawn through an opening in the bottom of the collector, picking up heat by contact with the front or back side of the absorber as it was pulled upward inside the collector on its way into the building. The innovative perforated-absorber collector was an improvement over earlier collectors, in which the glazing was eliminated, and the outdoor air was drawn directly through small holes in the face of the collector. Eliminating the glazing component made the collector less expensive, and drawing the air through the face of the collector had the effect of increasing the efficiency of transferring the absorbed solar energy to the air being heated, by reducing both convective and radiative heat losses.

This report contains information of interest to the designers and prospective purchasers and operators of solar air-heating systems using perforated absorbers. In it you will find descriptions of, and performance data for, the perforated-absorber collector systems on the Ford of Canada auto assembly plant and the General Motors battery plant in Canada, the NREL waste handling building in the USA and the Göttengen utility co-generation plant in Germany. Measured performance data from these four systems demonstrate a progressive improvement in cost/performance, with current systems achieving a 40% performance improvement and a 25% cost reduction over earlier versions. Three other projects using perforated-absorber collectors, that were developed during this Task with input from the Air Systems Working Group, are also described: the Ispra Ecocentre project in Italy, a solar tea dryer in Indonesia, and a cocoa drying installation in Malaysia. Two software tools, UTCFLOW and SIMAIR, are described that engineers can use to aid in the design of such systems.

Part II of this report contains details of the tests that were performed at Canada's National Solar Test Facility, as well as summaries of the theoretical, monitoring and data analysis work done at the National Renewable Energy Laboratory in the USA and the University of Waterloo in Canada during Task 14. Insights gained from the theory and from analysis of measured performance data help explain how these simple collectors work to heat ambient air, and explain why they can be remarkably efficient.

Executive Summary

The Air Systems Working Group of IEA SHC Task 14, Advanced Active Solar Systems, concentrated on the study and improvement of a type of air-heating collector called the unglazed perforated-absorber collector (referred to in this report as the perforated collector or perforated absorber for short). This type of collector was developed for and used initially for preheating ventilation air in large industrial buildings. The air to be heated is drawn from outdoors through many small holes distributed over the face of the absorber plate. It is mixed with some indoor air (via a recirculating damper) to maintain a set delivery temperature, and then it is distributed to the building interior. There is no glazing on the collector, so the collector has no transmission losses, and is less expensive to install than a glazed collector. It is easily installed on the south vertical wall of a building, and resembles conventional wall cladding. Since ambient temperature air is being heated, the absorber plate temperature is only a few degrees above ambient temperature, so radiant heat losses are small. The heated air in the boundary layer next to the perforated absorber is sucked through the absorber plate into the collector, so convective losses are also small, and wind has only a secondary effect on collector performance. The system delivers preheated ventilation air to the building via ducts located near the ceiling level, where the incoming air mixes with room air and tends to destratify air temperatures in the building. All these attributes of the perforated collector system make it very cost effective.

During the time that the Air Systems Working Group was active, industrial practice for solar preheating of ventilation air for large buildings improved both in terms of energy delivered per square metre of solar absorber (collector efficiency), and also in terms of the energy delivered per dollar. In 1989, when Task 14 was set up, there were no large perforated air-heating collector installations; the standard for solar preheating of ventilation air was a glazed collector. The first large unglazed perforated collector was installed on the Ford of Canada automotive manufacturing plant in 1990, the year that Task 14 started, and that 1877 m^2 installation became the first air-heating demonstration project of Task 14. Monitoring of the unglazed collector showed that the unglazed perforated collector performed better than either the glazed collector or a non-perforated canopy type of collector that was tried before the perforated collector was developed.

In total, four demonstration systems were installed and monitored as part of IEA SHC Task 14: the Ford of Canada auto assembly plant and the General Motors battery plant in Canada, the NREL waste handling building in the USA, and the Göttingen utility co-generation plant in Germany. The monitoring results from the earlier systems were helpful in identifying design improvements, and this experience was applied to the design and construction of the later systems.

Monitoring of the Ford of Canada perforated collector system revealed the importance of 1) controlling air leakage through the summer by-pass damper 2) reducing pressure drop in the air distribution system inside the building 3) placing the control sensor for the recirculating damper downstream of the fan to achieve good control of the air delivery temperature, and 4) maintaining high collector air flow for maximum solar heat collection. As a result of the flow non-uniformity observed in the Ford of Canada system, the GM battery plant system was built with a canopy across the top of the collector that acted like a plenum to even out the air flow over the whole collector face. Monitored active solar collection efficiency averaged 72% for the GM system, an improvement over the 54% achieved by the Ford of Canada system. Monitoring of the GM battery plant system also proved the importance of good design of the air distribution system inside the building, so that adequate air flow through the collector is maintained and good solar efficiency is achieved. The economic payback of the GM battery plant system over conventional make-up air units was calculated to be 2.3 years.

The perforated absorber was used in a new way in the Göttingen district heating plant in Germany. Here the heated air was used as the combustion air for the natural gas fired boilers in the plant. Preheating the combustion air has the effect of increasing the combustion efficiency of the boilers, thereby displacing fossil fuel and reducing CO2 and other emissions from the plant. Measured solar efficiency of the perforated collectors was as high as 62% with high air flow rates. In the summer time, when demand for combustion air is low, the temperature of the air delivered from the solar collector is higher, but the efficiency is low due to the low average air flow rate.

The 27.9 m^2 perforated collector installed on the Waste Handling Facility at the National Renewable Energy Laboratory (NREL) in the USA has no header across the top as those on the GM battery plant and the Göttingen district heating plant have. Another difference is that the NREL collector operates at a constant air flow rate. Monitored data from this installation were therefore useful in better identifying the heat losses due to wind. The average measured collector efficiency was 63% for an average suction velocity of 0.036 m/s over the face of the collector. The wind was measured to have the effect of reducing the collector efficiency by from 2.5 to 3.5 percentage points for every metre per second of wind speed.

Three other projects using perforated-absorber collectors, were also developed during this task with input from the Air Systems Working Group: the Ispra Ecocentre project in Italy, a solar tea dryer in Indonesia, and a cocoa drying installation in Malaysia. The Ispra Ecocentre collector is about 485 m^2. It is used to preheat the air that is supplied to one of the two air handling units that provide ventilation for the building on which the solar collector is mounted. The tea dryer installation uses a 600 m^2 roof-mounted perforated absorber oriented 22 degrees from the horizontal and facing west. The cocoa drying installation uses a 370 m^2 roof-mounted collector. Performance data are not yet available from either the cocoa drying installation or the Ispra Ecocentre project, but during the month of September 1994 the tea dryer system displaced about 11 880 litres of diesel oil.

Basic research that was carried out during Task 14 lead to a better understanding of how these collectors worked, and helped to improve the engineering tools available for the design of perforated collector systems. The two software design tools UTCFLOW and SIMAIR were developed or improved during Task 14. SIMAIR can be used to calculate monthly or annual performance of a perforated collector system. During Task 14, the efficiency equation used in SIMAIR was changed from a simple polynomial fit to the collector efficiency measurements made at the National Solar Test Facility (NSTF) in Canada to a more physically-based model that was empirically calibrated to fit the NSTF measurements. UTCFLOW was developed by NREL during Task 14 as an aid to configuring the collector to achieve uniform flow over the absorber surface.

Chapter 1:

Introduction to Solar Air Heating Using Perforated Absorbers

1.1 What is a Perforated-absorber Collector?

A perforated-absorber solar energy collector is an air-heating, unglazed solar collector that consists of a dark-coloured metal absorber plate (usually corrugated) that is perforated with many small holes to allow outdoor ambient air to pass through before being drawn into the building to provide it with fresh-air ventilation. The absorber, exposed to the sunlight, acts as an effective solar radiation-to-air heat exchanger. The many small holes in the absorber provide close contact between the solar absorber and the air to be heated. Thermal losses from this type of collector are small, because the continual flow of fresh air towards the absorber almost eliminates the normal heat losses from ambient wind (convective heat loss), and the flow of outdoor-temperature air through the absorber keeps the temperature of the absorber within a few degrees of ambient temperature, so that energy losses by radiation from the collector to the surroundings are also small. The result is that this simple collector is remarkably efficient — about twice as efficient as glazed collectors designed to collect heat at higher temperatures.

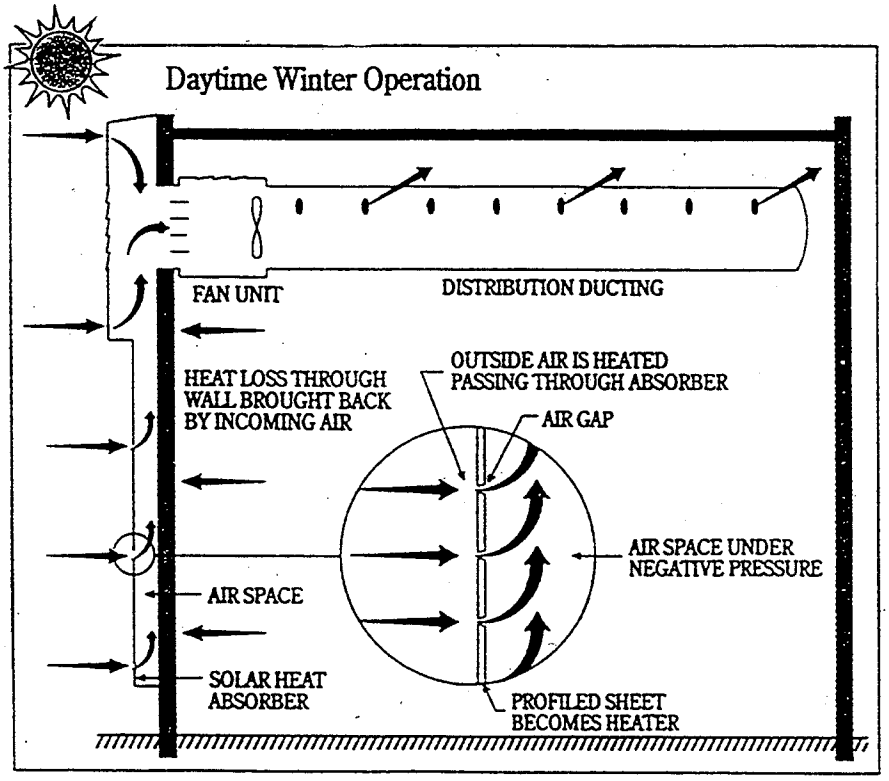

Figure 1.1 Perforated-plate collector cross-section.

Detailed Description

The perforated air-heating collector system is composed of two parts, the collector (outdoor components) and the air handler and controls (indoors components). Figure 1.2 is an isometric view of the perforated collector system, in which each component is shown. A detailed description of each part is given below.

Collector

The perforated absorber is made of 0.8 mm thick corrugated aluminium sheet. Figure 1.3 is a detail drawing of the perforated absorber. The sheet is of a thin gauge to minimize weight, material, and cost; the corrugations provide structural rigidity. The perforations are small round holes, 1.6 mm in diameter, spaced regularly across the face of the sheet. The void fraction (i.e., amount of surface area in holes) varies with the application. A larger void fraction is used (e.g., 2%) for applications where high-efficiency but low temperature rise is required. In applications where a higher temperature rise is required, a lower void fraction is used. Void fractions as low as 0.1% have been laboratory tested. The total collector area is based on the volume flow rate per unit area that will provide the desired temperature rise to the system's total airflow. Maintaining the airflow per unit area at a high value increases the suction pressure drop and reduces the convective losses.

The perforated absorber is connected to the existing building wall by a support structure of vertical and horizontal Z-channels. The horizontal Z-channels may be perforated to provide both a vertical air channel and structural support with a single element. The vertical channels are fastened to the existing wall, horizontal channels are attached to the vertical channels, and then the perforated absorber is fastened to the horizontal channels.

A summer bypass damper is installed on those systems where year-round ventilation is required, but where heating of the ventilation air is not wanted in the summer. The bypass damper allows ambient air to enter the building directly, bypassing the collector entirely. The bypass damper is located opposite the collector outlet opening (fan inlet duct). It is a motorised two-position damper that is controlled by an outdoor ambient-air thermostat. Typically the control is set to open the damper (bypass the collector) when the ambient temperature is above 18 °C and to close the damper when ambient temperatures drop below 18 °C. The damper is larger than the fan inlet opening to reduce the entrainment of collector air into the ventilation air stream.

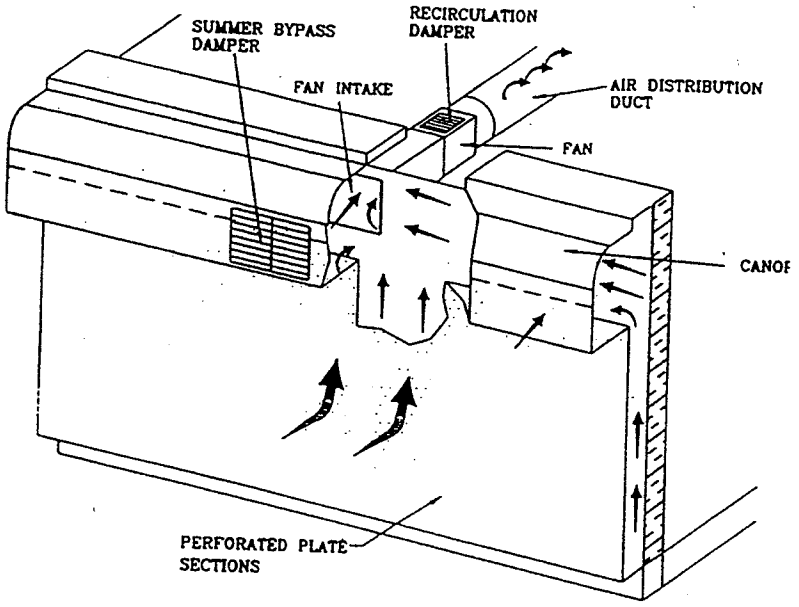

Figure 1.2 Isometric view of the perforated-plate/canopy collector.

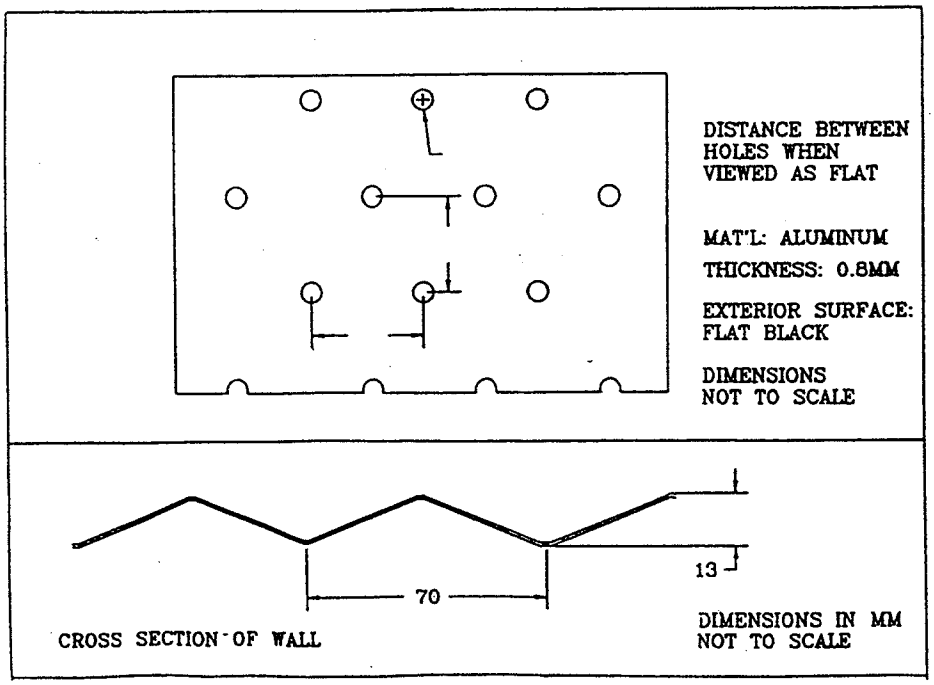

Figure 1.3 Perforated absorber plate material.

Air Handling and Control Systems

Figure 1.4 shows the air handling and control systems. The air handling system is comprised of a constant speed fan, a recirculation damper, and a fabric distribution duct. The fan and recirculation damper are installed as a pre-manufactured component. The fan is a V-belt drive, propeller-type.

A recirculation system, controlled by a thermostat at the fan outlet, is used to ensure that the air delivered to the building is maintained at a pre-set minimum temperature. The recirculation system consists of two dampers operated simultaneously by a modulating motor. The motor drives the dampers in opposite directions to vary the mix of ceiling-level indoor air with collector outlet air, thereby maintaining a constant delivery temperature to the building. As the temperature of the collector outlet air drops, collector airflow is decreased and indoor airflow is increased. The delivered air temperature is set using an adjustable temperature controller. As shown in Figure 1.4, the outlet temperature sensor was located upstream of the fan in the early system. The sensor is now located downstream of the fan to provide a more accurate reading of the mixed air temperature.

The preheated ventilation air is delivered through a high-density polyethylene duct with discharge holes along its length. The holes are evenly spaced along the length of the duct and positioned to spread the air perpendicular to the tube and towards the building ceiling, destratifying the building air. Hole diameters vary, but are usually approximately 60 mm in diameter. The size and number of perforations were calculated to produce a pressure drop of 65 Pa across the duct at the design flow rate.[1]

[1] Dunford, John (1991) Personal Communication. Energy Jet Inc., 2 Carson Court, Brampton, ON, 905-793-7400.

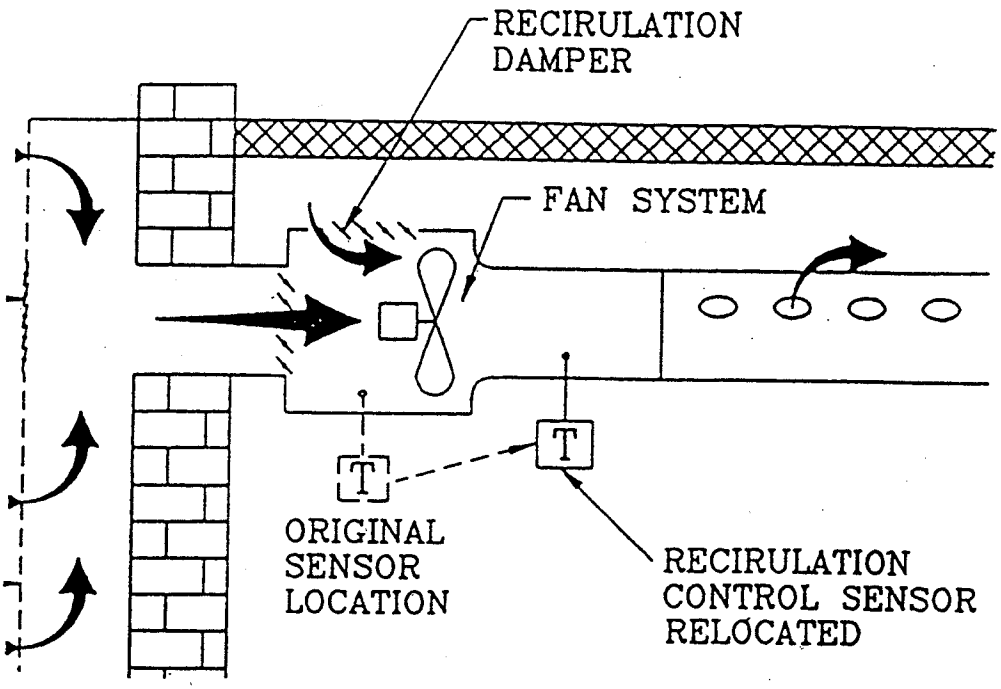

Figure 1.4 Air handling and control system for the perforated collector

1.2 Uses

The first application of the perforated absorber solar collector was the preheating of ventilation air for industrial buildings. This type of collector is particularly well-suited for that application, because the temperature of the inlet air is equal to ambient air temperature. In the few years since its invention, other uses for the collector have been introduced, including ventilation air preheating for commercial and multi-story residential buildings, crop drying, and preheating of combustion air. Virtually any application that requires the heating of outdoor air can benefit from using the perforated absorber collector technology, by simply passing the air through the solar collector before delivering the air to the intended system.

1.3 Advantages and Limitations

The perforated collector system was designed to heat large quantities of fresh air in a single pass. By providing ventilation air heating via the collector system, significant quantities of fossil fuels can be displaced. The collector system is designed to be attached to the existing building structure, to facilitate installation and minimize costs. The building frame is the support system, eliminating racking requirements and costs. The original building wall is the collector back, eliminating the need for a back absorber and insulation. Placing the collectors vertically reduces the need for waterproofing and structural rigidity, and reduces the potential loss of performance due to snow loading, since all these problems are associated with sloped glazings.

Attaching the collectors to the building wall provides energy benefits in addition to the active solar heat collected. Drawing air up the building wall and then into the building will recapture heat normally lost to the atmosphere through the south wall. Blowing the pre-heated (but cooler than indoor) air into the building at ceiling height can destratify building air, reducing heat normally lost through the ceiling and, to a greater extent, normally lost through high-temperature exhaust air.

Since this collector is unglazed, it can exchange radiant energy directly with its surroundings. Therefore, it is suitable only for applications in which the average absorber temperature (and thus the temperature of the delivered air) is not too much higher than the surrounding ambient air. The collector achieves its greatest efficiency when heating high volumes of air only a few degrees. For some applications, such as crop drying, higher temperatures are required. For those applications, the collector efficiency will be lower, and so a larger collector area and a lower average flow rate of air will be required. On the other hand, since the capital cost of this collector is much less than conventional glazed collectors, it is still cost effective to operate it with these higher temperature rises.

1.4 Collector Performance

Numerous laboratory tests have been done at the NSTF over the course of Task 14. Temperature rise data was assembled and put into graphic form, and is given in Figure 1.5. The Chart gives temperature rise through the collector as a function of solar radiation. Each of the lines corresponds to a single airflow rate per unit area of projected collector surface area. The highest temperature rise is achieved with the lowest airflow rate.

1.5 Perforated Collector Applications Described in this Book

Seven example applications of the perforated absorber collector are described in this book. The four demonstration systems listed in Table 1.1 were installed and monitored as part of IEA SHC Task 14. The Ford of Canada auto assembly plant and the General Motors battery plant in Canada are examples of ventilation air preheating systems for industrial buildings. The collector on the NREL waste handling building in the USA provides the only space heating and ventilation for this building. The Göttingen utility co-generation plant in Germany is an example of using the perforated collector to preheat combustion air for gas-fired boilers, thereby increasing the combustion efficiency. These applications are quite diverse, and the reader

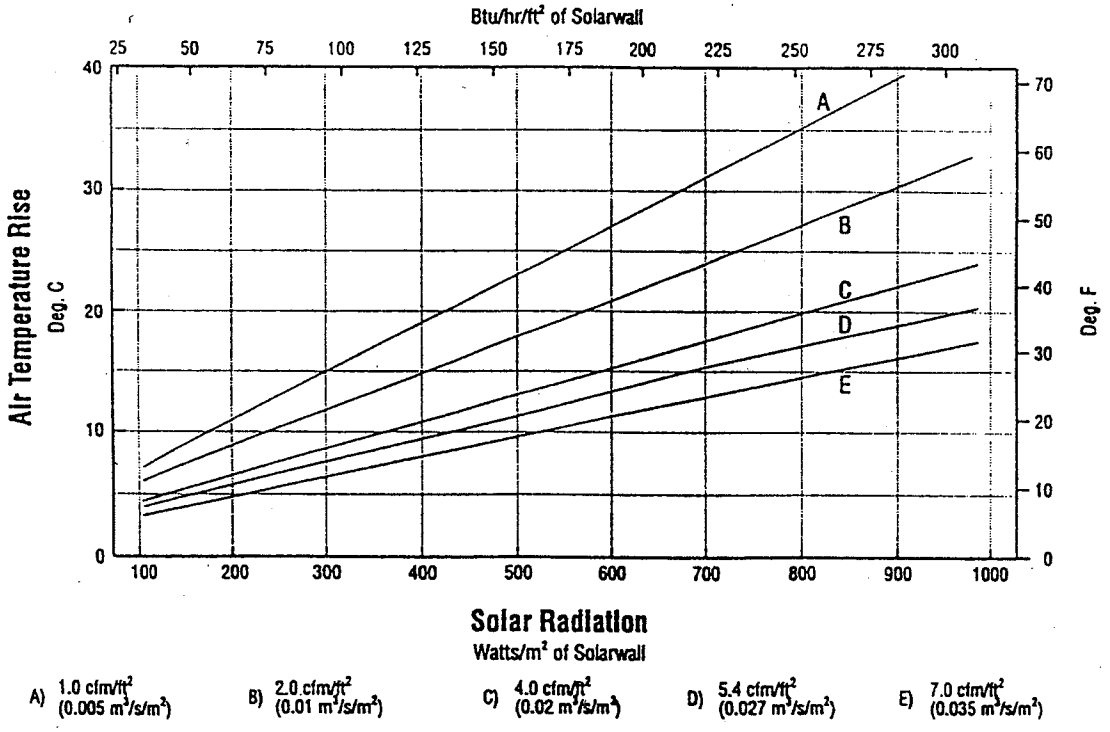

Figure 1.5 Air temperature rise versus solar radiation for various airflow rates.

is directed to the text of the relevant sections in Chapter 2 for details of how the energy collection, cost and efficiency data listed in Table 1.1 were calculated.

Three other systems, installed or planned during Task 14, demonstrate other uses of the perforated absorber collector. The few details available for these systems at the time of writing are given in Table 1.2. The Ispra Ecocentre building retrofit project includes both liquid and air-heating collectors in an integrated building heating and ventilation system. Two crop drying applications (tea drying in Indonesia and cocoa drying in Malaysia) demonstrate the suitability of the perforated absorber for operation in non-vertical orientations and for higher delivery temperatures than typical of the building ventilation applications.

The crop drying applications are particularly unique. A Canadian funded project is investigating the use of solar energy to dry a variety of crops in the ASEAN region. Two of the countries, Indonesia and Malaysia are demonstrating the perforated plate solar collector. The results of these two projects will be compared with the conventional air-based solar collectors being demonstrated at other locations in the Philippines, Singapore, and Thailand. Many different crops are being dried including tea, cocoa, beans, bananas, and rubber. The ASEAN-Canada project is a five year program which began in 1992. The systems were installed during 1994 and will subsequently be monitored.

Solar energy is ideally suited to the drying of crops, especially with commercial operators who currently use non-renewable fuel to heat the air. Designing the solar heater is relatively straight forward once the air volume and temperature rise for the particular crop are known. Many of the commercial dryers operate 24 hours per day year round. The day-to-day solar radiation near the equator is fairly constant which provides uniform solar drying throughout the year.

Table 1.1: Summary of Demonstration Project Costs and Performance

	Ford of Canada *(ventilation air preheating)* (1990)	GM, Oshawa *(ventilation air preheating, Sep.-May heating season only)* (1991)	NREL Waste Hand. Facility *(ventilation air heating)* (1992-1994)	GöttingenUtility Co-generation *(Preheating combustion air)* (1993-1994)
Collector area and type	1877 m^2 vertical wall 2% porosity with 1% on canopy	420 m^2 gross (net perforated area = 365 m^2) 2% porosity on wall, 1% on canopy	27.9 m^2 2% porosity constant air flow rate system	343 m^2, 1% porosity, dark brown wall oriented southwest
Available Insolation per m^2 per year	2.5 GJ (700 kWh)	2.28 GJ (632 kWh)	n/a	2.6 GJ (on horizontal surface)
Solar energy collected per m^2 per year	1.44 GJ (400 kWh)	1.64 GJ (456 kWh)	n/a	0.9 GJ (250 kWh)
Annual average efficiency	57%	72%	68% (1992/93) for G>1500 Wh/(m^2day) 63% in 1994 Jan.1 -Mar.22	Up to 63% for V_s= 0.02 m/s Ave. is 34% *
Total Energy Savings per m^2 per year	3.3 GJ (917 kWh)	2.71 GJ ** (754 kWh)	n/a	0.9 GJ (250 kWh)
Installed Cost (1993 US$/$m^2$)	84	159	100	188
Maintenance cost ($/$m^2$ yr)	0.05	n/a	1.00	4.40
Cost of an annual GJ of delivered energy ($/(GJ yr))	25.00 *	59.00	n/a Energy cost is $6/GJ based on 20 yr analysis)	209.00 (Energy cost is $30.52/GJ based on 20 yr analysis)
Economic Payback time	n/a	1.0 to 1.3 yrs compared to steam; 3.6 yrs compared to natural gas	n/a	n/a
Other Comments	***Cost of energy is $58/ (GJ yr) if only active solar gains are considered.**	****"Total energy savings" doesn't include all the destratification savings.**		***Low avg. efficiency is due to the very low average flow rate of 0.008 m/s**

Table 1.2: Summary of New Applications

	Ispra Ecocentre (Ventilation air pre-heating)	Tea Drying in Indonesia	Cocoa Drying in Malaysia
Collector area and type	370 m^2 vertical wall, plus 180 m^2 canopy. 0.7% porosity	600 m^2 roof-mounted, 1% porosity, west-facing at 22 degree slope	370 m^2 roof mounted, 0.25% porosity south-24 degree slope.
Suction Air Flow Rates	"Operating Mode 2": 0.003 to 0.015 m/s	0.03 m/s	Adjusted to deliver a maximum air temperature of 65 °C
Solar Energy Available per m^2 per year	n/a	5.97 GJ	6.59 GJ
Simulated Total Delivered Energy	n/a	2.1 GJ	n/a
Average Collector Efficiency	n/a	65%	n/a
Installed Cost (1993 US$/$m^2$)	n/a	95	104
Measured Performance	n/a	1.2 GJ oil equivalent saved in Sept. 1994	n/a

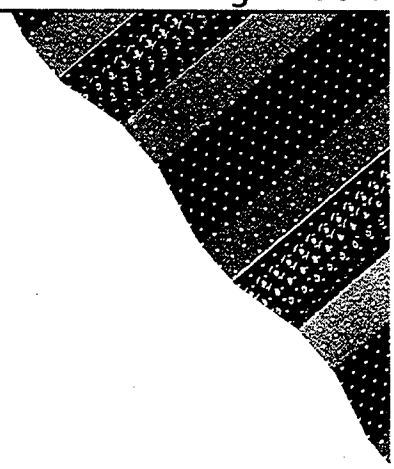

Chapter 2

Demonstration Projects

2.1 Ford of Canada, Oakville Assembly Plant, Oakville, Canada

General Project Information

The perforated collector installation at the Ford of Canada automobile assembly plant in Oakville, Ontario was one of the first installations of this technology. In 1990, the perforated absorber was retrofitted as a replacement for the glazed system that was originally installed. The perforated-plate system was installed to demonstrate improvements in system safety and appearance. The installed cost of the perforated-plate was lower than for the glazed system, and monitoring was undertaken to determine if efficiency was comparable.

System Description

System Operating Modes The operation of the perforated absorber is such that the air intake on the perforated collector is distributed across the entire surface of the absorber. The inlet across the bottom of the wall used by the glazed system was sealed. The operation of the system is described in Chapter 1.

Key System Parameters 16 fan units provide a total of 223,300 m^3/hr through 610 meters of air distribution ducting. In most areas, two void fractions (i.e., the amount of surface area covered by holes) were used on the absorber to obtain an even airflow distribution across the entire collector. A 1% void fraction was used near the fan, and a 2% void fraction was used farther away to smooth out the air flow.

Collector Description The collector is described in Chapter 1.

Collector Parameters Figure 2.1.1 is an elevation view of the monitored section of the Ford installation. The entire collector covers 1877 square metres. The monitored section consists of 237 m^2 of collector at the extreme east end of the plant. The surface is flat black (no selective coating). A 2% void fraction covers the entire area of the monitored collector section. A 2.44 metre by 2.44 metre summer bypass damper is mounted on the absorber skin directly in line with the fan opening. The bypass damper is larger than the duct opening to reduce induced flow from the collector into the building when the damper is in the open position. The summer bypass control was adjusted to close the damper at ambient temperatures below 18 °C and open the damper above 18 °C .

System Components The system components are described in Chapter 1, with reference to Figures 1.1 through 1.4.

Description of Advanced Features The perforated absorber removes the need for unsightly and non-fire rated fibreglass glazing, resulting in an estimated 35% reduction in cost. The glazed and unglazed systems were expected to have similar performance. Monitoring results showed that the annual solar heat delivered by the perforated collector was 1.4 GJ/m^2y, slightly higher than the 1.3 GJ/m^2y delivered by the glazed collector.

Justification of Advanced Features Laboratory testing at the National Solar Test Facility (NSTF) showed that the perforated collector had efficiencies up to 30% higher than the glazed collector under no wind and low wind conditions, while the glazed collector was 17% more efficient under high wind conditions. Table 2.1.1 below summarizes efficiency test results for both glazed and perforated prototypes. Figure 2.1.2 shows the test results for the aluminum absorber with 2% void area at various collector flows, wind speeds and radiation levels. Efficiency is a strong function of collector flow, but wind speed affects efficiency only at lower collector flow rates.

Table 2.1.1: NSTF Glazed and Perforated Collector Efficiency Results

Collector Type	No Wind	Low Wind	High Wind
Standard Glazing		0.57	0.54
FS Glazing		0.52	
Aluminum Soffit	0.75	0.65	0.39
Steel, 4% void area	0.69	0.62	0.34
Aluminum, 1% void area	0.72	0.62	
Aluminum, 2% void area	0.73	0.68	0.46

Notes:

Wind	High = 3.5 m/s	Low = 1 m/s
Incident Radiation	900 W/m^2	
Airflow	0.15 kg/s	
Gross Collector Area	4.655 m^2	

Monitoring of several systems consistently showed that local wind conditions along large south-facing building walls are much less severe than in open unprotected areas. This is illustrated in Figure 2.1.3 which shows monitoring results of the wind conditions on the rooftop and in front of the Ford perforated-plate system. For the period shown, the wind speed measured in front of the wall was on average about 60% lower than that measured 5.2 meters above the roof.

Combining the NSTF test results and the wind speed reductions expected at the perforated collector, simulations were run using the SIMAIR computer model. The predicted solar heat delivered for the perforated collector system was 1.44 GJ/m^2 annually. The original glazed collector system had a measured performance of 1.3 GJ/m^2 and a predicted performance of 1.48 GJ/m^2 annually. The overall cost/performance improvement of the perforated collector was therefore anticipated to be 30%, due to the lower cost of the perforated-plate system.

Description of Back-up System/Auxiliary Individual gas-fired unit heaters provide heat to the plant. No auxiliary heating system is used in conjunction with the solar system.

Description of Load The load is the heating of ventilation air to replace air exhausted during manufacturing processes. All of the ventilation air required by the building is drawn in through the solar collector. Solar energy provides between 5 and 20% of the energy required to heat this ventilation air.

Description of Controls The controls are as described in Chapter 1.

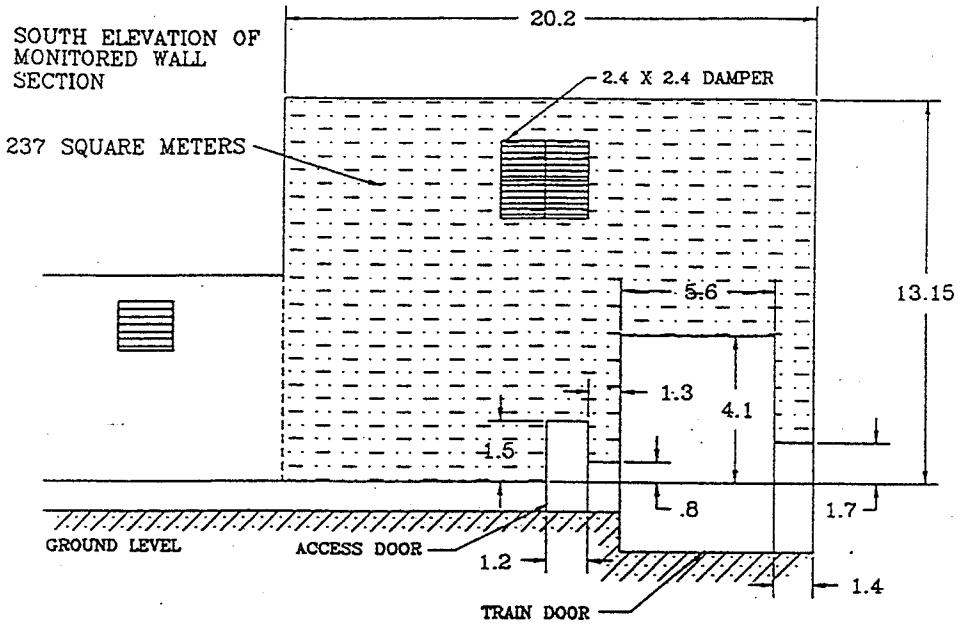

Figure 2.1.1 Elevation view of Monitored Perforated Collector at Ford

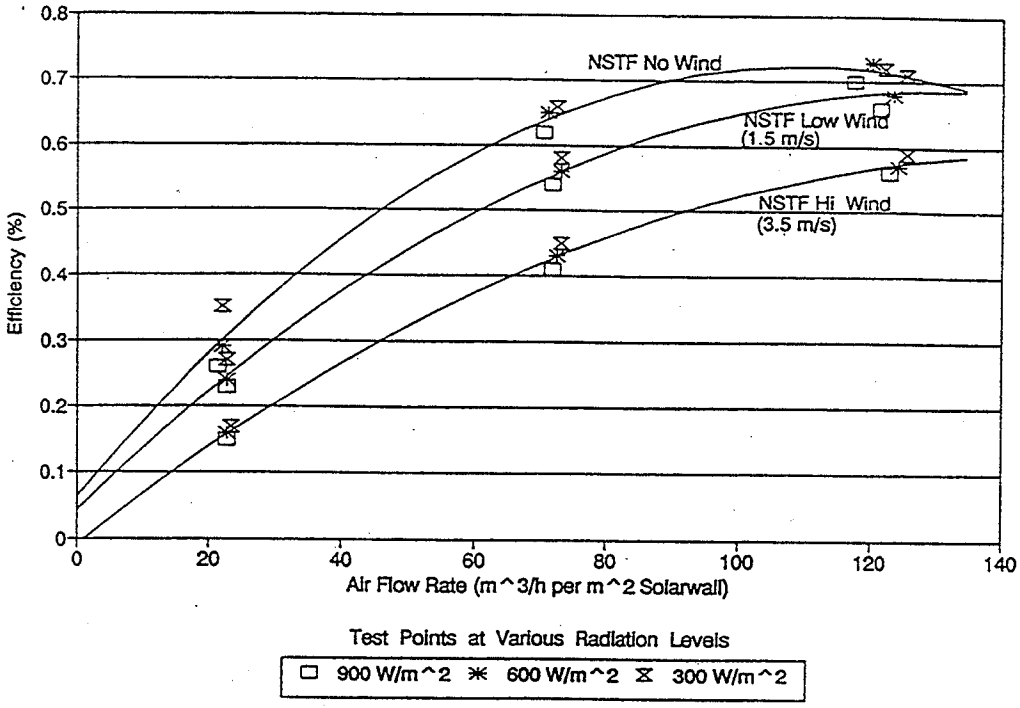

Figure 2.1.2 NSTF laboratory test results for the perforated-plate collector.

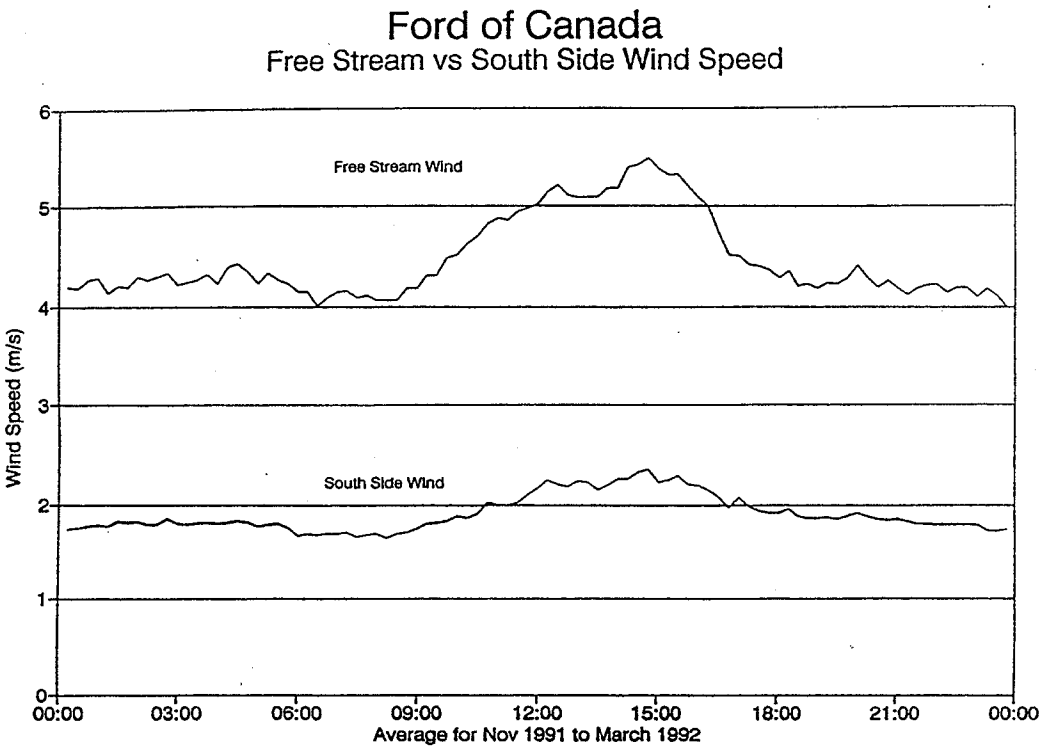

Figure 2.1.3 Free-stream and south-side wind speed at the Ford of Canada building.

Key Meteorological Data

Table 2.1.2 summarizes the atmospheric conditions measured at Ford over nine months of monitoring between March 1991 and April 1992. Solar radiation values are given for the vertical surface. The measured solar radiation for the nine month period were on average 12% lower than the Typical Meteorological Year

Table 2.1.2: Daily Average Atmospheric Conditions During Monitoring Period

Month	Days of Valid Data	VerticalSolar Radiation (kWh/m²/d) [MJ/m²/d]	Daytime Ambient Temp. (°C)	Nighttime Ambient Temp. (°C)
Mar-91	29	3.2 [11.4]	3.7	1.1
Apr-91	29	2.1 [7.6]	12.1	8.5
May-91	10	2.6 [9.3]	12.5	9.7
Nov-91	24	1.2 [4.2]	7.0	4.4
Dec-91	31	1.9 [7.0]	2.2	1.1
Jan-92	29	1.6 [5.6]	-2.2	-2.5
Feb-92	17	2.9 [10.4]	-1.8	-3.1
Mar-92	12	2.3 [8.4]	1.2	-1.0
Apr-92	21	3.0 [10.9]	5.2	6.2
9 Month Average	**202 (Total)**	**2.3 [8.3]**	**4.2**	**2.5**

(TMY) values for Toronto. The ambient temperatures, however, were generally above TMY conditions. For comparison, Table 2.1.3 presents Toronto TMY data for the same months.

Table 2.1.3: Toronto TMY Average Weather Data for November through May

Month	Solar Available (Vertical) (kWh/m²/d) [MJ/m²/d]	Daytime Ambient Temp. (°C)	Nighttime Ambient Temp (°C)
Nov.	1.9 [6.8]	4.1	2.1
Dec.	1.8 [6.3]	-3.5	-4.1
Jan.	2.6 [9.3]	-5.1	-6.2
Feb.	3.1 [11.1]	-5.8	-7.4
Mar.	3.7 [13.1]	-0.9	-3.3
Apr.	3.0 [10.7]	7.3	4.5
May.	2.5 [9.0]	12.0	9.7
7 Month Average	**2.6 [9.4]**	**1.2**	**-0.6**

Monitored Performance

Instantaneous Performance

Monitored instantaneous active solar efficiency of the perforated-plate collector is plotted in Figure 2.1.4 as a function of airflow rate. The "+" signs indicate quarter-hourly monitored values of instantaneous efficiency for representative days in the 1992 heating season. Wind speeds for these test points were between 0 and 3.5 m/s as measured in front of the collector, to provide results that can be compared to the NSTF data. All data points plotted are at radiation levels above 75 W/m². These field test data are superimposed over the three NSTF laboratory test curves. The solid curves "A" and "B" are curve fits to the field test data for March through May, 1991 and January through April, 1992 respectively. In both cases the average wind speed was slightly higher than the NSTF low-wind condition.

The following factors contributed to the better performance during the second year of monitoring compared to the first year. It should also be considered that a larger number of representative days were available in the second year, providing a statistically more significant sample.

- The bypass damper was manually closed and fastened for the second year of monitoring. This may have resulted in less air leakage through the damper and more uniform flow through the collector.
- The fan-belts were tightened after the first year of monitoring, resulting in a higher maximum collector airflow.
- The average wind speed across the collector face was lower on the representative days for the second year, thereby reducing convective losses and providing improved collector efficiency compared to the previous heating season.

- At low radiation levels (e.g. below 150 W/m2) the efficiency exceeds the NSTF test results. The representative days in the second year had more data points at lower radiation levels.

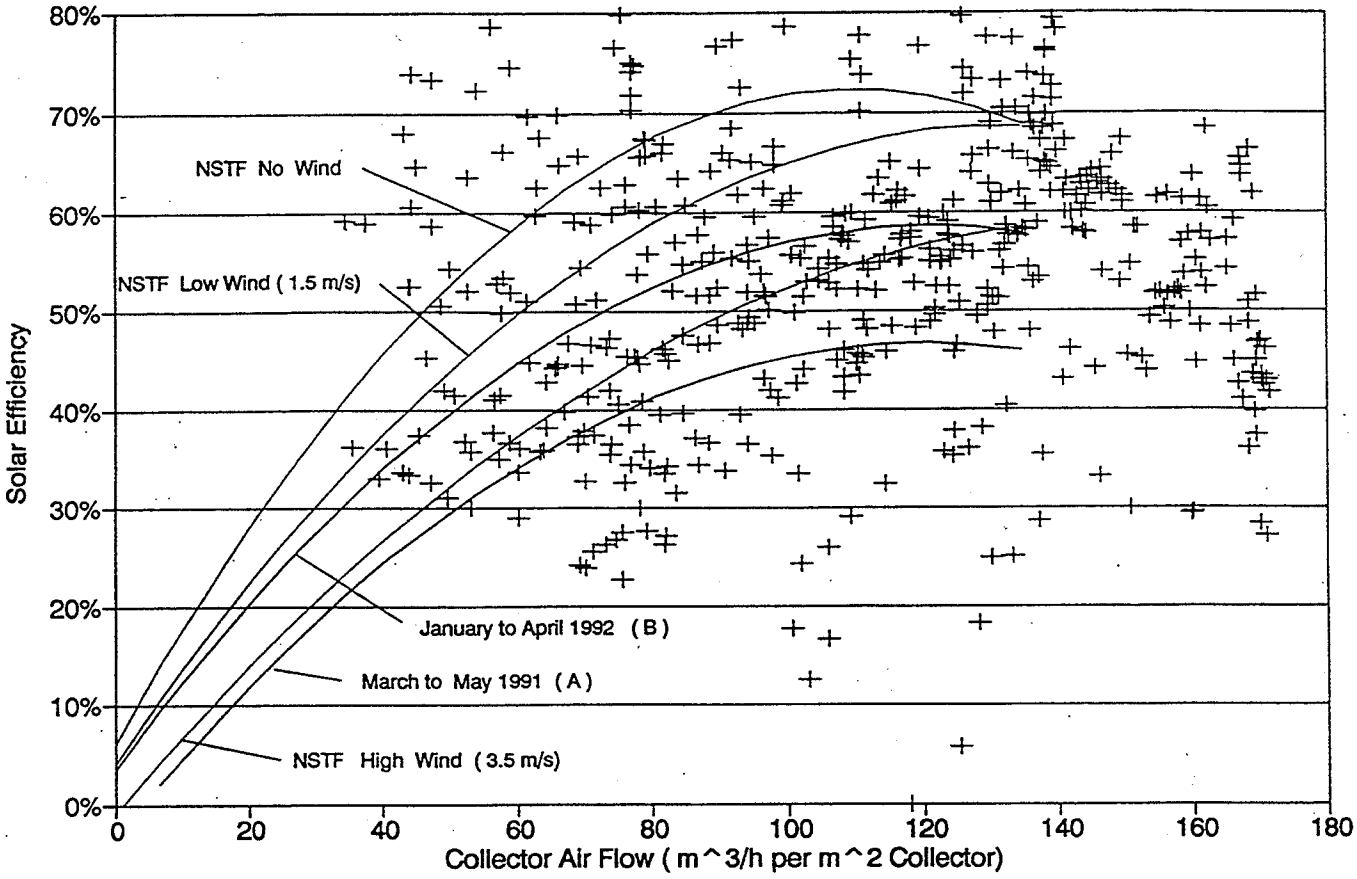

Figure 2.1.4 Ford of Canada field test data and NSTF lab test data.

Active Solar Heat Collected

The monitored daily average thermal performance for the perforated collector for the days of valid performance data are listed in Table 2.1.4.

The monitored and predicted values of daily average solar heat collected on a monthly basis over the monitoring period are compared in Figure 2.1.5. These data are also listed in Table 2.1.5. The predicted values of active solar heat collected were based on actual weather data where available. For months when there were more monitored weather data than monitored performance data, these performance data were extrapolated by multiplying them by the ratio of the performance calculated by SIMAIR for all days of valid weather data to that calculated by SIMAIR for the days of valid performance data. Missing weather data in any month was accounted for by multiplying monitored results by the ratio of total days in the month to the days of data available.

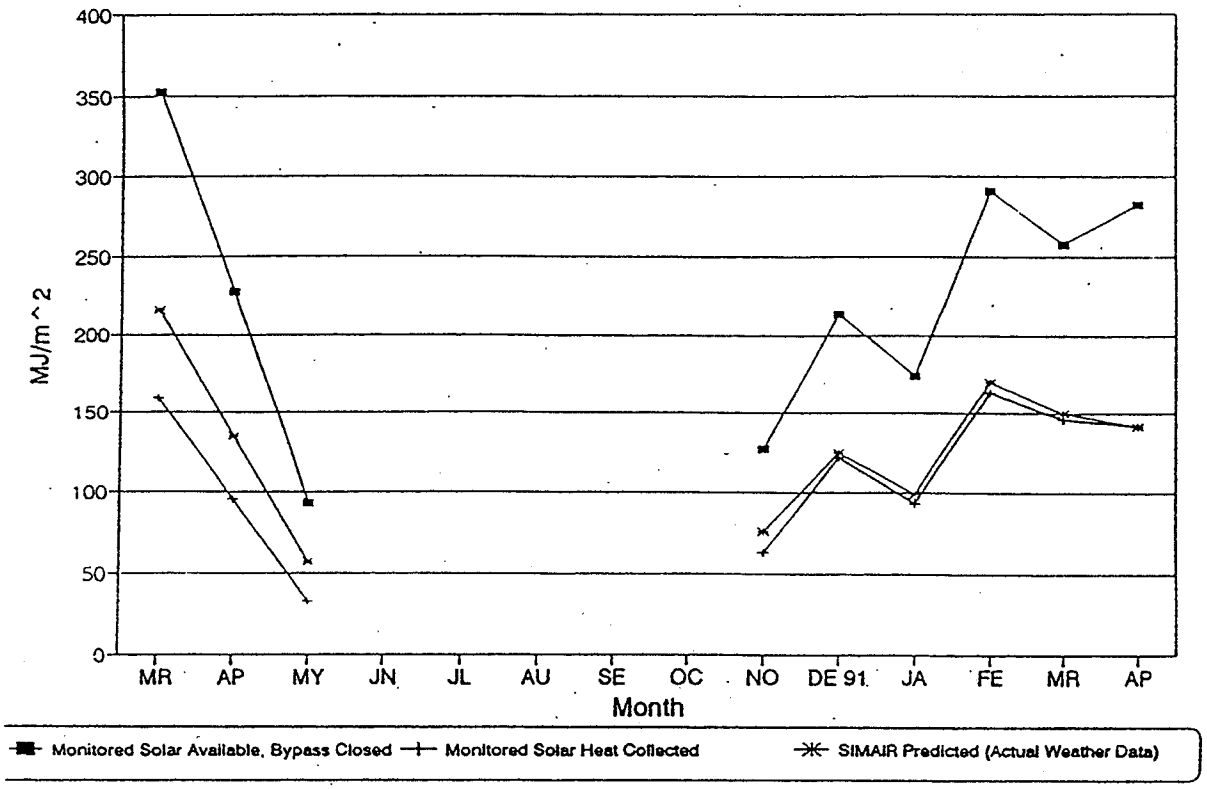

Figure 2.1.5 Comparison of simulated and monitored solar heat collection at Ford of Canada

Table 2.1.4: Monitored Performance for days of Valid Data

Month	Days Valid Data	Solar Available (kWh/m²/d)	Active Solar Heat Collected (kWh/m²/d)	Active Solar Efficiency (%)
Mar-91	22	3.2	1.5	46.5
Apr-91	19	2.4	1.1	45.4
May-91	10	2.6	0.9	35.5
Nov-91	18	1.5	0.8	50.9
Dec-91	31	1.9	1.1	56.6
Jan-92	27	1.6	0.8	53.6
Feb-92	17	2.9	1.6	55.9
Mar-92	12	2.3	1.6	56.6
Apr-92	21	2.6	1.3	50.0
Monthly Average	**177 (Total)**	**2.3**	**1.2**	**51.1**

* Summer bypass damper sticking. See "Monitored Solar Heat Collected" section.

Monitored Solar Heat Collected

Simulation results show the collector to be performing slightly below predictions in March 1991 and close to predictions in all other months. The maximum monthly predicted solar efficiency is 61.4% in March 1991. For the 10 days monitored in May 1991, active solar gains and efficiency appeared unexpectedly low. It was concluded that the summer bypass damper had opened for a short period in April but did not close properly afterward (air leakage through the bypass damper lowers the airflow through the collector and reduces the heat collected). The damper operating cable was later found to be sticking and the damper was manually fastened closed for the second heating season.

Air Temperature Rise

An important aspect of the operation of the perforated collector is the quality of heat delivered. The quality of heat is measured by the temperature rise of the air delivered to the building. The perforated collector can provide over 12 °C of temperature rise (on a sunny day) even with airflow rates exceeding 125 m^3/h per m^2.

Wind Effects on the Perforated Collector

The wind speed at the face of the collector followed a similar pattern to the free-air wind speed, but at a lower value. The overall average wind speed was 1.6 m/s, or 36% of the overall free-stream wind speed. During the day the average rose to 2.0 m/s, or 38% of the daytime free-stream value.

Table 2.1.5: Overall performance Analysis for Days of Valid Data

Month	Days Valid Data	Active Solar Heat Collected ($kWh/m^2/d$)	Night-time Heat Recaptured ($kWh/m^2/d$)	Passive Solar Temp Rise (C)	Destrat-ification Savings ($kWh/m^2/d$)	Reduced Wall Heat Loss ($kWh/m^2/d$)	Total Savings ($kWh/m^2/d$)
Mar-91	22	1.5	0.2	0.5	0.9	1.0	4.0
Apr-91	19	1.1	0.4	0.4	0.9	0.6	3.3
May-91	10	0.9	0.1	0.4	0.9	0.4	2.7
Nov-91	18	0.8	1.4	0.2	0.9	0.8	2.8
Dec-91	31	1.1	0.3	0.3	0.9	0.8	3.3
Jan-92	27	0.8	0.3	0.2	0.9	0.9	3.1
Feb-92	17	1.6	0.4	0.4	0.9	0.9	4.1
Mar-92	12	1.3	0.4	0.4	0.9	0.8	3.8
Apr-92	21	1.3	0.1	0.5	0.9	0.5	3.2
Monthly Average (Total)	**177**	**1.1**	**0.4**	**0.3**	**0.9**	**0.8**	**3.4**

The wind direction was always along the collector wall, either east-to-west or vice versa, regardless of the direction of the free-stream wind. Wind across the collector reduces performance, especially at low collector airflows. Sheltering of the perforated collector by the building therefore provides a natural benefit to performance.

Fan Power

As with any make-up air system, the perforated collector requires fans to move air into the building. For the second year of operation, a higher capacity fan was installed to increase air flow. An increase in motor power requirements resulted. Measurements showed that fan power requirements increased from 5.2 kW to 7.8 kW. This increase in fan power corresponds to the fan manufacturer's system curves, and resulted in a power requirement of 0.79 Watts per L/s of airflow. With the system operating 24 hours a day, 365 days a year, annual fan energy use is 68,000 kWh or 0.78 kWh/m^2 per day. It is important to note that approximately the same amount of fan energy, or more, would be required if a conventional make-up air unit were installed instead of the solar collector fans.

Passive Solar Heat Gains

Passive solar gains aid the performance of the perforated collector by heating ambient air before the collector brings it in. Air on the south side in front of the collector is on average 1°C above the free-stream ambient temperature. The south-side air is warmed by solar radiation absorbed by the ground in front of the collector. The benefit of this heating was calculated to be 0.3 kWh/m^2 per day of system operation. The monetary value of this benefit is dependent on how much this is above the temperature of air brought in by a conventional make-up air system. In a later monitoring project[1] it was found that passive solar gains are not always a net financial gain if, for example, the "conventional" make-up air system draws outside air from immediately above the roof of the building. This is because the air above the roof can be warmer than the air on the south side of the building.

Radiant Heat Loss from the Perforated Collector

There is a constant heat-loss from the absorber due to radiant exchange with the sky and terrestrial surroundings. The measured heat-loss is based on readings from an infrared radiometer (pyrgeometer) and measurements of the collector's absorber temperature. Between 15 and 25 W/m^2 were lost on average from the wall during March and April 1992. The losses were greater over the daylight hours because the absorber was hotter. The nighttime radiant heat loss is important because it reduces the benefit of nighttime heating of ventilation air from recapture of building heat loss.

If a selective surface with an emissivity of 0.1 were used instead of flat black paint, the radiant heat loss would be reduced by approximately 17 W/m^2. Over an eight-month heating season, the benefit of a selective surface is estimated to be 0.35 GJ/m^2.

Reduced Heat Loss Due to Added Insulation

The assembly plant's south wall was originally constructed of concrete and single-pane glass. When the perforated collector was installed, 38 mm of fibreglass insulation and a new steel skin were added to the exterior face of the building. The perforated-plate was then installed outside the new skin, enclosing an air cavity. The overall assembly reduced the heat-loss from the building by virtue of the insulation alone and by maintaining the air behind the perforated-plate at a temperature higher than the south wall would see if it were exposed to ambient temperatures. The "sol-air" effects of the original wall must also be accounted for in the calculation of the savings.

[1]Enermodal Engineering Ltd. (1994) Performance of the Perforated-Plate/Canopy solarwall at GM Canada, Oshawa. Report prepared for Natural Resources Canada - CANMET, June 1994.

The total savings due to reduced heat loss through the south wall are given in Table 2.1.5, and range from 0.4 to 1.0 kWh/m^2/d, depending on the average outdoor temperature. The average saving is 0.8 kWh/m^2/d, approximately 60% of the magnitude of the solar heat collection. Buildings with better insulation would, of course, show smaller savings.

Recapture of Nighttime Wall Heat Loss

The flow of ventilation air up the cavity behind the perforated-plate captures heat flowing out through the building shell and returns it to the building. The heat recaptured overnight was an average of 0.3 kWh/m^2/d, and is greatest in cold months.

Conclusions

The testing shows that

- instantaneous efficiencies over 70% are possible with the perforated- plate system;
- a high quality of heat can be delivered by the perforated collector, as typical sunny day temperature rise can be over 12 °C with a high airflow on a sunny day;
- monthly average solar heat collection efficiencies of over 55% were measured;
- extrapolating the monitored data, the active solar heat delivered annually is calculated to be 1.4 GJ/m^2 with an efficiency of 57%;
- the total energy savings attributable to the perforated collector was 12.2 MJ/m^2/day or 3.3 GJ/m^2 for the monitoring period;
- perforated collector performance could be improved if a low-leakage summer bypass damper and a selective coating on the absorber were used; and
- Perforated Collector airflows of over 120 m^3/h per m^2 of collector will ensure that maximum energy performance is realized.

Estimated Costs

This project was a replacement of the glazed solar collector. Since the support structures used for the glazing were re-used for the perforated absorber, the project costs were not representative of a typical complete installation. The actual project costs reported below are not used in the financial analysis, rather estimated costs for a typical complete installation are used. It is assumed that the distribution components (fans, ducts, controls) are needed for a standard make-up air ventilation system. The incremental solar cost is considered to be only the perforated collector outdoor components. The manufacturer estimates that the cost to supply and install the perforated absorber would be about US$158 000 or US$84/m^2 (1993 dollars). The labour portion of this cost was estimated at US$38 800 or about US$21/m^2. By comparison, the glazed system is estimated at US$131/m^2. The total solar energy contribution for the perforated collector of 6131 GJ per year is worth about US$30 000 per year at Canadian natural gas prices (US$3.40/GJ and 70% combustion efficiency).

The total ventilation heat load is about 38600 GJ/y, or about 21 GJ/m^2. The auxiliary portion of this would cost about US$177 000 (gas price and efficiency as above). The perforated collector itself requires no

maintenance. The fans and dampers in total need about four hours per year, costing about US$85/y or US$0.045/m^2. For the perforated collector itself, the cost performance ratio is approximately US$58/GJ/y.

2.2 General Motors Battery Plant, Oshawa, Canada

General Project Information

In 1991, an advanced perforated-plate collector system for preheating ventilation air was installed at a General Motors battery manufacturing plant in Oshawa, Canada. For the first time an unglazed perforated collector incorporating an overhanging canopy was used. The new design was intended to improve on earlier perforated-plate-only designs that did not include a canopy.

The GM system was monitored over 3 heating seasons, and modifications to improve the performance were made over that time. The monitoring provided information on the potential areas for modification and improvement. The performance results for the last year, incorporating all the modifications, are presented.

System Description

System Operating Modes The operation of the perforated-plate collector with a canopy is similar to the basic perforated collector described in Chapter 1. The canopy was included to balance air flows and to recapture any heat that may be convecting up the outside face of the absorber.

Key System Parameters The GM system has a total of 365 m^2 of vertical perforated-plate (including the bypass dampers). There is an additional 55 m^2 of vertical projected area in non-perforated-plate. A storage tank with 12 m^2 projected surface area shades a portion of the wall. (See Figure 1.2 in on Page 2.) Two 1.22 metre by 2.44 metre bypass dampers are located in the face of the canopy. These dampers are used as a summer bypass to allow ambient air to be fed directly into the building when no heating of ventilation air is required. The two-position damper is controlled by an adjustable thermostat that senses outdoor temperature. The thermostat was originally set to open the damper when the outdoor temperature was above 18 °C.

The GM perforated collector contains two fan/distribution systems. Each system consists of a constant-speed fan, a recirculation damper system and a fabric distribution duct. Two new high-efficiency fans were installed and ducting modifications were made in early 1993. The system changes increased the airflow to close to the original design flow of 74 700 m^3/h (20 750 L/s).

Collector Description The collector is described in Chapter 1, the major difference being that a canopy was added across the top of the collector, as illustrated in Figure 1.2 on page 2. The canopy was constructed of perforated collector sheet on the vertical and the downward facing horizontal sections so that the absorber and heat collecting areas of the collector are increased. On upward facing areas, the perforated collector was not perforated to prevent rain from entering the collector.

Collector Parameters The solar collection system installed at GM is a hybrid of a perforated-plate and a canopy-wall system. The lower 6.25 metres of the perforated collector is a black perforated aluminum-plate with 1.6 mm diameter holes covering 2% of the surface area. The absorber plate is fastened to the south face of the building wall with an average 150 mm air cavity behind. Air is drawn through the absorber, then rises up through the cavity to the canopy that forms a manifold (horizontally) across the top of the absorber. The fully enclosed canopy projects 900 mm beyond the surface of the absorber and has a cross-sectional area of 1.6 m^2.

The canopy acts as both a manifold for the airflow and a solar heat-collection device. As a manifold, the canopy carries solar-heated air horizontally to the fan opening. To increase solar heat collection, the canopy face is made of perforated-plate with a 1% void fraction, and serves as an extension of the absorber area. The underside of the canopy is also perforated with a 1% void fraction to collect any heated air that may be rising up the outside surface of the absorber.

System Components The system components are described in Chapter 1.

Description of Advanced Features The added canopy was the original advanced feature. 1991-92 monitoring results showed that the system was operating at below design airflow rates. An advanced air handling system (as described below) was retrofitted during the course of monitoring. Installation of the new high-efficiency air handling system was the second advanced feature.

Justification of Advanced Features A study was undertaken in 1992 to determine the cause of the low airflow and recommend ways that the flow rate could be increased while at the same time reducing fan electrical requirements and noise levels.[1]

The study recommended three changes to the perforated collector air handling system:

- installation of tapered intakes on the ducts leading from the collector to the fan systems,
- replacement of the existing fan/motor assemblies with high-efficiency vane axial fans complete with high-efficiency motors, and
- installation of a new fabric distribution duct with increased hole area.

The study concluded that

- airflow would increase to near design values;
- a lower system pressure drop curve would reduce fan power requirements,
- a more even distribution of airflow throughout the plant would result;
- fan noise would decrease; and
- airflow distribution across the face of the collector would improve.

Description of Back-up System/Auxiliary Individual steam-fired unit heaters provide heat to the plant. No auxiliary heating system is used in conjunction with the solar heating system.

Description of Load The load is the heating of ventilation air to replace air exhausted in the manufacturing process.

Description of Controls The controls are as described in Chapter 1.

---

[1]Enermodal Engineering Ltd. (1994) Performance of the Perofrated-Plate/Canopy Solarwall at GM Canada, Oshawa. Report prepared for Natural Resources Canada - CANMET, June 1994.

Table 2.2.1: Daily Average Ambient Conditions for Days of Valid Weather Data

Month	Days of Valid Data	Vertical Solar Radiation (kWh/ m²/d) [MJ/m²/d]	Daytime Ambient Temp. (°C)	Nighttime Ambient Temp. (°C)
Sep 93	16	2.71 [9.8]	13.1	11.7
Oct	31	2.07 [7.5]	8.9	8.2
Nov	30	1.81 [6.5]	4.1	3.6
Dec	26	2.04 [7.3]	-0.9	-1.7
Jan	31	2.68 [9.6]	-10.5	-10.9
Feb	28	3.83 [13.8]	-6.4	-7.0
Mar	9	2.35 [8.5]	-0.1	-1.1
Apr	14	3.02 [10.9]	7.2	5.0
May	27	2.08 [7.5]	10.2	9.2
Annual Average	**212 (Total)**	**2.89 [10.4]**	**1.7**	**0.8**

Table 2.2.2: Toronto TMY Weather Data

Month	Vertical Solar Radiation (kWh/m²/d) [MJ/m²/d]	Daytime Ambient Temp. (°C)	Daytime Ambient Temp. (°C)
Sep*	3.38 [12.2]	14.9	10.6
Oct	2.95 [10.6]	9.8	7.6
Nov	1.90 [6.8]	4.1	2.1
Dec	1.76 [6.3]	-3.5	-4.1
Jan	2.57 [9.3]	-5.1	-6.2
Feb	3.08 [11.1]	-5.8	-7.4
Mar	3.65 [13.1]	-0.9	-3.3
Apr	2.96 [10.7]	7.3	4.5
May*	2.49 [9.0]	12.0	9.7
Annual Average	**2.72 [9.8]**	**2.6**	**0.4**

*TMY data include only the last half of September and only the first hald of May.

Key Meteorological Information

Table 2.2.1 summarizes the atmospheric conditions measured at GM over the nine months of monitoring in the 1993/1994 heating season. Solar radiation values are given for the vertical surface. The measured solar radiation for the nine month period is very close to the Typical Meteorological Year (TMY) value for Toronto. The monitored ambient temperature is approximately 1 °C cooler than the TMY values. For comparison, Toronto TMY data for the same period are presented in Table 2.2.2.

Table 2.2.3: Fan System Performance Before and After Modifications

	Design Fan Airflow (m_3/h)	Original Fan Airflow (m_3/h)	Modified Fan Airflow (m_3/h)
East Fan	37 350	23 290	31 570
West Fan	37 350	26 350	36 370
Total	74 700	49 640	67 940
Collector Airflow ($m^3/h/m^2_{collector}$)	**178**	**118**	**162**

Note: Collector airflow is based on a collector area of 420 m^2.

Table 2.2.4: Fan Power Before and After Modifications

	Total Power (kW)	Energy per Unit Area Perforated Collector ($kWh/m_2/d$)	Air Moving Efficiency [W/(l/s)]
Before Modifications	9.2	0.53	0.68
After Modifications	8.3	0.47	0.44

Performance Data

The results of the fan system modifications are indicated by the data listed in Tables 2.2.3 and 2.2.4. The total fan airflow increased by 36% to 67 940 m^3/h or 162 m^3/h per m^2 of collector (within 9% of the design value). Had no changes been made to the fan or ducting system, the fan laws state that the fan power requirement should have increased 152% to achieve this 36% increase in flow. In this case, the changes to the fan system actually resulted in a 10% decrease to 8.3 kW. The specific air moving power decreased 35% to 0.44 W per litre/sec of airflow.

Active Solar Heat Collected

Figure 2.2.1 presents instantaneous values of active solar efficiency for the GM system for two typical months (November 1993 and February 1994). The individual points are 15-minute instantaneous efficiencies when the solar radiation was greater than 300 W/m^2. The monitored data were screened to eliminate large changes in solar radiation and fan airflow from one fifteen-minute period to the next, to ensure that the system was operating at steady-state conditions. Monitored data were separated into two categories. The solid triangles represent efficiency points calculated when the south-side wind speed was below 1.2 m/s (the average value for November). Hollow circles represent performance at wind speeds above 1.2 m/s. The solid line on the graph is a second order polynomial curve-fit to the low-wind-speed data points, and the dashed line is a curve-fit to the higher-wind-speed data points. These data are evidence that the system is capable of instantaneous efficiencies over 80% at high airflows.

The monitored data suggest that the wind has less effect on efficiency at high collector flows. At low collector airflow rates, the high-wind-speed efficiency points are generally below the low-wind-speed data points. At high collector airflow rates, the two sets of data points overlap, indicating less sensitivity to wind speed.

Building Wall Heat Loss and Recapture

The average power collected by the solar collector in November is plotted in Figure 2.2.2 as a function of the time of day. Using a stacked format, the height of the diagram shows the sum of the active solar heat gain rate and the wall heat recapture rate. During the day, the heat recaptured is reduced because the warm air in the collector cavity reduces heat flow through the building wall.

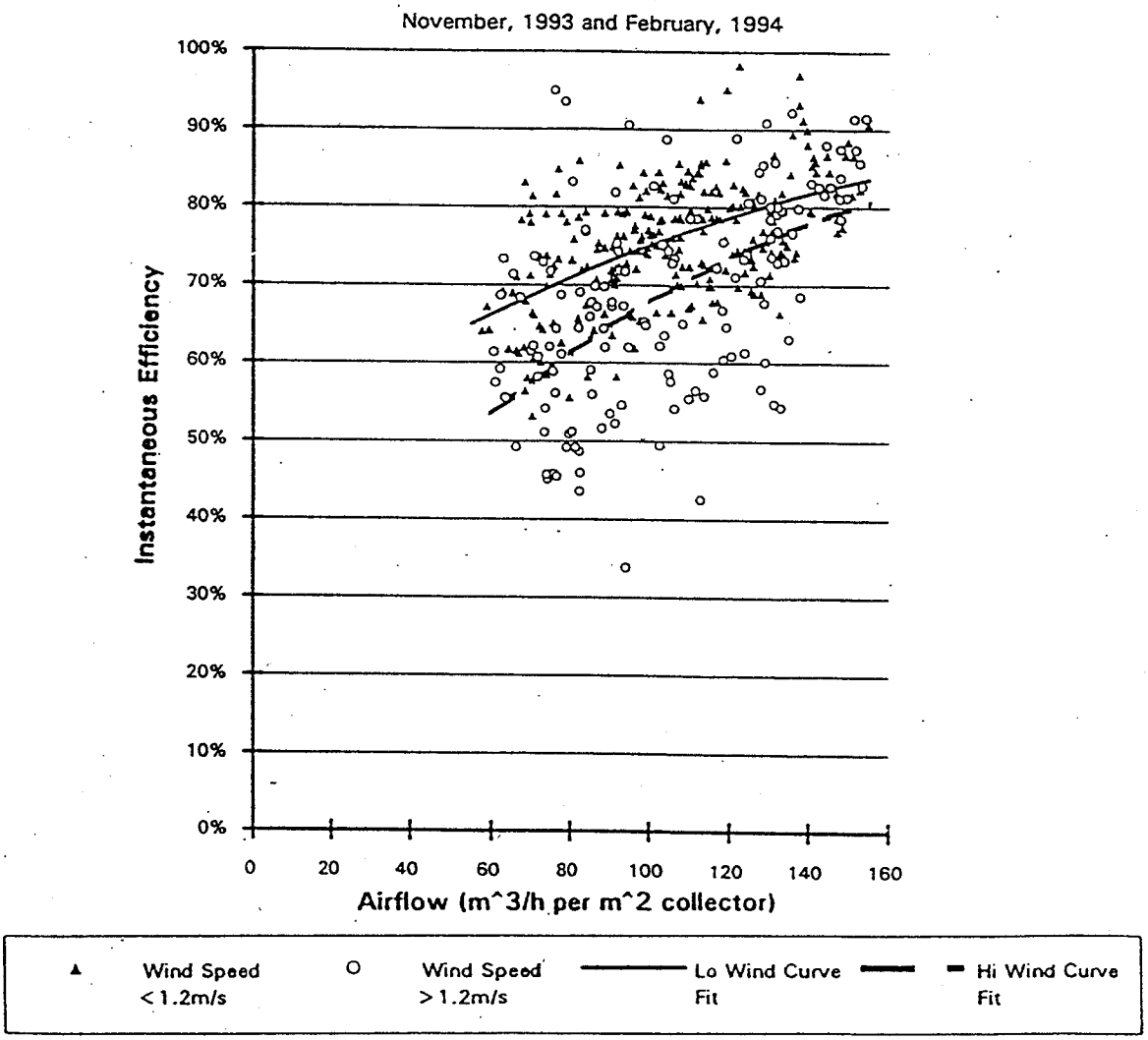

Figure 2.2.1 Collector efficiency for low and high wind speeds.

Reduced Building Heat Loss

The presence of the collector reduces heat loss through the portion of the building wall over which it is installed, by raising the air temperature next to the original building cladding. The savings due to the collector are greatest during the day, because the air in the cavity has been warmed by the solar radiation absorbed by the perforated-plate. The presence of the air space inside the collector provides some insulation value even at night. Nevertheless, the savings due to this mechanism are small. This is partly because the solar collector shades the building wall. (Solar heating of the original building cladding by short-wave radiation reduces the heat loss compared to heat loss based on air temperature differences only. This effect is accounted for by calculating the equivalent "Sol-air" temperature.)

Destratification Savings

Cool air delivered from the collector to the underside of the ceiling reduces the ceiling air temperature and destratifies building air. The lower ceiling air temperature reduces the heat loss through the ceiling and reduces the amount of heat exhausted by ceiling exhausts. A comparison of monitored ceiling temperatures

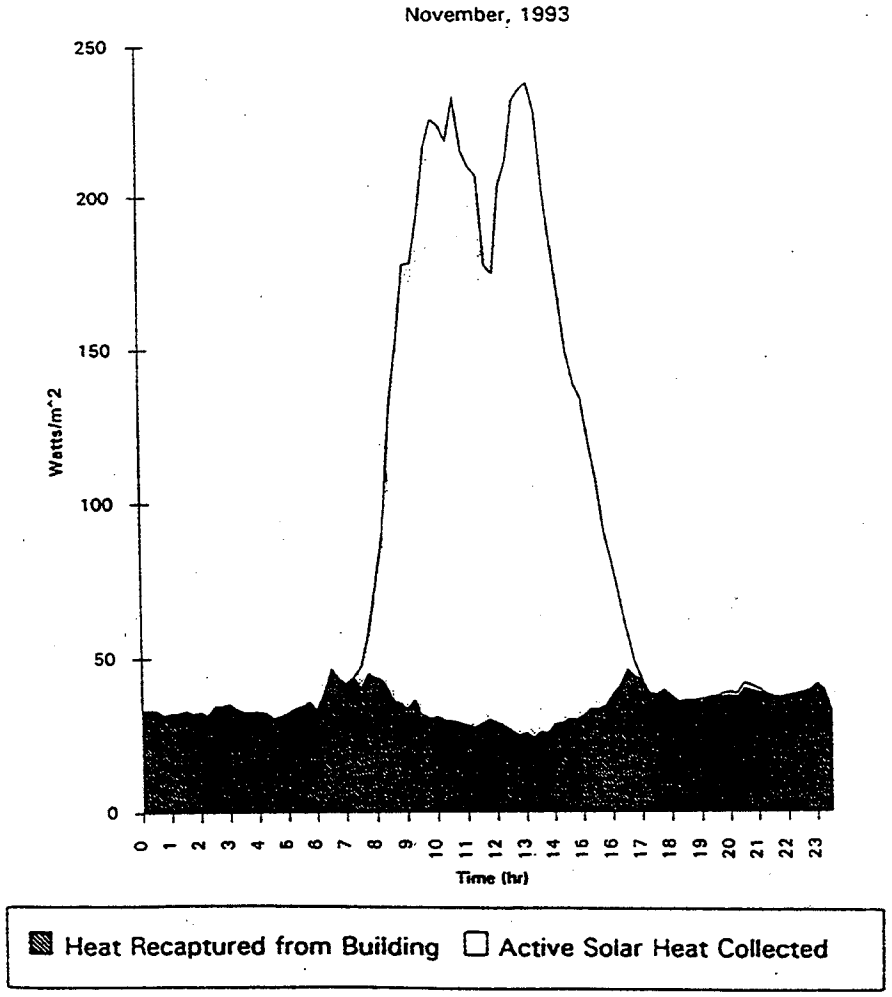

Figure 2.2.2 Total heat collected over the day.

with both fans on and both fans off showed that the operation of the perforated collector fan reduces the ceiling temperature by an average of 2.2 K. Only two temperature sensors were used to monitor ceiling temperature over the entire plant. Any localized production heat sources or other variations in temperature have not been monitored. Destratification savings could therefore be higher or lower.

Air delivered from the collector affects approximately 3,900 m^2 of building ceiling area. The exact insulating value of this ceiling is not known but, it was common practice to insulate ceilings with 50 mm of fibreglass insulation on industrial buildings in the early 70's. This would provide a thermal resistance of 1.0 m^2K/W.

In the building on which this collector is installed, the exhaust fans are at head height, and are located over battery charge tables. Monitoring showed that the temperature of air at exhaust hood height did not drop when the perforated collector fans were operating compared to when they were turned off. For this building, destratification savings are calculated for reduced conduction through the ceiling only.

Total System Performance

The performance results for the GM perforated collector are summarized in Table 2.2.5. Several changes were made to the system over the course of monitoring. The major changes included modifying the duct work and fan to achieve higher airflows, repositioning the temperature control on the recirculation damper, and lowering the delivered air temperature setting to 13 °C .

The average monthly active solar efficiency varied from 66% to 76% (excluding May 1994). The total monthly savings obtained by the perforated collector ranged from 2.6 to 3.7 kWh/m²/day per square metre of collector. Destratification savings averaged 0.49 kWh/m²/day.

Table 2.2.5: Monitored Performance for Days of Valid Data (in kWh/m²/day)

Month	Solar Available (kWh/m²/d)	Solar Heat Collected (kWh/m²/d)	Active Solar Efficiency (%)	Total Savings (kWh/m²/d)	Fan Energy (kWh/m²/d)
Sept 93	2.71	2.05	76	4.40	0.47
Oct	-	-	-	-	-
Nov	1.81	1.33	74	3.61	0.46
Dec	2.04	1.54	75	3.64	0.48
Jan	2.68	1.83	68	3.65	0.41
Feb	3.83	2.54	66	4.54	0.39
Mar	2.35	1.64	70	4.16	0.48
Apr	3.02	2.25	75	4.92	0.56
May	2.08	1.83	88	4.69	0.46
Annual Average	**2.54**	**1.86**	**72**	**4.15**	**0.45**

Estimated Costs

Perforated-absorber collector systems for preheating ventilation air have been installed on many industrial buildings. Most of these projects were retrofits, each requiring slightly different installation procedures to account for site variations. Nevertheless, the GM perforated collector project, although smaller than most perforated collector projects, is typical in many respects. The costs (in 1993 US$) for the GM project are summarized in Table 2.2.6. The costs for larger projects or for new construction are expected to be slightly lower. The "initial cost" refers to the total installed cost of the project as initially installed. The "upgrade cost" refers to the estimated increase in initial costs had the fan, motor, and ducting changes (described earlier in this section) been made with the initial installation. The total cost is the sum of the initial and upgrade costs, which in this case is US$159 per square metre of collector area. The operating costs are expected to be the same as for the Ford system. (See Monitored Performance under Section 2.1.)

Table 2.2.6: Cost of GM Perforated Collector System (in US$/m²)*

Component	Initial Cost	Upgrade Cost	Total Cost
Perforated-plate with Canopy	56	0	56
Fan System and Ducting	31	9	40
Labour	58	5	63
Total	**145**	**14**	**159**

* - Costs based on a 420 square metre system and two fan systems;

Total System Payback

As installed at GM, the perforated collector saves 1140 GJ annually. The economic benefit of these savings depends on the heating source assumed to be displaced. Two conventional make-up air systems are possible alternatives to the perforated collector: a steam-fed fan-coil or a direct-fired natural gas make-up air unit. In most cases the least cost alternative will be the system of choice. However, GM's decision on the most desirable alternative installed would be based on a combination of economics and familiarity with the equipment. For example, the cost of installing and operating a steam system is higher than for a direct-fired natural gas system. Still, the decision might be to go with the more expensive system because personnel are familiar and comfortable with operating it, spare parts are already in-house, and in-house expertise exists for maintaining the equipment.

The steam-fired option would be considered because steam is the primary heating source presently at GM. Installation would require a packaged roof-top steam-operated system with roof curb, steam piping, and outlet ducting. These systems are installed for about US$1.27/m³/h. The perforated collector system delivers 43 680 m³/h of airflow continuously. The installed cost of a steam system to deliver the same airflow would be US$55 500. The fan on the steam system would also require 3.6 kW more power to operate than the modified perforated collector system. The additional savings for the perforated collector system amount to annual electricity cost savings of US$1430.

The installed cost of the perforated collector system was US$66 530, an incremental investment of US$11 030 over a steam operated make-up air system. Based on steam costs of US$14.70/1000 kg, the savings using a perforated collector system, rather than low-pressure steam, are US$10 200/year. The payback on the perforated collector system is 1.3 years. If, as in most industrial buildings, the exhaust fans were located at the ceiling, the annual savings (including increased destratification savings) would be 1530 GJ for a total cost savings (including fan savings) of $15 300 with a payback of 1 year.

A direct-fired natural gas make-up air system costs approximately US$1.15/m³/h to install. To supply the same amount of air as the perforated collector, this make-up system would cost US$49 800. Fan power for the make-up air system would be equivalent to the perforated collector system because both the fan efficiency and the airflow are lower. The US$16 700 incremental cost would represent a payback of 4.9 years. If, as in most industrial buildings, the exhaust fans were located at the ceiling, the annual energy savings (including increased destratification savings) would be 1530 GJ, providing a total annual cost saving of US$4590 and a payback of 3.6 years.

Incremental Fan System Payback

Modifications to the fan and ducting systems saved energy in two ways and costs in three ways. First, increased airflow produced energy savings associated with all four heat collection mechanisms. Using SIMAIR to calculate these savings, it was found that, over the year, 98 kWh/m^2, or a total of US$720/year, was saved.

Second, electrical savings accrued over what the system would have consumed if only the fan blade had been changed. Based on the manufacturers recommendation, a new propeller of a similar type as originally used, but designed for higher throughput, was chosen. The heavy duty propeller fan required 10.0 kW input per fan to provide the higher airflow. Assuming electricity and demand charges of US$0.0408/kWh and US$3.78/kW respectively (current local rates) the total electrical savings are US$3200/year. A total savings of US$3920 annually. Based on a US$14/m^2 installation cost, the payback is 1.5 years.

Based on the total cost of the project and the benefits described above, the cost/performance ratio is US$58/(GJ/y). If the exhaust fans were located at the ceiling the cost/performance ratio would be US$44/(GJ/y).

2.3 NREL Waste Handling Facility, USA

General Project Information

There are two small outdoor transpired collector ventilation preheat projects at NREL: a 27.9 m^2 perforated collector mounted on the new Waste Handling Facility and a 25.4 m^2 experimental adjustable transpired collector on the Bulk Storage Facility. The first collector is a commercial installation designed and installed by Conserval Systems, Inc. and the NREL Facilities Management Branch. After completion in the fall of 1990, it was instrumented by the NREL Solar Heating Research Group, and it serves as the U.S. air heating project for Task 14. This collector, its performance and cost are described in this section of the report. The second collector was designed and built by the NREL Solar Heating Research group for experimental research purposes. It uses a 1% porosity collector surface and a constant velocity header to improve flow uniformity across the absorber. It is discussed in Part II, Chapter 2.

System Description

The Waste Handling Facility is located approximately 30 meters north of the new Solar Energy Research Facility (SERF) on the NREL premises. It is a 120 square meter concrete block building used to handle hazardous waste materials from the labs at NREL. The building contains two rooms: an explosives containment room and a general hazardous waste handling room. This small building requires very high ventilation, hence the heating load is comparable to that of a much larger structure.

The transpired collector (see Figure 2.3.1) is located on the south wall of the building. The collector surface is corrugated aluminum with a porosity of 2%. The collector has a total surface area of 27.9 square meters. A bypass damper provides a direct route for outside air to reduce the heating of the air by the collector during warm days when no heat is needed. This system is similar to the Ford of Canada, Oakville system, in that it has no header across the top of the collector to even out the airflow across the collector.

The building HVAC system is comprised of three exhaust fans each rated at 1500 cfm and one two speed supply fan rated at 3000 cfm. The supply air fan is a vane axial fan that is located downstream of the electric air heater. Air is drawn through the collector, heated if necessary, and delivered to the two interior rooms via two ducts approximately 50 cm in diameter.

System operation is extremely simple; ventilation air is always drawn through the collector even during the night, except in the summer when the collector is bypassed and outdoor air is drawn directly into the building. See the attached system diagrams.

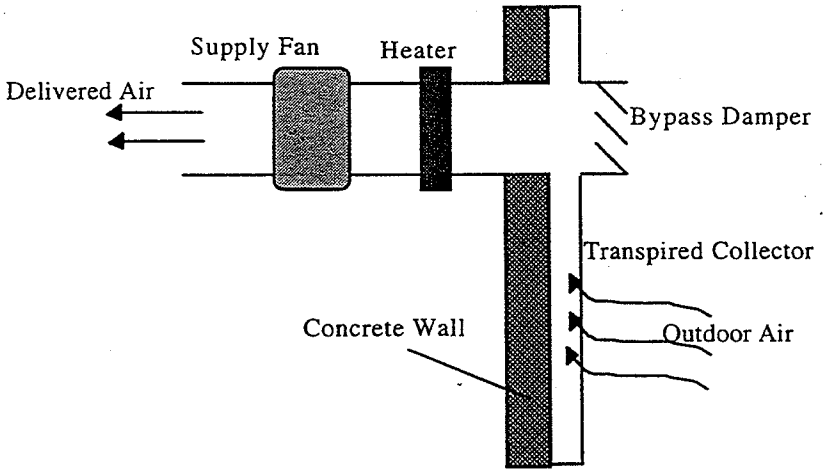

Figure 2.3.1 Waste Handling Facility Schematic

A thermopile is installed across the heater and fan assembly. The purpose of this thermopile is to get an accurate measurement of the temperature rise across the heater so that the mass flow rate delivered to the room can be determined from

$$MassFlow = HeaterPower \;/\; c_p \Delta T_{heater}.$$

Using the same sensor locations used by the delivered air temperature sensor and the inlet air temperature sensor, the effects of infrared radiation from the heater and collector were reduced to a minimum. Tests have shown that this thermopile is not noticeably effected by the presence of the hot heater element or warm collector surface. Figure 2.3.3 shows the location of the thermopile.

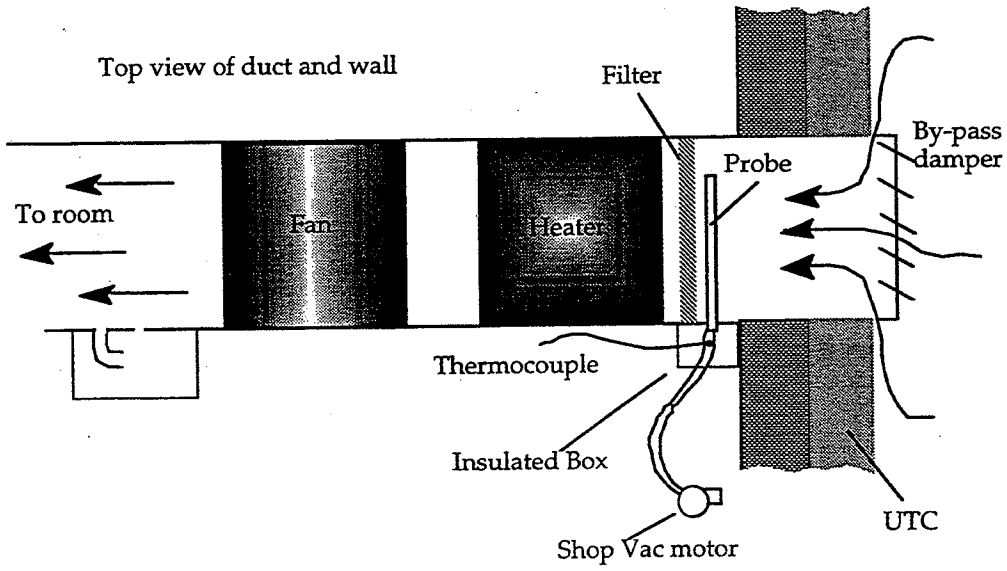

Figure 2.3.2 Inlet Suction Probe Location

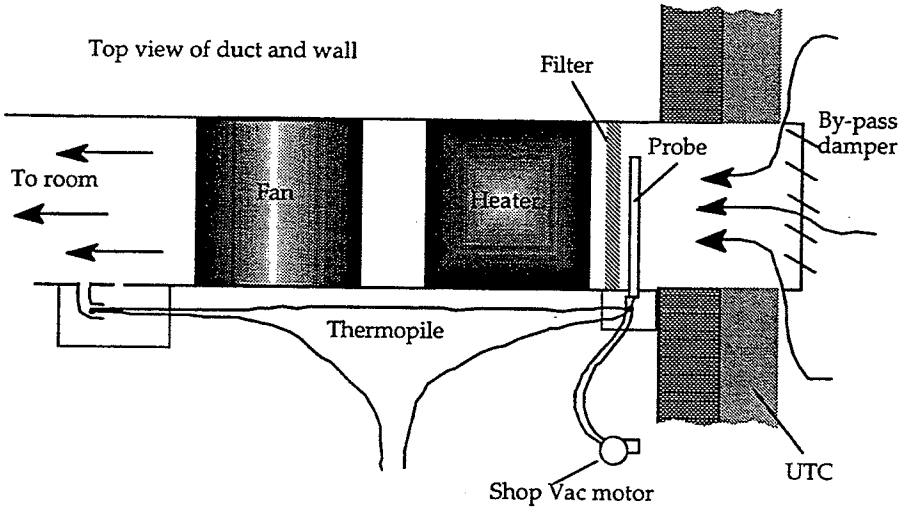

Figure 2.3.3 Thermopile Location

Performance Data

Two sets of performance data are presented here. The first set of data covers the period from the spring of 1992 through the spring of 1993. These data showed that the collector operated at approximately 68% efficiency, when the energy absorbed by the concrete wall behind the collector was taken into account. Following subsequent modifications to the data acquisition system, an independent set of data was taken during the first two and a half months of 1994, for which period the average collector efficiency was measured to be 63%.

1992-1993 Results

As a result of limitations in the instrumentation and the effects of the building itself on the performance of the collector, measured daily efficiencies had an estimated accuracy of ±20%. The primary reasons for this level of uncertainty were: accuracy of the thermocouples, uncertainty in the measurement of the mass flow rate, effects of infrared radiation from the collector and the heater on the thermocouples, and the heat transfer through the uninsulated concrete wall behind the collector.

The average efficiency of the collector during the heating season (September through April) was found to be approximately 68% for days with total incident solar energy greater than 1500 Wh / m^2day. Below 1500 Wh / m^2 day of insolation the uncertainty in data became excessive, and results for those days were therefore not included. Figure 2.3.4 shows the measured efficiency of the collector from September 1st 1992 through April 30th 1993.

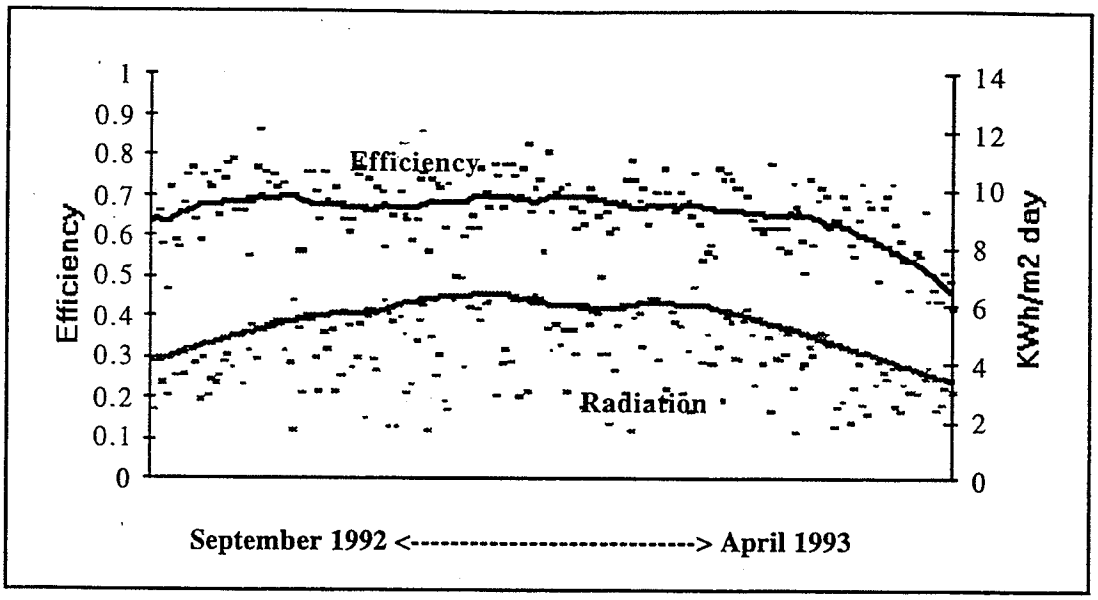

Figure 2.3.4 Average Daily Efficiency

The collector efficiency reported here accounts for the heat transfer to the concrete wall by modelling the heat transfer through it. During winter months the heat delivered to the concrete wall represents between four and ten percent of the total energy delivered depending on the outside conditions.

Besides the daily average efficiency of the collector, the other issue of primary importance to this collector is its performance as a function of wind speed. The following plot shows the daily average collector efficiency as a function of daily average wind speed (incident energy-weighted).

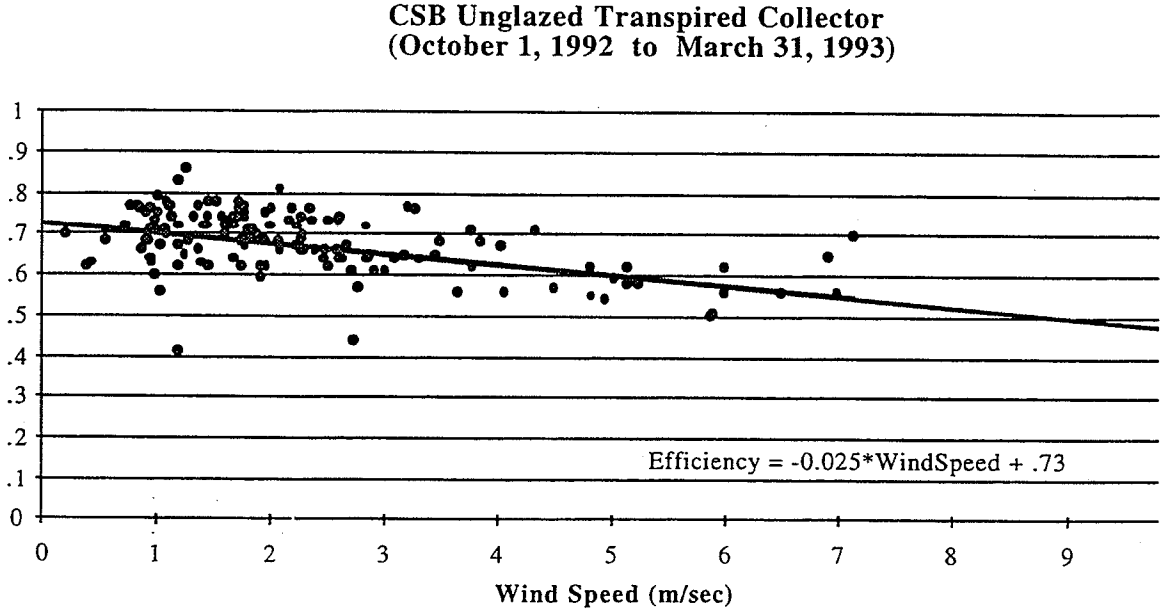

Figure 2.3.5 Efficiency versus Wind Speed

Figure 2.3.5 shows a moderate degradation of the collector performance with increasing wind speed. The effect is larger than expected; however, it must be kept in mind that the average face velocity of this

collector is only 0.036 m/sec, and there are areas with much lower flow rates. This value is considerably less than the 0.05 m/sec that the system was designed for. Because of the low flow rate and the fact that most of the wall has 2% porosity, the pressure drop across the collector is quite small, and thus the collector is more susceptible to wind effects. Areas of the collector may not be used effectively if wind flow around the building results in a lower local pressure than that of the air inside the collector.

1994 Results

Improvements to the data acquisition system were completed on December 21, 1993. Since that time data has been recorded with a few days missing due to problems with the data logger communications. The following section presents the data that was recorded from the January 1, to March 22, 1994.

Figure 2.3.6 is a plot of 30 minute average collector efficiencies for February 11th through February 20th. In this plot both the raw collector efficiency and the reduced collector efficiency are shown. The reduced collector efficiency accounts for the heat transfer into and out of the concrete wall behind the collector plenum by using a finite difference model of the heat transfer. By comparing the two efficiencies one can see that the raw efficiency has more spikes and efficiencies exceeding 100%. The reason for this is because when a cloud suddenly casts a shadow across the collector the energy stored in the concrete wall is released to the air stream and the efficiency is artificially increased. Although the finite difference model used to generate the reduced collector efficiency does improve the measurements of the actual energy collected it does not completely solve the problem of interaction with the concrete wall.

Figure 2.3.7 shows the radiation and ambient temperatures for the same period shown in Figure 2.3.6. Notice that the days of low efficiency shown in Figure 6 correspond to days that are significantly warmer than the previous day. During these days the thermal mass of the building wall and collector is absorbing some energy from the air stream, thereby reducing the measured energy delivered by the collector. Thus the variation in the ambient temperature from day to day or hour to hour directly effects the measured efficiency of the collector, and therefore the collector efficiency should be evaluated over weekly or longer periods of time.

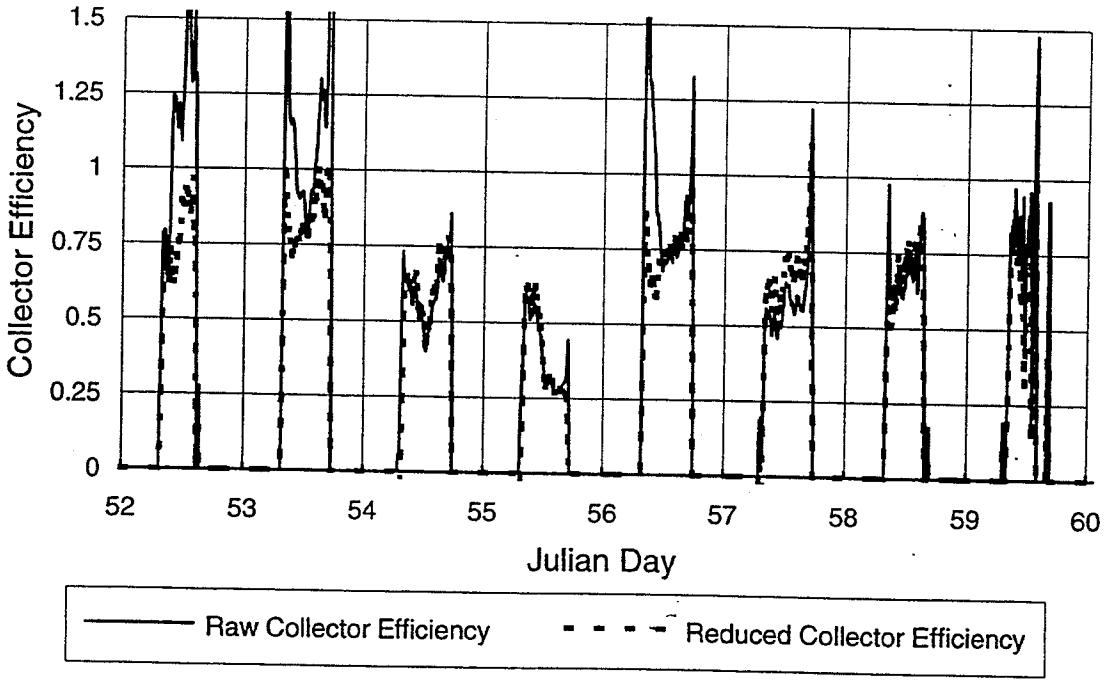

Figure 2.3.6 Collector Efficiency

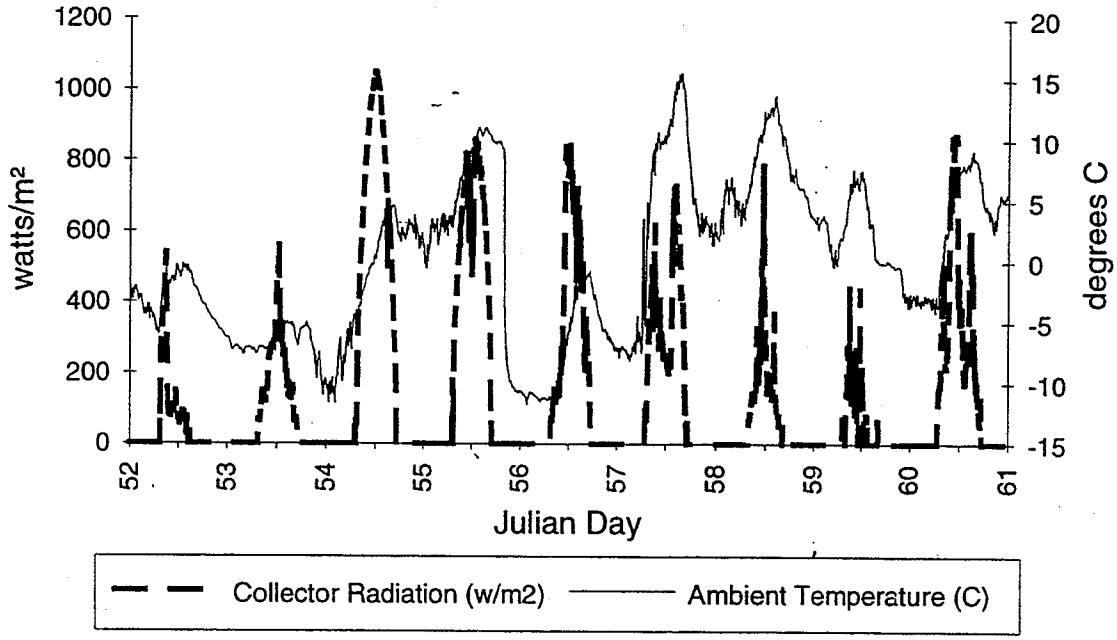

Figure 2.3.7 Ambient Temperature and Solar Radiation

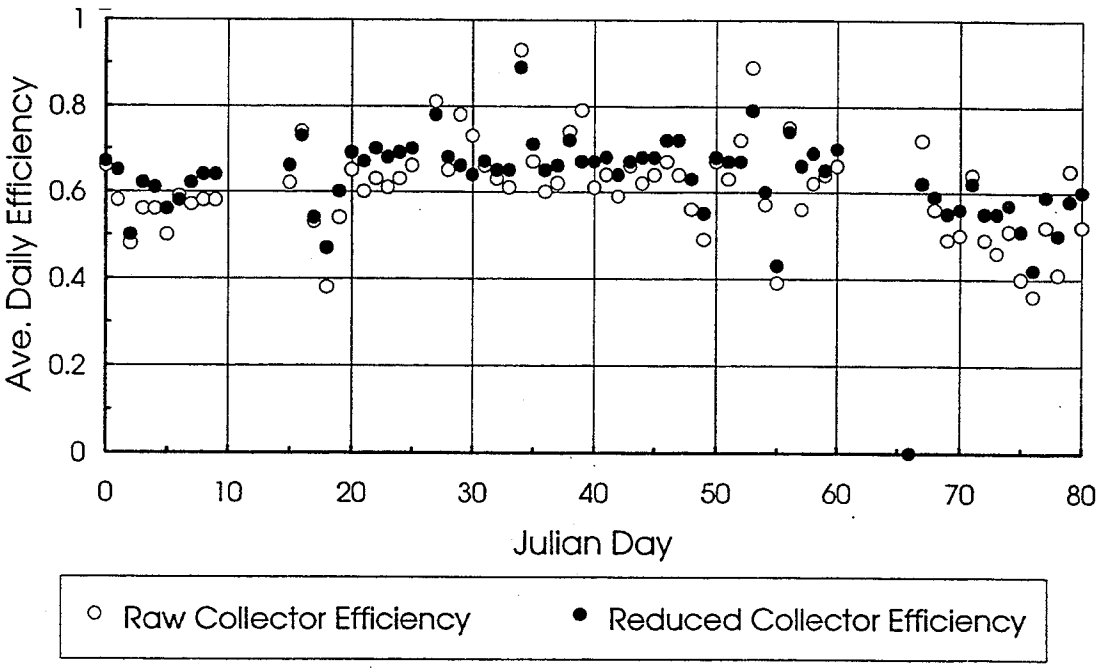

Figure 2.3.8 Daily Average Collector Efficiencies

Figure 2.3.9 is a plot of the collector efficiency versus wind speed for the first two months of 1994. Similar to Figure 2.3.5, Figure 2.3.9 shows a small degradation of performance with wind speed. Because of the thermal storage of concrete wall, it is difficult to accurately asses the effect of wind speed on collector efficiency. The time delay introduced by the thermal capacity of the wall means that efficiencies recorded under high winds may be higher than they actually are because energy is being dumped into the air stream

from the warm wall. As mentioned before the finite difference model used to account for the heat transfer into and out of the wall improves the accuracy of the measurements, but because it is based on the measured temperatures it too has time delays and can not completely compensate for the thermal storage of the wall.

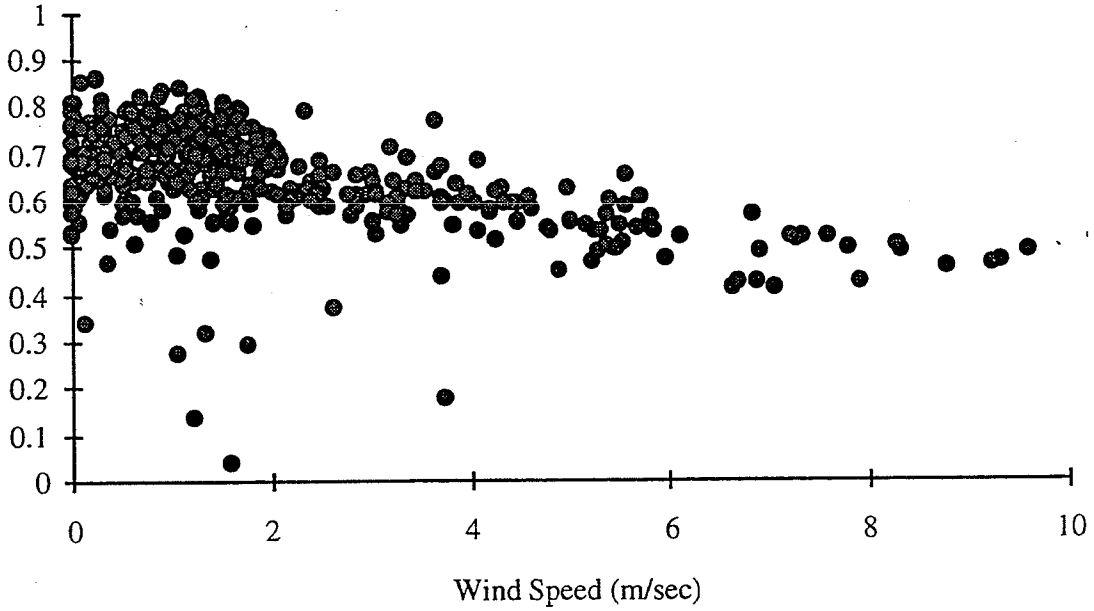

Figure 2.3.9 Collector Efficiency versus Wind Speed

Summary of the Monitoring Results

The average efficiency of the Waste Handling Facility from January 1st through March 22nd, 1994 was found to be 63%, which compares well with data collected prior to January 1994. One reason why it is lower than earlier measurements is that, in the later measurements, the ambient temperature was measured in front of the collector rather than behind the building. The new temperature measurement is warmer than the old measurement and therefore the measured efficiency of the collector is lower. The old temperature measurement was lower because the air behind the building did not experience any passive solar gains due to the solar-warmed ground and it was also exposed to colder sky and ground temperatures.

The improvements to the data acquisition system virtually eliminated the effect of infrared radiation on the temperature sensors, improved the measurement of the ambient temperature and mass flow rate, and improved the measurement of the energy collected by using a finite difference model to account for the heat transfer into and out of the concrete wall. As a result, the new figure of 63% for an average collector efficiency is now more accurate and can be considered a good value for the efficiency of the unglazed transpired collector on NREL's Waste Handling Facility under typical Golden, Colorado conditions.

Description of the Load

The building ventilation heating load is due to outdoor air entering the building to replace the volume of air that leaves the building through exhaust fans. The building envelope heating load is due to heat conduction through building components, e.g., walls, roof, etc.

With the solar ventilation preheat system, incoming ventilation air is drawn through the solar collectors and is delivered at a temperature that depends on the intensity of incident solar radiation and the ambient

temperature. If the air temperature is less than the indoor temperature, then the solar preheat system meets a percentage of the ventilation load. If the delivered air temperature is above the indoor temperature, then the solar system meets all of the ventilation load, and part or all of the building envelope heating load.

Description of Controls

Normal operation of this system requires no controls; outdoor air is drawn through the collector whenever the ventilation system operates. Summer bypass can be activated by manual seasonal switch-over or based on outdoor air temperature.

Key Meteorological Information

Typical Meteorological Year (TMY) data for Denver, Colorado, United States is listed below.

	Total Horizontal Radiation (kJ/m²/day)	**Average Outdoor Temperature (°C)**
Jan	9534.0	1.16
Feb	12790.0	0.44
Mar	17368.0	2.77
Apr	21328.0	8.61
May	24229.0	13.88
June	26678.0	18.88
July	25792.0	22.77
Aug	23198.0	22.00
Sept	19597.0	17.11
Oct	14759.0	11.11
Nov	10027.0	4.11
Dec	8305.0	0.33
Ann	17880.0	10.05

Estimated Costs

Total Project Costs (1989 U.S.$/m²)

Fan and ducts can be considered to be part of the ventilation system that is installed whether or not the solar collector is part of the ventilation system.

	Materials	Installation	Total
1) Glazed Front-pass	100	60	160
2) Unglazed Transpired	40	60	100

Estimated Installation Labour (person-hours)

Labour for design, engineering drawings, and field supervision is approximately 1 percent of total system costs for large systems. These costs are included in the installation labour costs listed below.

	$/m²	person-hours/m²
1) Glazed Front-pass	60	1.7
2) Unglazed Transpired	60	1.5

Estimated Annual Operating Costs

Fan power and fan maintenance can be considered to be part of the ventilation system operation that occurs whether or not the solar collector is part of the ventilation system. Maintenance costs for the collector and solar controls are assumed to be 1% of system costs per year.

Cost/Performance Ratio ($/GJ)

The economic analysis period is 20 years, and the interest rate is 8 percent. The general inflation rate and the fuel cost escalation rate are assumed to be zero.

	Annualized Costs ($/GJ)
1) Glazed Front-pass	16
2) Unglazed Transpired	6

Additional Information

Expected Technical Lifetime

Glazed collectors in some solar ventilation preheat systems have employed fibre-reinforced glazing (FRG) materials to achieve minimum system costs. These materials degrade when exposed to outdoor conditions, exhibiting reduced solar transmission and deteriorated appearance. Effective lifetime will probably not be more than 10 years.

Unglazed collectors for ventilation preheat systems employ dark-coloured metal siding materials. These types of materials can last 20 to 30 years or longer.

Fans and ducts can be considered part of the building ventilation system.

Economic Lifetime

1) Glazed Front-pass	20 years
2) Unglazed Transpired	20 years

Other

F', the collector efficiency factor, represents the ratio of the actual useful energy gain to the useful energy gain that would result if the collector absorbing surface had been at the local fluid temperature. In a unglazed transpired collector, the air drawn through the absorber comes, in theory, from the layer of air adjacent to the surface, and air temperature is equal to the surface temperature. For this situation F' would

be equal to 1.0, and this may hold true for absorbers with many small, closely-spaced openings. For real absorbers with more widely-spaced openings, portions of the absorber may be at elevated temperatures, so that the average absorber temperature is greater than the temperature of the transpired air, and F' is less than 1.0. Transverse flow due to wind or buoyancy is expected to reduce absorber temperature non-uniformities.

F", the collector flow factor, accounts for the temperature distribution in the direction of flow. For conventional collectors, the temperature distribution is exponential along the absorber from the inlet temperature to the outlet temperature. For unglazed transpired collectors, the entire absorber is at the outlet air temperature (if F' equals 1.0).

F_R is the product of F' and F". A low-emittance surface on the absorber would make heat losses less sensitive to elevated absorber temperatures, overall or due to absorber temperature non-uniformities. It remains to been seen if it would be cost-effective and practical to develop and use a weatherable selective surface.

2.4 Göttingen Utility Co-Generation Plant, Germany

General Project Information

The first perforated collector wall to be built in Europe was constructed in Göttingen, Germany (latitude: 51.55° ; longitude: 9.93°; altitude 155 m). The project partners are the Göttingen utility, the University of Stuttgart (ITW) and the Institute for Solar Energy Research (ISFH). A national research project has been set up in Germany in order to investigate the possibilities of solar assisted preheating of combustion air in an existing power station.

The solar collection system is a perforated unglazed aluminum-plate absorber. The preheated air is collected by the duct system and distributed to the three different boilers. The total peak power of these gas fired boilers is 40 MW. The solar preheating of the combustion air will save fossil fuel and will reduce the emission of air pollutants. Therefore, the system was installed in autumn 1992 when a retrofit of the facade was necessary anyway. The system performance was monitored during the fall of 1993 and from May until September 1994.

System Description

System operating modes The district heating power plant of Stadtwerke Göttingen consists of two high-pressure superheated-steam boilers with two subsequent turbines delivering a maximum electrical output power of 5 MW. Furthermore, two high-pressure steam boilers are installed in order to cover on-peak heat demand in winter and low loads in summer. The whole available heating capacity in the cogeneration plant amounts to approximately 65 MW.

In standard power plants, the combustion air is sucked in from the ambient and heated up in the combustion process itself. Solar preheating of this air reduces the primary energy demand. As the temperature of the incoming air is increased by only a few degrees, the solar collector system used to heat the air can show a high efficiency.

There are two different operating modes of the system, depending on the level of the solar radiation on the collector plane (see "Description of controls"). Either room air or solar preheated air can be used as combustion air. During the monitoring period, the room air junction was not used in order to measure the temperatures in the collector plenum during the night time for heat loss calculations.

Key system parameters The total collector area is 343 m^2; the net absorber area without the manifold is 305.6 m^2. The design suction air flow is 40 800 m^3/h, but the measured air flow during the non-heating period was much lower (about 7500 m^3/h). This was the consequence of some changes in the boiler system (exhaust gas recirculation) that were performed after the construction of the solar wall.

Collector description The air cooled solar collector is unglazed. The absorber is manufactured of aluminium sheets (thickness 0.7 mm) that have trapezoidal folds for mechanical stability reasons. In addition, the plates are perforated. The void fraction is 1% throughout. The suction flow through the holes of the absorber sheet ensures that nearly all heat that is normally lost by natural convection can be collected. An air gap of approximately 10 cm separates the absorber sheet from the back of the collector which is simply the exterior wall of the building. This exterior wall is constructed as a metal facade with 8 cm mineral wool for insulation.

The collector is separated into four equal panels (see Figure 2.4.1).

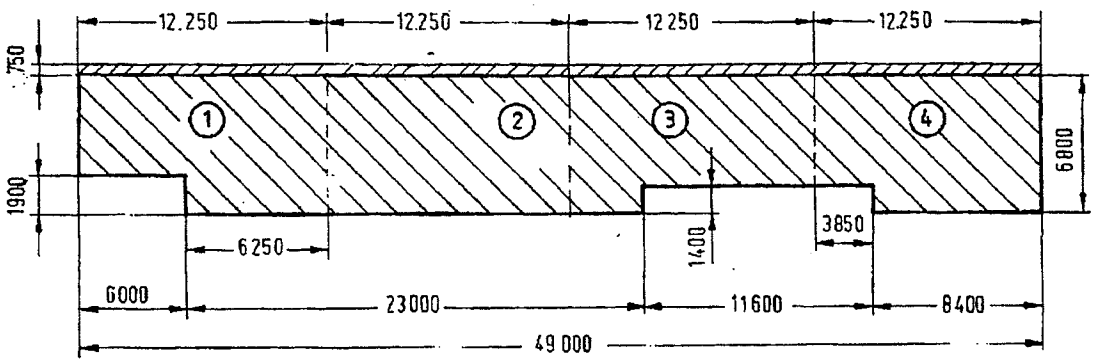

Figure 2.4.1 Vertical face of the perforated collector showing dimensions.

Each collector panel has a manifold at the top of the facade. A manually driven flap is mounted at each manifold to adjust the pressure drop in the collector. Thus an evenly distributed collector air flow is ensured. During the monitoring period the flaps where also used to cut off one or more panels.

Collector parameters

Table 2.4.1: Collector Parameters

Net collector area	305.6 m²
Panel 1	71.9 m²
Panel 2	83.3 m²
Panel 3	72.5 m²
Panel 4	77.9 m²
Thickness of the aluminum	0.7 mm
Colour	dark brown (Zieglebrown)
Void Fraction	1%
Plenum width	10 cm

System components

The combustion air preheating system in Göttingen consists of

- the wall-integrated air-cooled solar collector
- the air duct system
- the control system

The collector is located at a vertical wall in front of the boiler house. The wall is oriented to Southeast (compass direction 122 degrees).

The function of the duct system is to collect the preheated air and to distribute it to the three different boilers. Four ducts (cross section area 0.4 m²) are connected to the collector manifold (see Figures 2.4.2 and 2.4.3). In addition, room air is optionally sucked through a duct located under the roof of the boiler house. The air temperature under the roof is over 40 °C due to the thermal losses of the boilers and pipes. Thus, a further preheating of the combustion air is possible, utilizing low temperature heat which is normally vented off the building. The duct system is not insulated because in most cases the room air temperature within the plant building is even higher than the air in the duct. After this second preheating, the air flows down to the boilers. The air flow is forced by the original fans of the combustion chambers.

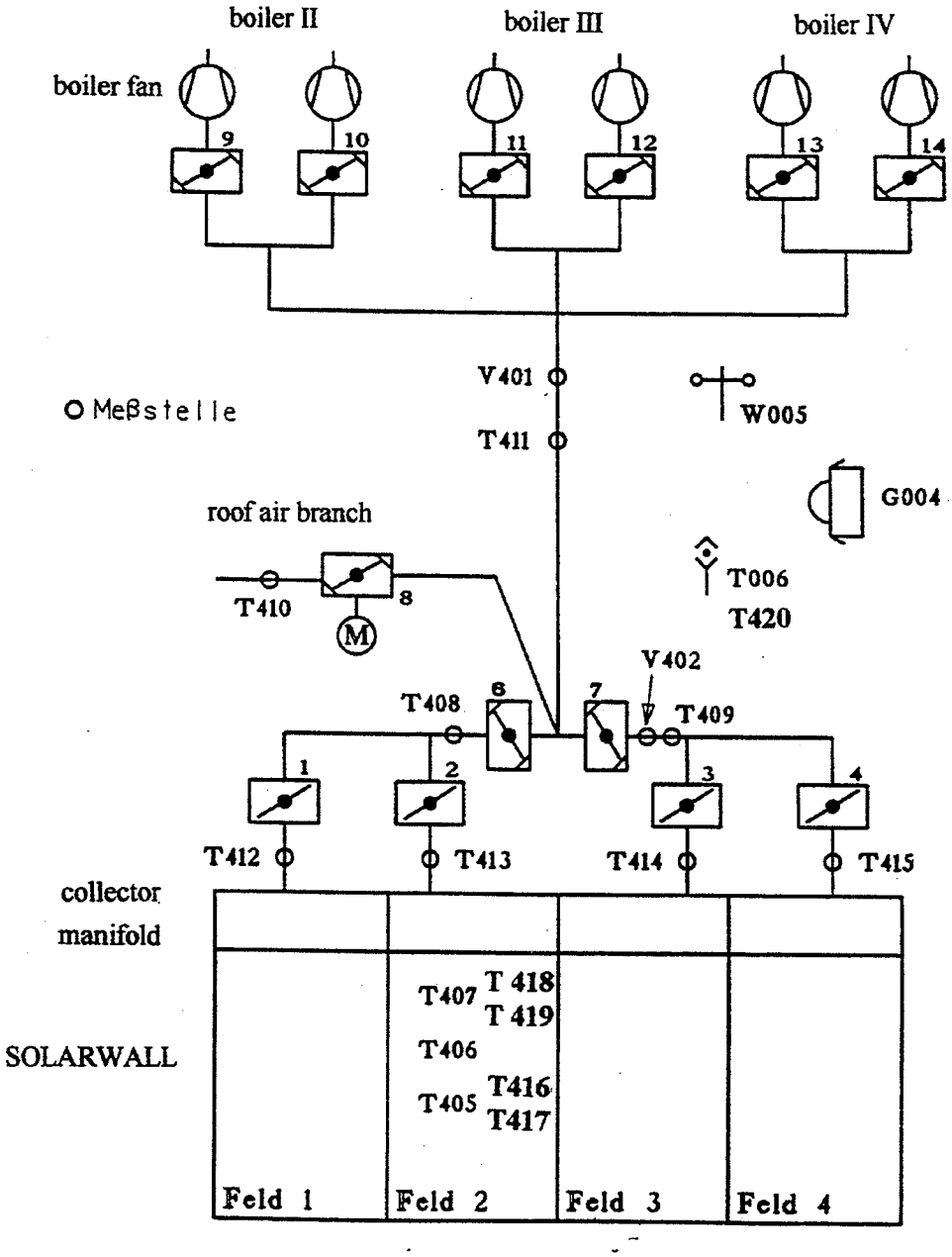

Figure 2.4.2 Schematic of the Duct System and Sensor Positions

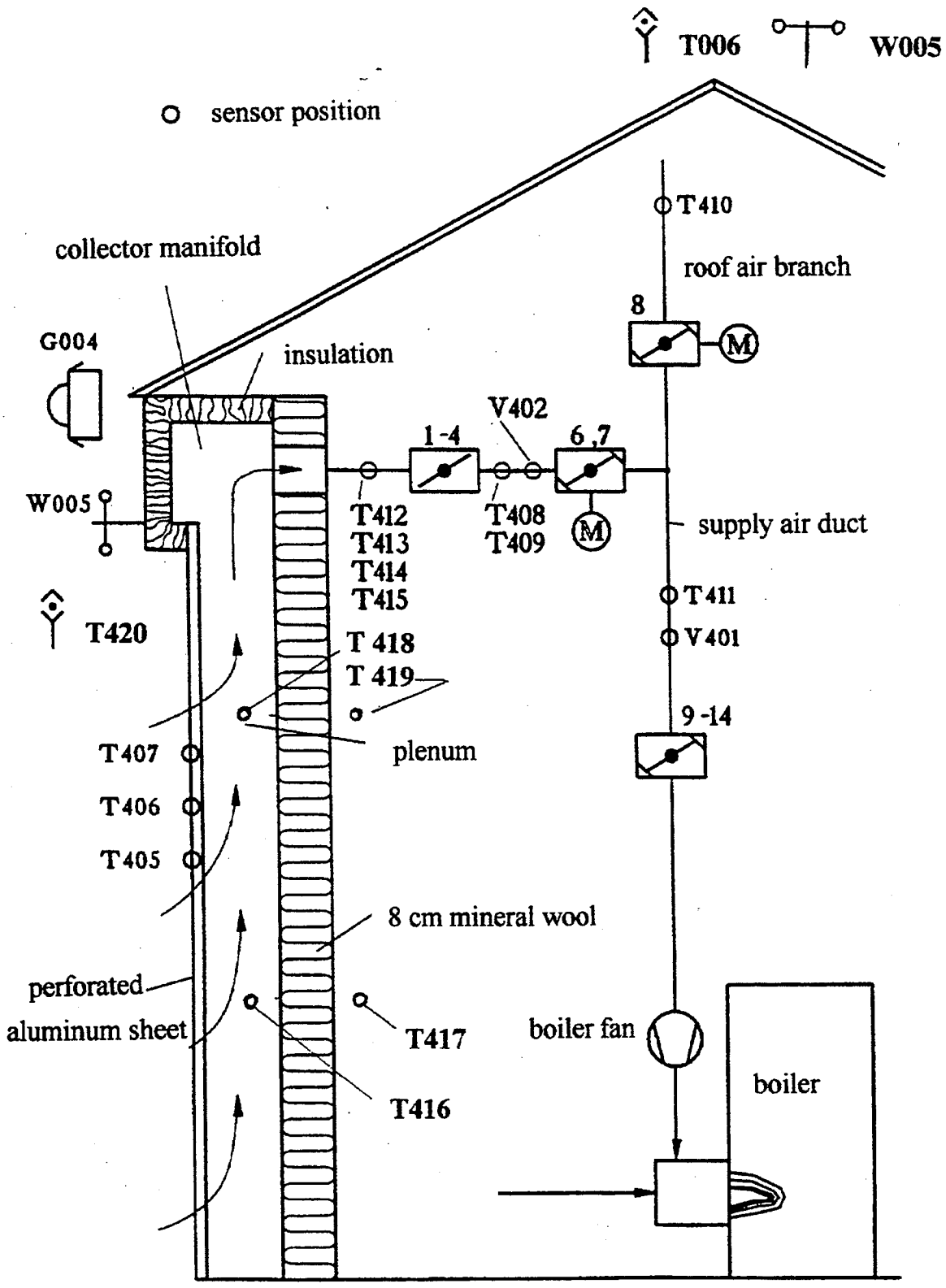

Figure 2.4.3 Vertical Section of the Plant Building

Description of Advanced Features One of the significant features of the system is the manifold at the top of the wall. This channel has a rectangular cross- section (see Figure 2.4.4) with a height of 75 cm. The purpose of the manifold is to gain a better flow uniformity (especially at the upper corners of the panels). As a matter of cost efficiency, the manifold was not designed as a constant velocity header. To minimize heat loss from the air in the header to the ambient air, the channel walls are insulated with mineral wool.

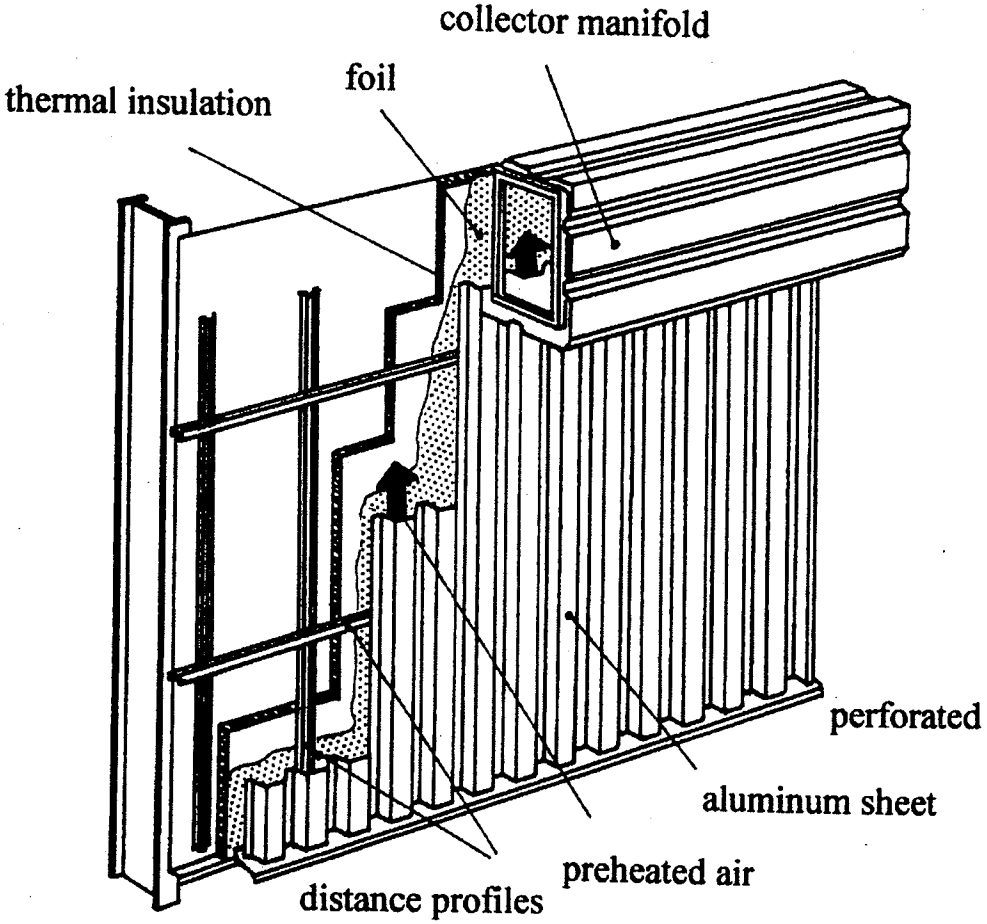

Figure 2.4.4 Construction Details of the Perforated Collector Wall

Justification of Advanced Features The total length of the perforated collector is 49 m. There are four outlets, hence the width of each panel is 12.25 m. This relatively wide horizontal dimension (the height being only 6.8 m) is the justification for constructing a manifold at the top of each panel.

Description of Back-up system/auxiliary The perforated collector works as a preheater of the combustion air. If there is no solar energy available, ambient air or room air (from the top of the plant building) is used. Hence, no auxiliary heater was necessary.

Description of load The load of the boilers depends mainly on the ambient temperatures. During the "non-heating period" only heat for hot water or industrial processes is necessary. Hence, from May till

October, the volume flow is less than half of the flow during the heating season. The monthly design combustion air flow is shown in Figure 2.4.5. As already mentioned, the measured flow was much smaller. The monthly mean values are shown in Table 2.4.2.

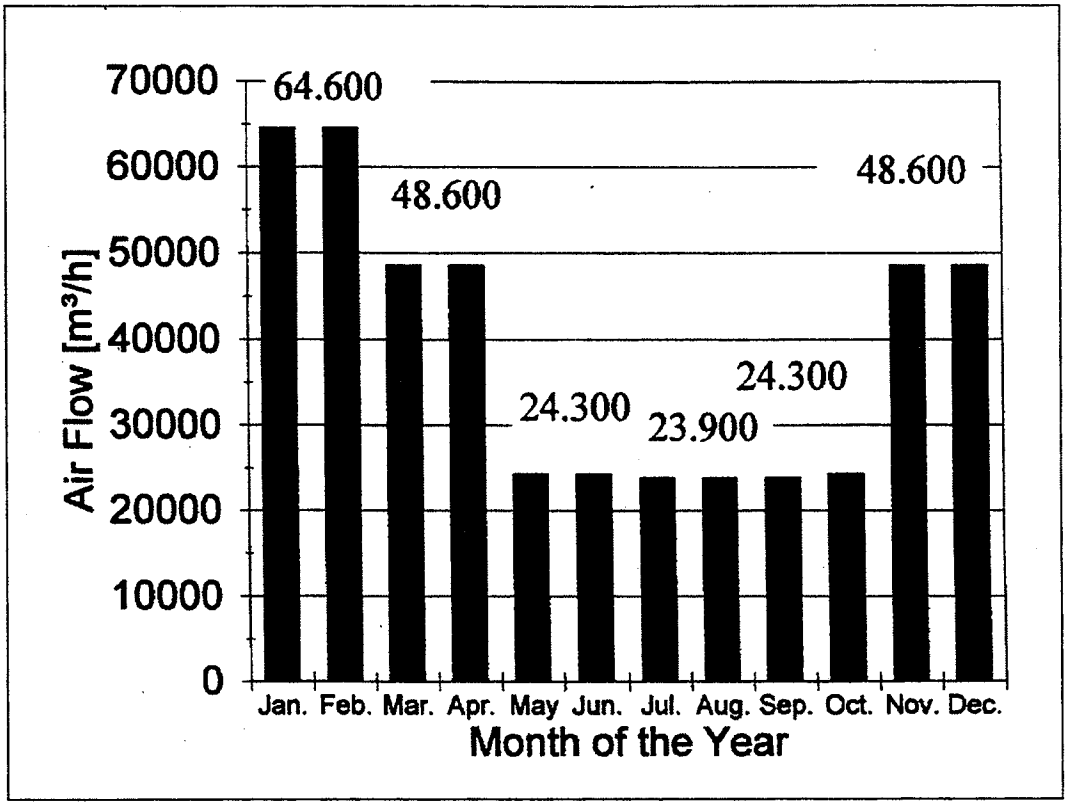

Figure 2.4.5 Monthly Design combustion Air Flow.

Table 2.4.2: Mean air flow

months of 1994	May	June	July	August	Sept.
mean air flow [m³/h]	2186	2148	1576	1966	2603

Description of controls Since not all three boilers are operated constantly, the amount of air must be adjusted according to the actual requirement. This is done by the blast regulation of the boilers. Furthermore, for combustion with low emission (esp. NOx), the inlet temperature must be monitored and adjusted. In addition, the concentration of oxygen is kept below 20% with the recirculation of exhaust gas. In regular operation, the control system opens the flaps of the solar collector array only if the solar radiation on the collector plane is more than 100 W/m². During daytime, the flaps to the collector field are fully opened, and the flap (No. 8 in Fig. 2.4.2) to the room air junction is closed. At night, the flaps are closed, and all the combustion air is taken from the room air junction.

Key Meteorological Information

Table 2.4.3 shows the monthly average horizontal radiation (MJ/m²) and ambient air temperature of the TRY (Test Reference Year) of the meteorological region relevant for the location of Göttingen.[1]

Table 2.4.3: Key Meteorological Information

Month of the TRY	Vert. Solar Rad. [MJ/m² per month]	Ambient Temp. [°C]	Wind Speed [m/s]
January	62.1	0.4	4.6
February	87.6	1.6	4.6
March	139.3	5.0	3.9
April	326.9	8.9	3.3
May	384.4	12.6	3.2
June	358.47	14.8	2.8
July	439.25	17.2	2.9
August	349.8	17.7	2.8
September	265.4	14.5	2.7
October	99.6	9.0	3.5
November	54.2	5.3	3.4
December	32.94	1.7	5.4
Ann. Average	**216.7**	**9.06**	**3.6**

Performance Data

A PC- based monitoring system has been set up to record the main operating conditions of the solar system, such as collector field outlet temperature and volume air flow. In addition, the weather conditions are monitored (ambient temperature, global solar radiation in the plane of the collector, wind speed). The sensor locations are shown in Figures 2.4.2 and 2.4.3; the sensor descriptions are listed in Table 2.4.4.

[1] Blümel, Klaus; Hollan, Eberhard; Jahn, Axel; Kähler, Malte; Peter, Rainer (1986) "Development of Test Reference Years (TRY) for Climatic Regions in the Federal Republic of Germany" BMFT-FB-T 86-051, July 1986

Table 2.4.4: Description of the sensors

Parameter Measured	Sensor Location	Units	Meter Type	Accuracy + -	Label
Temperatures:					
Delivered Air	Supply Duct in Front of Fan	deg C	PT100	0.2K	T411
Roof Top Air	Roof Air Branch	deg C	PT100	0.2K	T410
Collector outlet	In front of Flap No.1 to	deg C	PT100	0.2K	T412
	No.4 respectively				T413
					T414
					T415
Branch duct					
panel 1 and 2	After Flap No. 2	deg C	PT100	0.2K	T408
panel 3 and 4	After Flap No. 3	deg C	PT100	0.2K	T409
Absorber Plate	Three Locations at Centre	deg C	PT100	0.2K	T407
	of Panel 2 distributed vertically	deg C	PT100	0.2K	T406
		deg C	PT100	0.2K	T405
Free Air Ambient	At the Top of the Building roof	deg C	PT100	0.2K	T006
Southeast-side					
Ambient	2 Meters from Solarwall Panel 2	deg C	PT100	0.2K	T420
Plenum Air	Lower Part	deg C	PT100	0.2K	T416
	Upper Part	deg C	PT100	0.2K	T418
Building Air	Lower Part	deg C	PT100	0.2K	T417
	Upper Part	deg C	PT100	0.2K	T419
Delivered Air Flow	Supply Duct	m/s	METEO DIGIT	0.2m/s	V401
Vertical Solar	Parallel to Solarwall	W/m^2	CM 11	4%	G004
Wind Speed	Top of the Roof	m/s	Anem.	3%	W004

Monitoring Results for the Period in 1993 Continuously collected data of the air-cooled solar system are available since August 2, 1993. The first monitoring period was from the thirty-first till the fortieth week of 1993. Since the thirty-second week, the flap positions of the flaps Nos. 1, 3 and 4 were weekly changed according to the schedule of Table 2.4.5. In the last column, the total mean mass flow of the delivered air is printed.

Table 2.4.5: Schedule of the Flap Position of the Modules 1 to 4

Week of the year 1993	Flap No.1	Flap No.2	Flap No.3	Flap No.4	MassFlow kg/s
31	open	open	open	open	2.18
32	close	open	close	close	2.09
33	close	open	close	close	2.08
34	close	open	open	close	2.12
35	open	open	open	open	2.13
36	close	open	close	close	2.09
37	close	open	close	close	2.06
38	open	open	open	open	2.19
39	close	open	close	close	2.03
40	open	open	open	open	2.57

In this way, different suction face velocities occurred at panel 2 which was continuously in operation in spite of the more or less constant total air flow. The flaps Nos. 6 and 7 where kept continuously open, whereas flap No. 8 was closed. With this concept, it was possible to estimate the heat flux through the building wall (temperature rise during night time) and to subtract it during day-time. The solar output and the heat gain from building air are shown in Figure 2.4.6. The collector efficiency and the corresponding suction face velocity are plotted in Figure 2.4.7.

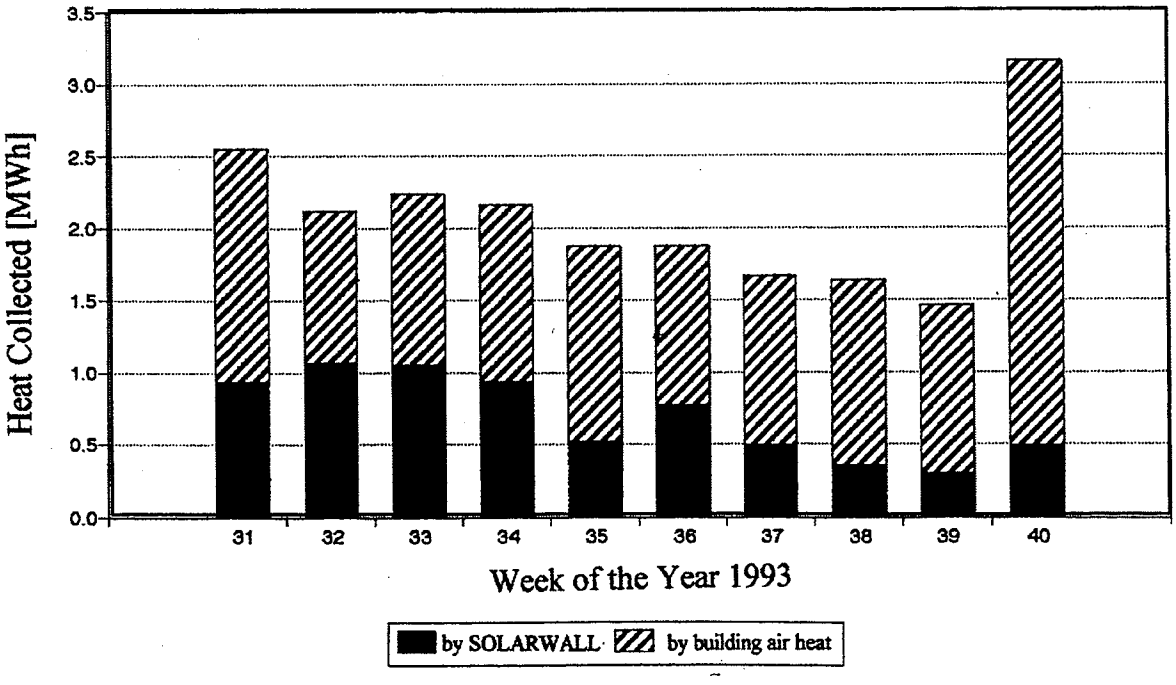

Figure 2.4.6 Solar Output and Heat Gain form Building Air

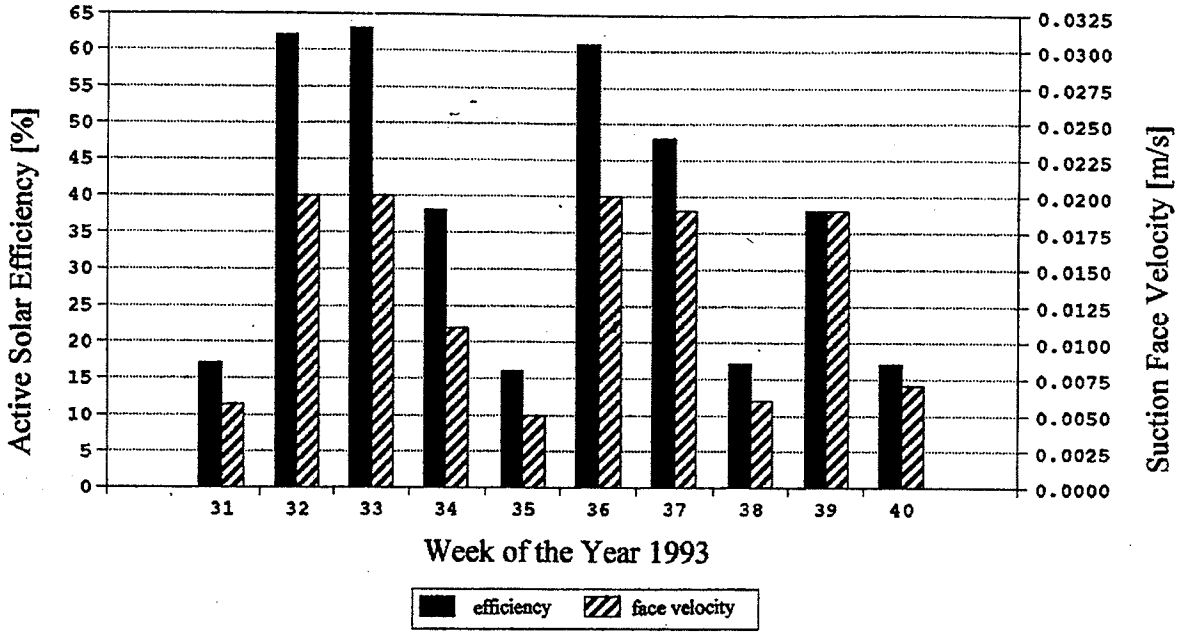

Figure 2.4.7 Collector efficiency and Suction Face Velocity

Monitoring Results of the Period from May until September '94 The amount of heat delivered from building air appeared not to be negligible. Hence, it was decided to mount some additional temperature sensors in order to investigate the heat transfer through the building wall more in detail. The sensors T416, T417, T418 and T419 were installed in May '94. At the same time, the ambient air temperature sensor T420 was mounted in front of the perforated collector. Because of the different micro-climate in front of the building, this sensor showed slightly higher temperatures (up to 2 K) compared to the air temperature measured at the top of the roof (T006). The accuracy of this sensor is very important, because the reading of this sensor is used for calculation of the temperature rise of the delivered air.

The data evaluated are from the period from May 16th until September 22nd, 1994. Within this period, five minute data were continuously stored and evaluated. In total, a lack of less than three days had to be interpolated. At the end of September, a serious break down of the data acquisition system occurred; hence data from 8 days of September are lost. Weekly-averaged monitoring results are presented hereunder.

Table 2.4.6: Vertical solar radiation

months of 1994	May	June	July	August	Sept.
Vert. Solar. Rad. [MJ/m²]	450	424	526	447	297

The ratio of the energy consumption of the district heating plant to the demand of process heat and hot water of the district is reduced drastically during the non-heating period. Because of important changes in the operating strategy of the plant, the actual air flow was much lower than the design combustion air flow as already mentioned. Considering the low combustion airflow rate, it was decided to use only one collector field (flaps No. 1, 3 and 4 closed) during the monitoring period in 1994.

Due to the low suction ratio of about 30 m³/h per m² collector area, high surface temperatures occurred (up to 55 °C peak values). Figure 2.4.8 shows a plot of the weekly mean temperatures.

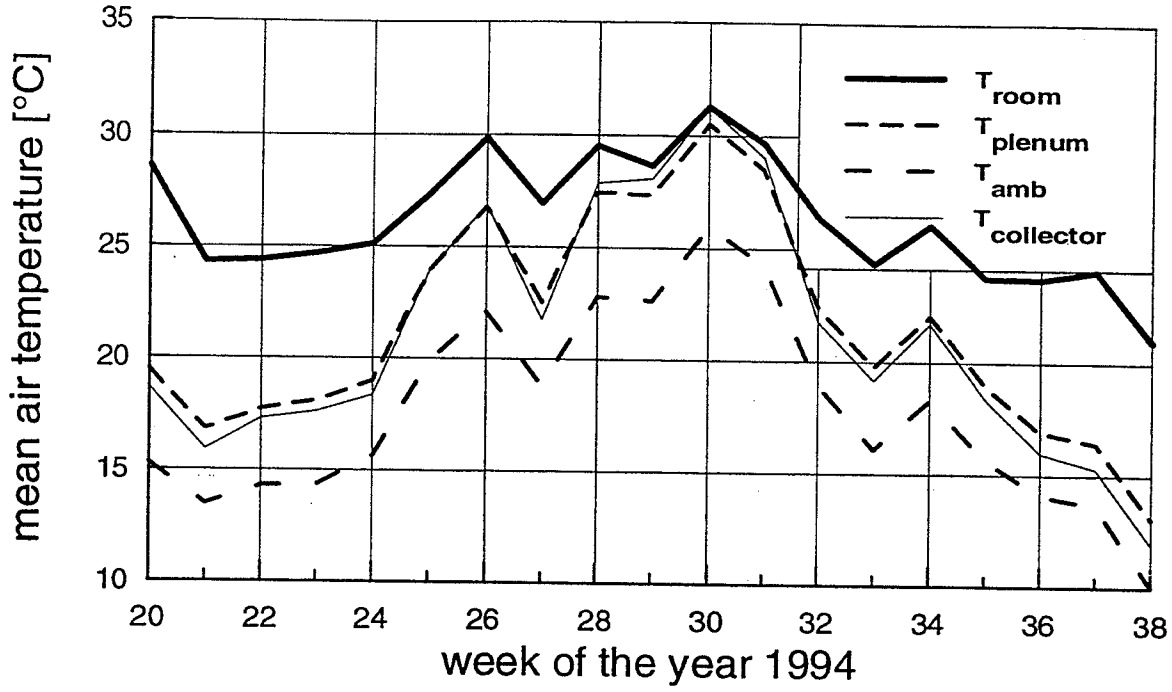

Figure 2.4.8 Weekly Mean Air Temperature and Collector Surface Temperature

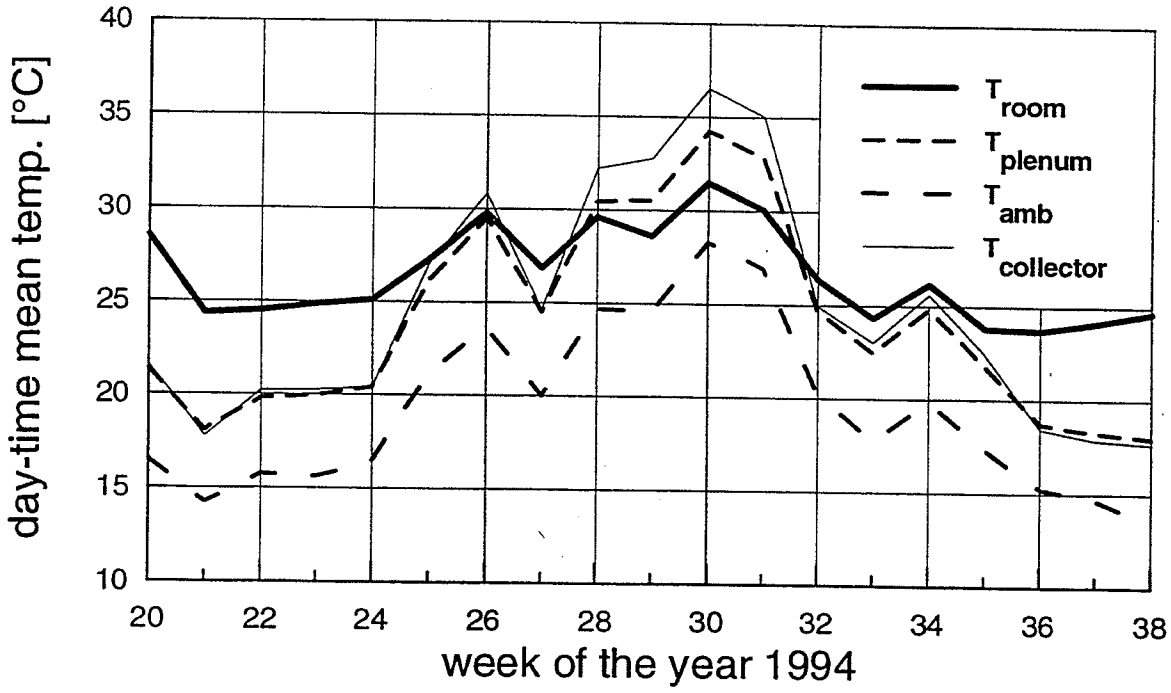

Figure 2.4.9 Weekly Day-Time Mean Temperatures

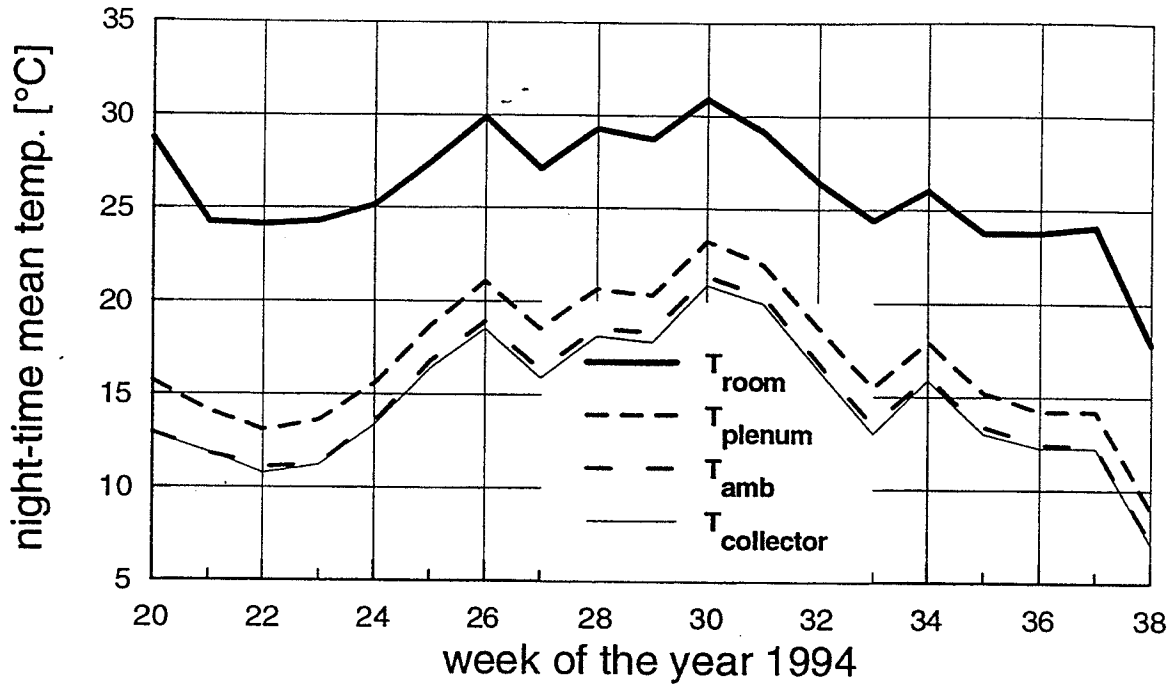

Figure 2.4.10 Weekly Night-Time Temperatures

Figures 2.4.9 and 2.4.10 illustrate the different situations during day-time and night-time. Due to radiation, the mean night-time collector surface temperature $T_{collector}$ is about 2 K lower than the ambient temperature T_{amb} (see Figure 2.4.10). The room air temperature of the plant building exceeds the 25 °C level during summer time. Hence the heat flux passing the building wall cannot be neglected. The U-value of the insulation system with thermal bridges included was calculated by finite difference calculations (U=0.70 W/m^2K).

Two heat balances (day-time and night-time) where used in order to calculate the net heat delivered by the perforated collector. The total heat was split into the portions contributed by

- the heat flux through the wall (Q_{wall}),
- the heat transported into the plenum by air leaking from the room (Q_{leak}),
- the solar gains (Q_{solar}), and
- the heat recovery / losses through the duct system (Q_{duct}).

The weekly total heat savings are plotted in Figure 2.4.11, whereas in the Figures 2.4.12 and 2.4.13 the weekly heat losses and savings are specified.

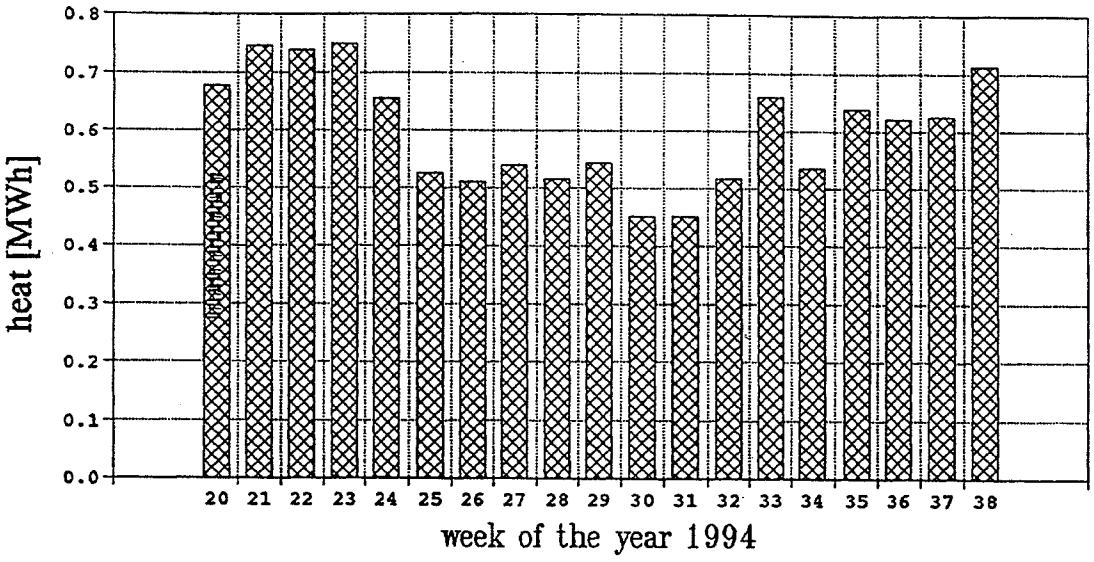

Figure 2.4.11 Weekly Total Savings

The weekly collected solar heat is as high as 0.5 MWh. In July and August (day time hours), the solar preheated air is significantly hotter than the room air. Hence certain heat losses through the wall and the duct system occur (Q_{wall} and Q_{duct} negative). During night-time however, the situation changes; there is no solar gain, but there exists some heat recapture through the wall and the duct system and a contribution by a leakage air flow from the room into the plenum. (Q_{wall}, Q_{duct} and Q_{leak} are positive. See Figure 2.4.12).

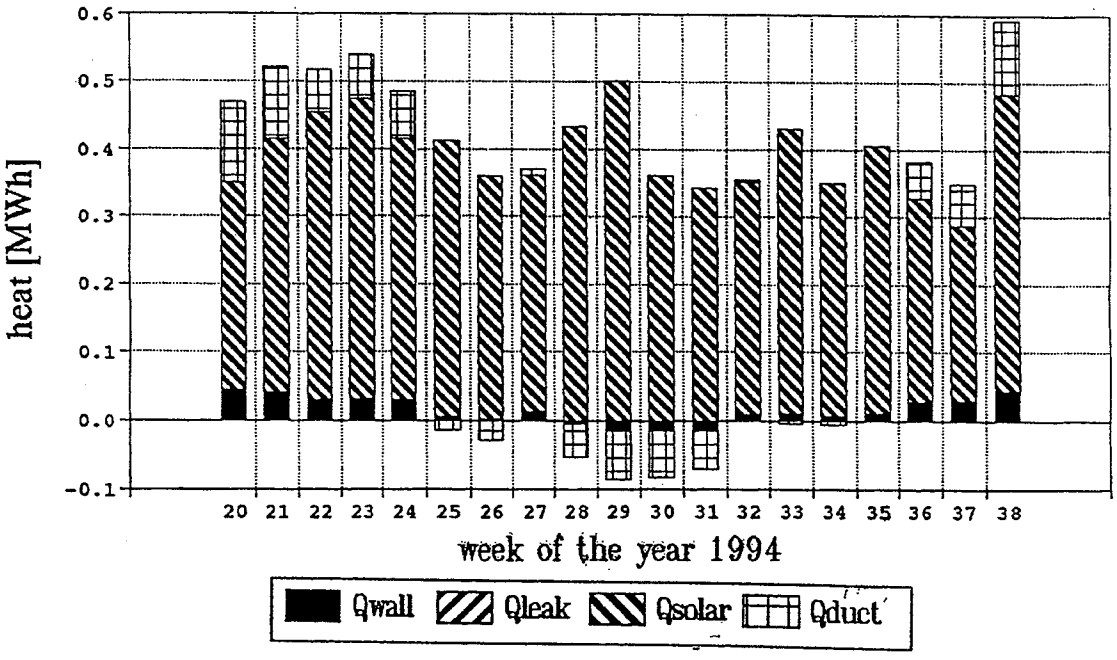

Figure 2.4.12 Weekly Heat Balance for the Day-Time Hours

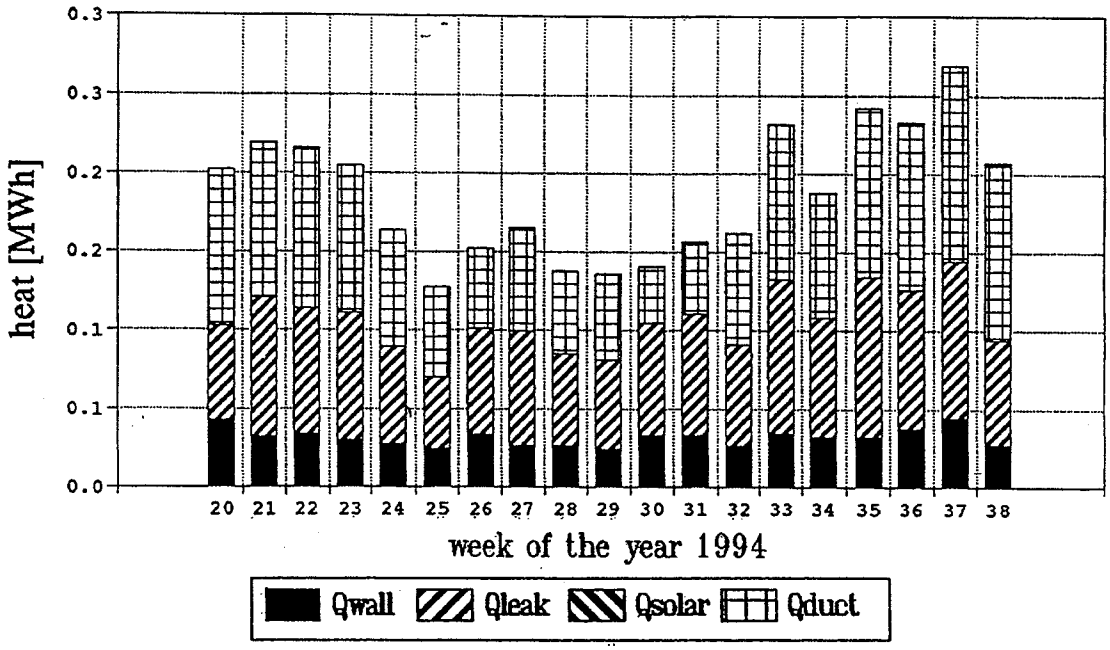

Figure 2.4.13 Weekly Heat Balance for the Night-Time Hours

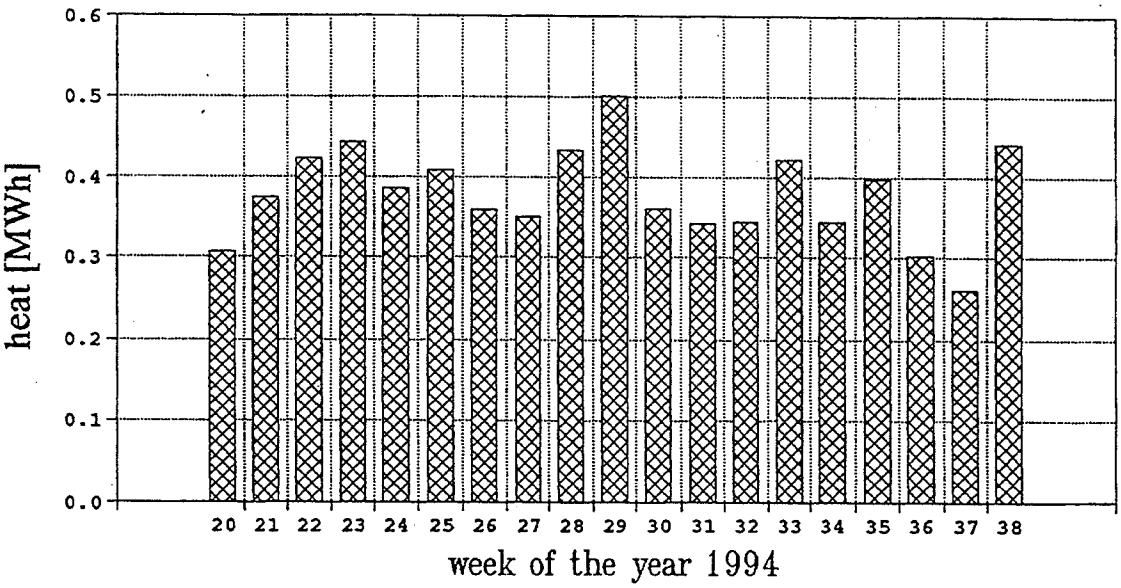

Figure 2.4.14 Solar Heat Collected

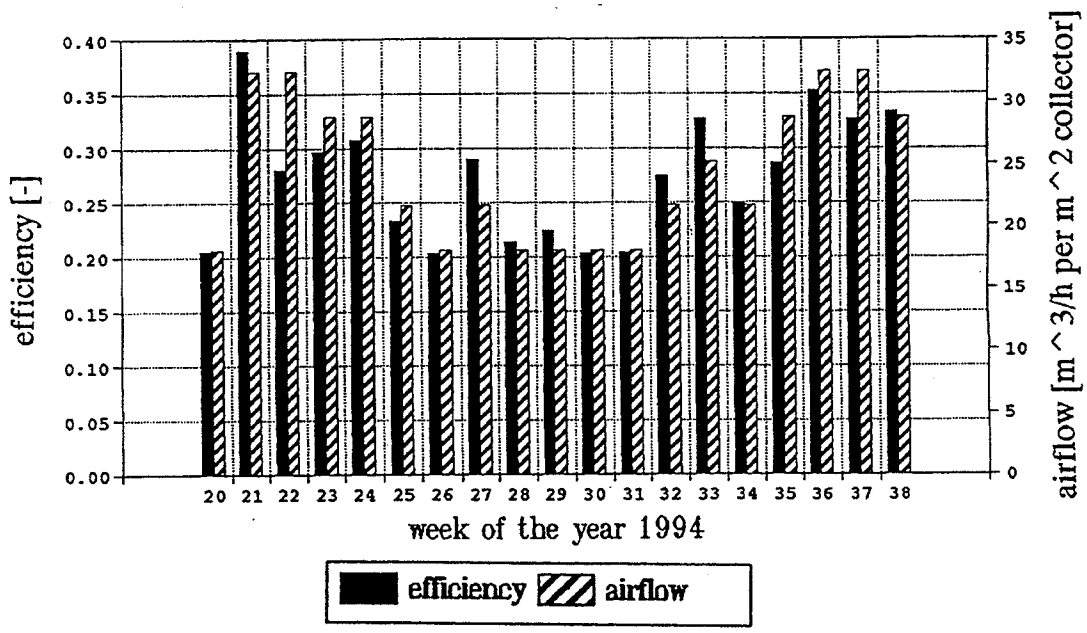

Figure 2.4.15 Weekly Mean Efficiency and Mean Air Flow Rate

Due to the low air flow rate (< 35 m^3/h per m^2 collector) the efficiency of the perforated collector does not exceed 40% during the 1994 monitoring period. Figure 2.4.15 shows the weekly mean efficiency of the perforated collector.

Usually the efficiency characteristic is plotted as efficiency versus suction face velocity w [m^2/s] (i.e. flow rate in (m^3/h per m^2 collector). The second order regression line is calculated by

$$\text{efficiency} = 50.954\ w - 1483.9\ w^2$$

The measured data points (solid squares) and the regression line (dotted line) are shown in the Figure 2.4.16.

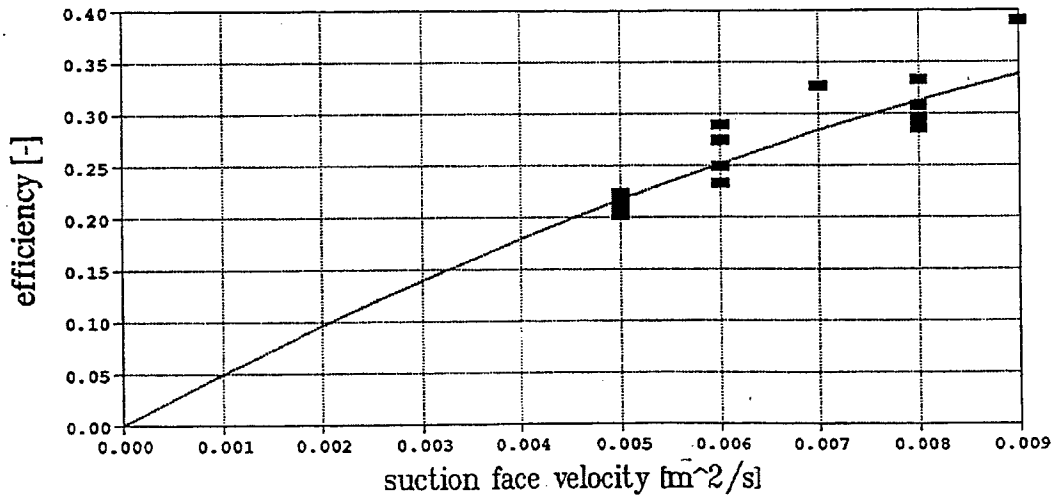

Figure 2.4.16 Perforated Collector Efficiency Characteristic

Estimated Costs

The project costs are given in Table 2.4.6 in 1993 US dollars (balance currency 30.12.93: 1 US$ = 1.7269 DM). The perforated collector was not only built to reduce energy consumption, but also as necessary retrofit of the building facade. Hence, for the calculation of the cost/performance ratio only the additional cost for the solar system was considered.

Table 2.4.6: Estimated Costs

Additional Costs of the perforated collector (compared to a conventional facade)	US$ 33 572
Air Duct and Control System	US$ 23 130
Net Investment Costs total (VAT 14% inc.)	US$ 64 641
Annual Operating Costs	US$ 1517
Total Economic Life Time	20 Years
Annuity	10.2%
Annual Maintenance Costs	US$ 289.13
Performance GJ/m²yr	0.9
Cost / Performance Ratio $/(GJ/m²yr)	209
Energy costs $/(GJ)	30.52

Expected technical lifetime As there are no moving parts (besides the flaps) and because corrosion-resistant materials (aluminum) were used, the expected technical lifetime will be more than 40 years with a minimum need of maintenance.

Economic lifetime Calculations of the cost/performance ratio are based on an economic lifetime of 20 years.

Other information As the pressure drop of the system is low, no additional fans besides the boiler fans were necessary to run the system. However, the additional electrical energy demand for the solar collection system, was considered for the economic calculations.

2.5 Ispra Ecocentre Project for Building Retrofit, Italy

Ispra Site and the Ecocentre

The Joint Research Centre of Ispra - Italy, and its infrastructures were originally laid out for a technologically-oriented nuclear research centre. It was established by the Italian Government in 1956 and transferred to the Euratom Commission in 1962. Most of the buildings were built in the period 1959-1968 and host a total of 1800 people.

Of all JRC sites, Ispra has undergone the profoundest change in its orientation, towards "soft" environmental research, which calls for significant modification in the site infrastructures. For this reason the conversion of the Ispra site into an environmental-optimized model site (ISPRA ECOCENTRE) was proposed. The intervention will involve

- large air solar collectors,
- combined heating and cooling system,
- reduction in energy consumption (less than 100 kWh/m² y in office building),
- biodegradable building materials,
- flexible and compact building structures,
- avoidance of destruction of natural habitats,
- use of electric cars,
- separation and recycling of waste.

The main aim of the environmental assessment of the Ispra site and of its buildings is to make a reduction in energy consumption using the most advanced and innovative techniques available. So the use of renewable energies, like an active solar system, becomes very important. The project will become a showcase where visitors can appraise the effectiveness of the technologies employed. To complete the ECOCENTRE project, 36 MiECU for funding were foreseen from 1993 to 1996. The first term of the project concerned the retrofitting of 4 existing buildings according to the following aims.

- Low energy consumption
- Cost-effectiveness
- Environmental friendliness
- Technological originality
- Aesthetic appeal

General Project Information

Further to a call for tenders published in the Official Journal of the E.U., a "restricted invitation to tender" was issued by the European Union Joint Research Center / Ispra for the renovation of buildings of the Ispra Establishment (ECOCENTRE PROJECT for BUILDING RETROFIT). CO.GE.IN. S.p.A. (Savigliano-CN) together with METEC srl (Torino) and CENERGIA a.p.s. (Ballerup-Copenhagen) were awarded the contract for Building no. 45 (EPBR-B45). The final design was presented in the middle of June 1994. The construction started on July 1994. The tender called for proposals which (in line with one of the ECOCENTRE Project's main goals) would allow for a substantial reduction in energy consumption, using advanced and innovative but economically justifiable techniques, so that their effectiveness could be appraised and their use accepted by the building industry.

The criteria followed by the design team in assembling the bid proposal, and in developing it through the design phase, met the aims and basic concepts of the tender and the best pay-back time. The project consists of the following main elements.

Architectural changes: To build an air solar collector (Canadian Solarwall™) covering 60% of south facade, install water solar collectors partly covering the existing top row of windows on the south facade, add new roofing, dismantle the existing steel-frame windows and replace with aluminium-frame windows with new facade design, install shading blinds to windows on south facade.

Fabric changes: To upgrade roof and wall insulation, upgrade single glazing to low-E double glazing.

Technical system changes: To install solar collectors (air and water solar collectors), install a buffer storage tank connected to the District Heating Network and a solar storage tank connected to building water solar collector circuit, have a new air distribution system, install an "Energy Management System" compatible to Ispra main system for control and monitoring, have a new lighting system with lighting control.

Civil Works

Civil works are mainly associated with the intervention needed for the reduction of energy consumption. For this reason a reduction of the U-value for walls and windows was foreseen. The proposed solution compared with the existing situation will allow a strong reduction in U-values. The south wall covered by the air solar collector is not insulated. Its U-value still remains the same as the U-value of the existing building.

Table 2.5.1: U-Values for Building 45 Hall - Ispra Ecocentre Project (values in W/(m²K)

Description	Existing	Proposed
External E-W Walls	1.10	0.30
External N-S Walls	1.28	0.32
Concrete Beams	2.29	0.35
Concrete Walls	2.90	0.35
Roof Hall	0.52	0.21
Roof Annexed Bldg	1.59	0.29
Main Doors	2.99	0.80
Windows	5.92	1.90

The Existing System.

First, a brief description of the existing system is presented. Heating and cooling stations of the Ispra site are centralized with a distribution pipe network. At present the fluids used are super-heated water at 120 °C for heating and both industrial (lake) water at 10 °C and chilled water at 6-7 °C for cooling.

The technological hall of building 45 at the moment is heated and cooled by two air handling units and the operation mode is CAV (Constant Air Volume). The machines are placed on platforms on the East and West sides of the building. There is no heat recovery from the exhaust air.

The two machines are connected to a large main duct for air supply. The air supplies installed in the duct are not high-throw industrial diffusers, but normal air supplies. They are placed at the 14.0 m level and for this reason the vertical throw is not sufficient to avoid a temperature stratification in the building.

The New System.

The existing air handling units are modified by introducing an air solar collector connected to the west air handling unit and a heat recovery system to the east one. Two storage tanks are introduced as a heat storage for the water solar collectors and as a buffer for the district heating system to allow pulse operation.

The two air handling units will be retrofitted to allow several operation possibilities, and to introduce a variable air volume system. New works will be done to connect the existing air handling unit to the solar wall system and to the buffer tanks, and to install new diffusers.

Tropical fans, arranged in two evenly spaced rows, will be installed at the high ceiling level. These anti-stratification fans operate in the winter season when a big temperature difference between 1.5 m and the ceiling level is measured.

Design conditions. The inside and outside design conditions were assumed as follows.

Outside design conditions:	
Winter Temperature	-6 °C
Summer Enthalpy	67.8 kJ/kg referring to a Temperature of 33.2 °C and RH 40%, or a Temperature of 27°C and RH 75%
Inside design conditions:	
Winter Temperature	20 °C
Summer Temperature	26 °C
Summer R.H.	60%

The maximum supply air temperature to the hall is set to 35 °C. The maximum air flow through each air handling unit is set to 20 000 m²/hour. The minimum fresh air intake is set to 4000 m²/hour.

Collector description. The main outside impact, from an aesthetic point of view, is the presence of a large dark air solar collector installed in front of 9 bays on the south facade. The collector is an innovative system for active solar heating of ventilation air, offering high solar-collection efficiency and providing energy saving benefits.

A perforated unglazed plate was proposed and designed. The system was developed by Conserval/Solarwall (Canada) and it is composed of two principle parts, the solar collector and the canopy.

The solar collector is made of 0.7 mm thick prepainted perforated aluminium sheet fixed through the support structure to the existing concrete column and south brick wall of the technological hall. There are round holes that allow the air to be drawn into the cavity included between the metallic surface and the walls of the hall. Air is preheated as it passes into this cavity, providing energy savings during the heating season on sunny days.

The canopy acts as both a manifold for the air flow and a solar heat collection device. As a manifold, the canopy carries air flow horizontally to the fan opening on the west side of the building. The system has a total surface of about 370 m² of vertical perforated plate and about 180 m² of semicircular canopy.

The solar collector is a perforated aluminium plate, rollformed to Alcan profile 45/200 with about 1.5 mm diameter holes covering about 0.7% of the surface area. The absorber plate is installed vertically on south face of building walls with a variable air cavity (from 20 cm to 50 cm). The semicircular cross-section canopy is placed in a horizontal position at the top of the perforated absorber. The plate used for the canopy is the same as the perforated collector one, but it is not perforated. The cross-sectional diameter of the canopy is 2 m.

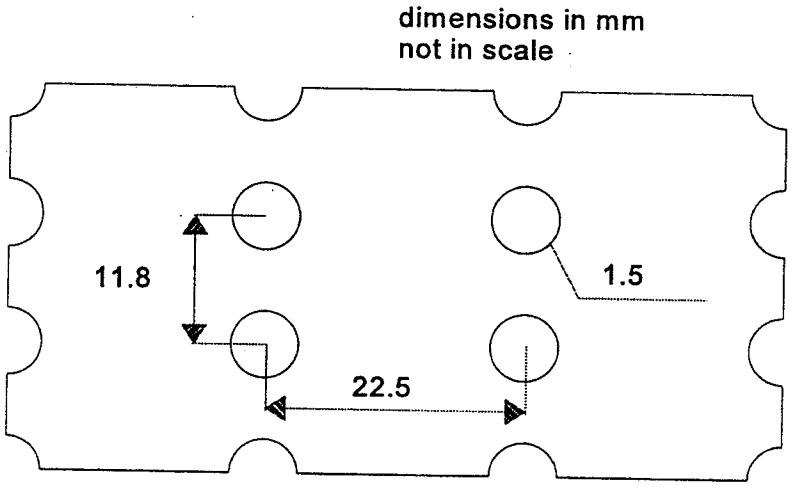

Figure 2.5.1 Distance Between Holes

A maximum air flow of 20 000 m²/h will be taken from the perforated collector by the west side fan and carried from the canopy to the inside distribution air duct.

Although the main benefits are available during a sunny day with outside temperature not very low, the use of the solar wall in the winter season is useful. In this case the inlet air temperature from the perforated collector could not be sufficient for the space heating. The heating coils could provide an additional heat to preheated air.

Air handling unit retrofitting. Both the two existing air handling units will be dismantled and retrofitted. The works include the installation of new vertical filters (complete with instrumentation for indication of filter pressure drop), the installation of new outside air dampers with electric motors controlled by the Energy Management System and an opening cut into the bottom and lateral panel to accommodate the connection duct to the canopy, the minimum fresh air duct and the return air damper. Existing fans and motors will be changed. A new high efficiency fan type CBI model VKA560 is proposed. At 20 000 m²/h the efficiency is greater than 80%. One of the aim of the design is the reduction of electricity consumption, for this reason a variable speed AC drive type Danfoss VLT series 2000 or equivalent is foreseen.

Rotary heat recovery & exhausted air fan description. A rotating heat exchanger, recovering heat from exhausted air, will be installed on the east wall of the building near the existing suspended platform. A FACO exchanger model RCR 1250 is foreseen. The air flow is 4000 m²/h, and the efficiency 78%. A Woods model UNO U450/4M fan will provide the expulsion of exhausted air.

Diffuser descriptions. One of the most important problems of the Building 45 hall is winter stratification of air temperature inside the building. The existing air supplies will be covered by metallic panels

and new diffusers will be installed. The diffusers will be placed under the existing air distribution duct at 14.5 m. It is proposed that 8 model Shako IKA 600 diffusers be installed. Each diffuser consists of an air entrance piece, an inner and outer outlet-basket. The outlet has openings at the circumference and at the front face. In the heating case, the openings on the front face will be totally open, and those on the circumference will be totally closed. In this position, the supply air jet enters vertically into the room. Through the great number of individual air jets, a high induction and great penetration depth will be reached. The openings at the circumference and at the front face were sized in a way that a change of the position of the openings has no influence on pressure loss and noise level.

The Energy Management System analyzes the readings from two temperature sensors: one placed inside the building, and the other in the distribution duct. The EMS chooses the most efficient throw for air supply inside the building (i.e. vertical, horizontal, or intermediate). In the winter time, with a maximum air supply temperature of 35°C, the air throw is totally vertical to allow an efficient heating of the air space near floor level. In the summer season, the air supply temperature is lower than the inside air temperature. In this case the throw is horizontal, and the maximum air velocity at 1.8 m is fixed to be 0.27 m/s in accordance with DIN regulations n. 1946 part II. Obviously, several different operation modes are available between these two extreme conditions.

Three diffusers will be provided with on/off air dampers. These dampers will be closed when, during the winter season, the total air flow in the duct is lower than 20 000 m²/h. In this case only 5 diffusers are required for heating of the hall, and the vertical throw is sufficient to reduce air stratification. If the total air flow is greater than 20 000 m²/h, the three diffuser dampers are totally open, because both air handling units are working, and 8 diffusers will supply warm air for the space heating.

Tropical fan description. Six tropical fans will be installed to provide a destratification effect in winter time. They will be arranged in two rows evenly spaced and installed at the high ceiling level. The anti-stratification fans operate in the winter season, when a set temperature difference between the 1.5 m and 15 m levels is measured. Six type Nordik 160/60" fans allow an air flow of 15 800 m²/h with an installed power of 70 W each. The benefit to the reduction of air temperature stratification is high, especially when compared with their low electricity consumption.

Buffer and solar storage. Two metallic tanks will be installed outside the building. Both of them are vertically-mounted galvanized metal sheet tanks certified for a maximum pressure of 8 bar. The volume of each tank is 7.5 m². The first tank is a buffer storage connected to the main district heating. The second one is a solar storage used for the accumulation of heat gains from the solar collectors.

The buffer storage tank will operate in accordance with a pulse operation strategy. The hot water will arrive from the district heating to the top of the storage and a return pipe to district heating will be provided at the bottom. Through the Energy Management System the buffer tank will call for heating only when it is needed. In three months (April, May and October) with operation of the district heating network, it will be possible to control the filling according to a pulse operation strategy. At the beginning of the day the district heating will fill the 7.5 m² buffer storage with hot water and the heat will be used for day heating.

A solar storage is connected to a secondary collector circuit. Water is heated in a heat exchanger by warm water running in the primary collector circuit. Both storages will provide water for the heating coils of the air handling unit and for fan coils in the annexed building 45G (north side). A 3-way valve will control the supply temperature, with priority of solar storage. On a sunny day, a total energy of 400 kWh can be obtained by the solar collectors. In this case the solar storage will be able to supply warm water for the total heating of the building. If heat from the solar storage exceeds the heat demand from the building, it will be transferred to the buffer storage.

Water solar collector description. The water solar collectors will provide heating for the building during sunny winter days or in the spring and fall seasons. A total surface of almost 80 m² is covered by the solar collectors on the south wall (5 bays) in front of the existing top windows. On the south wall, 40 galvanized steel-frame mounted solar collectors will be installed. The collectors are composed principally of an external glass about 4 mm thick and an aluminium absorber plate painted with special black colour. The thermal insulation is 6.5 cm thick mineral wool.

EMS - System operating modes. The system comprises a control sub-station (SAUTER) installed in the hall, and engineered for control of the total energy system. The sub-station will be connected to the JRC main control station which, through a PC installed with a graphic system, displays the operating conditions by changing colours, shapes and flashing symbols, and displays analog measured values which can be shown as graphs.

Control of the solar heating system. In what follows, the sensor and component identification numbers refer to the labels on the drawings at the end of this section. Pump number P4 starts when the temperature difference ST15 - ST18 is higher than the set point of the start differential for pump P4. Pump P3 starts when the temperature difference ST16 - ST17 is higher than the set point of the start differential for pump P3. Pump P4 stops when the temperature difference ST15 - ST18 is lower than the set point of the stop differential for pump P4. Pump P3 stops when the temperature difference ST16 - ST17 is lower than the set point of the stop differential for pump P3.

Set points:

P4 : Start differential = 5 °C Stop differential = -2 °C
P3 : Start differential = 2 °C Stop differential = 0 °C

Control of the buffer storage. The 3-way valve V12 will control the temperature ST23. The set point of ST23 is the highest temperature of the set points of ST24 and ST25. The inlet is from the buffer and the solar storage. By using the control strategy in this way, the heat from the solar storage has first priority. The valve V11 will open if the buffer is empty of heat. The valve V11 will open when ST22 < ST23, and close again when the temperature difference ST26 - ST27 is lower than a set point (for example 15 °C). In the summer period from May 1st until September 30th, the valve V11 will be closed completely. The pump P5 will start, and move heat from the solar storage to the buffer tank, when the temperature in the top of the solar storage is higher than a set point of 80 °C. The pump will stop again when the temperature is below 70 °C. The heat from the solar storage will be transferred to the buffer storage when the temperature in the solar storage ST19 is more than the temperature in the buffer ST22 and there is no pulse operation.

Control of flow temperature. The flow temperature ST24 to the air handling units will be controlled depending on the outside air temperature ST7.

ST7 = -6 °C	ST24 = 85 °C
ST7 = 10 °C	ST24 = 46 °C
ST7 = 18 °C	ST24 = 40 °C

The flow temperature ST25 to the fan coils will be controlled depending of the outside air temperature ST7.

ST7 = -6 °C	ST24 = 65 °C
ST7 = 10 °C	ST24 = 40 °C
ST7 = 18 °C	ST24 = 33 °C

Control of the tropical fans. The tropical fans are controlled depending on the temperature difference ST8 - ST9, and the tropical fans will only operate when heating is required (modes 1, 2 and 3). The fans start when the temperature difference ST8 - ST9 is higher than the set point of the start differential, and stops when the temperature difference ST8 - ST9 is lower than the set point of the stop differential.

Start differential = 6 °C
Stop differential = 4 °C.

Control of diffusers. The diffusers will allow different modes for the air intake into the hall. Three diffusers have an on/off motor damper. The control strategy for the diffusers is the following.

Air flow < 13 000 m²/h	winter supply temperature 30 °C, the three dampers are in the off postion, throw vertical.
Air flow > 13 000 m²/h and < 20 000 m²/h	winter supply temperature 35 °C, the three dampers are in the off postion, throw vertical.
Air flow > 20 000 m²/h	winter supply temperature 35 °C, the three dampers are in the on postion.

In operation modes 4, 5 and 6 (free-cooling or cooling), the three dampers are open and the throw is horizontal or intermediate, changing gradually according the difference between the supply temperature and the inside temperature.

Control of the air handling unit. The air handling units will operate in one of six different modes. The six modes are described here. Operation modes 1 and 2 are alternative and manually selected. This solution will allow JRC to compare, for the same outside conditions, two different solutions. The air handling units will work in one of the following five modes according to inside and outside conditions and the JRC strategy.

Mode 1 - heating with heat exchanger operation. Minimum fresh air intake through damper D5 will be controlled by the fan F2 and set at 4000 m²/h. The fan F3 will operate with the same air flow. If heating is required, the air flow through air handling unit B will increase gradually until a maximum level of 20 000 m²/h; heat will be provided by the heating coils. The air handling unit A will work in addition for recirculation.

Mode 2 - heating without heat exchanger operation. Minimum fresh air intake (set at 4000 m²/h) through damper D1 (air solar collector) will be controlled by the fan F1. If heating is required in operation mode 2, the heating coils will supply additional heat. Both the two air handling units will work (unit B only in addition for recirculation) with variable air volume.

Mode 3 - heating and solar wall. When the temperature of inlet air from air solar collector is higher than the set point then the following will happen. Heat required will be provided by the solar collector, and if the thermostat calls again, the air handling unit B will work in addition for recirculation. Maximum air flow from solar collector is set at 20 000 m²/h.

Mode 4 - cooling with outside air. If cooling is required when the outdoor temperature is sufficiently lower than the inside temperature, the air handling units will act in free cooling mode.

Mode 5 - cooling with cooling coils. During the summer season, maximum outside air is set at 4000 m³/h, and the minimum air supply temperature is set at 14 °C. Cooling coils provide air cooling.

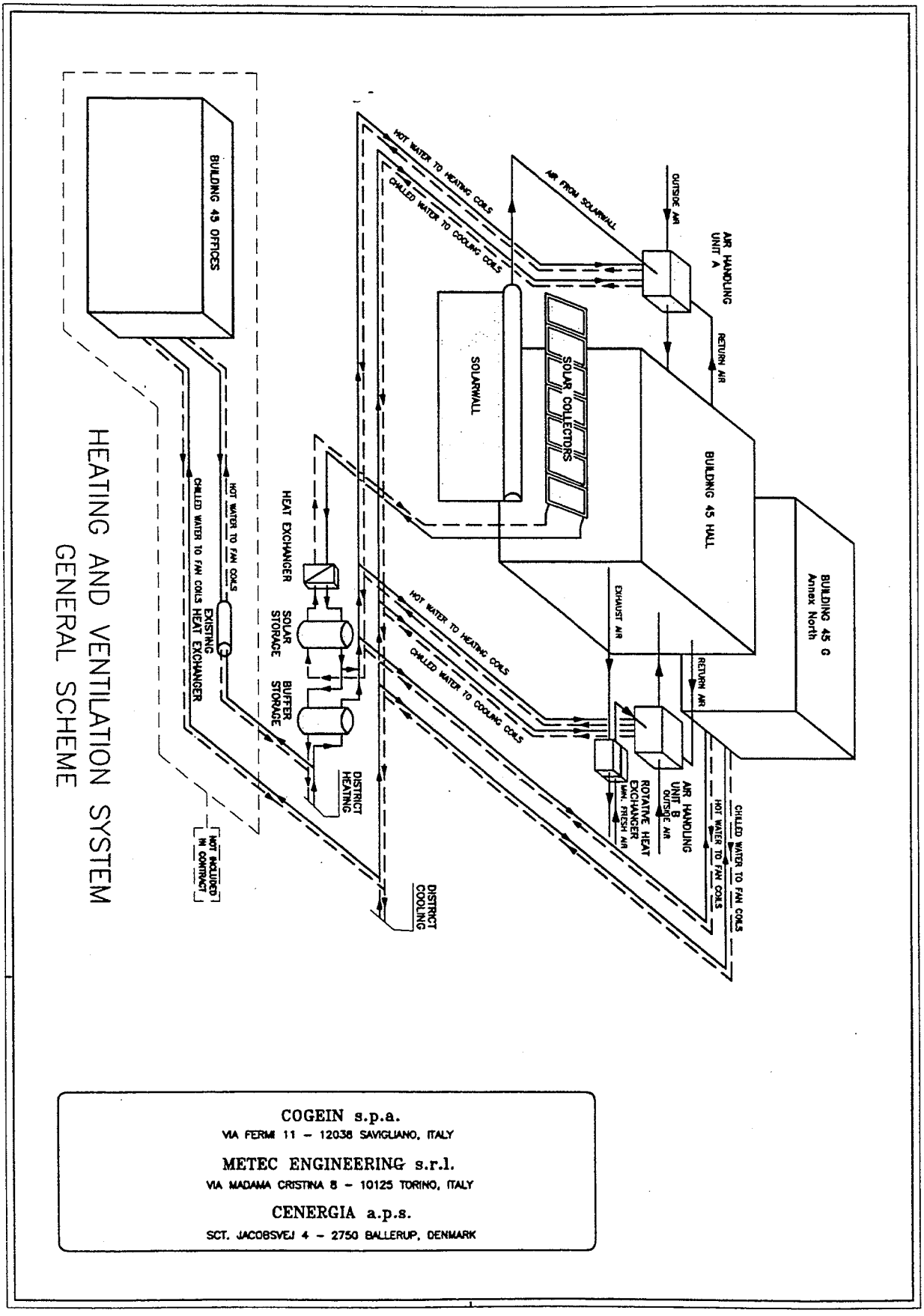

COGEIN s.p.a.
VIA FERMI 11 – 12038 SAVIGLIANO, ITALY

METEC ENGINEERING s.r.l.
VIA MADAMA CRISTINA 8 – 10125 TORINO, ITALY

CENERGIA a.p.s.
SCT. JACOBSVEJ 4 – 2750 BALLERUP, DENMARK

LIST OF SYMBOLS

UNIT A	AIR HANDLING UNIT A – WEST SIDE OF THE BUILDING
UNIT B	AIR HANDLING UNIT B – EAST SIDE OF THE BUILDING
D1	SOLARWALL DAMPER
D2	EXTERNAL AIR DAMPER – UNIT A
D3	RETURN AIR DAMPER – UNIT A
D4	RETURN AIR DAMPER – UNIT B
D5	MINIMUM FRESH AIR DAMPER – UNIT B
D6	EXTERNAL AIR DAMPER – UNIT B
HE1	HEAT EXCHANGER – AIR
HE2	HEAT EXCHANGER – WATER
SC	SOLAR WTER COLLECTORS
BT1	BUFFER TANK 1
BT2	BUFFER TANK 2
ST1	TEMPERATURE SENSOR – INLET TERMPERATURE FROM SOLARWALL
ST2	TEMPERATURE SENSOR – RETURN AIR UNIT A
ST3	TEMPERATURE SENSOR – OUTLET FROM UNIT A
ST4	TEMPERATURE SENSOR – SUPPLY AIR DUCT
ST5	TEMPERATURE SENSOR – OUTLET FROM UNIT B
ST6	TEMPERATURE SENSOR – RETURN AIR UNIT B
ST7	TEMPERATURE SENSOR – OUTSIDE AIR
ST8	TEMPERATURE SENSOR – INSIDE TOP OF THE HALL
ST9	TEMPERATURE SENSOR – INSIDE AT 1.5 M
ST10	TEMPERATURE SENSOR – INSIDE AT 1.5 M
ST11	TEMPERATURE SENSOR – INSIDE AT 1.5 M
ST12	TEMPERATURE SENSOR – CANOPY
ST13	TEMPERATURE SENSOR – SOLARWALL
ST14	TEMPERATURE SENSOR – SOLARWALL
ST15	TEMPERATURE SENSOR – TOP OF SOLAR COLLECTORS
ST16	TEMPERATURE SENSOR – PRIMARY SOLAR COLLECTOR CIRCUIT
ST17	TEMPERATURE SENSOR – SECONDARY SOLAR COLLECTOR CIRCUIT
ST18	TEMPERATURE SENSOR – SOLAR STORAGE
ST19	TEMPERATURE SENSOR – TOP OF SOLAR STORAGE
ST20	TEMPERATURE SENSOR – BOTTOM OF BUFFER STORAGE
ST21	TEMPERATURE SENSOR – MIDDLE OF BUFFER STORAGE
ST22	TEMPERATURE SENSOR – TOP OF THE BUFFER STORAGE
ST23	TEMPERATURE SENSOR – FLOW TEMPERATURE
ST24	TEMPERATURE SENSOR – FLOW TO AIR HANDLING UNITS
ST25	TEMPERATURE SENSOR – FLOW TO FAN COILS
ST26	TEMPERATURE SENSOR – FROM DISTRICT HEATING
ST27	TEMPERATURE SENSOR – TO DISTRICT HEATING

SH1	HUMIDITY SENSOR – INSIDE THE HALL
SH2	HUMIDITY SENSOR – OUTSIDE AIR
MD	MOTOR FOR VARIABLE THROW DIFFUSERS
DP1	DIFFERENTIÁL PRESSURE GAUGE – FILTER UNIT A
DP2	DIFFERENTIAL PRESSURE GAUGE – FAN UNIT A
DP3	DIFFERENTIAL PRESSURE GAUGE – FAN UNIT B
DP4	DIFFERENTIAL PRESSURE GAUGE – FILTER UNIT B
DP5	DIFFERENTIAL PRESSURE GAUGE – ROTATIVE HEAT
AG1	EXCHANGER
AG2	ANIT-FREEZE SENSOR – UNIT A
MP1	ANIT FREEZE SENSOR – UNIT B
MP2	PNEUMATIC MOTOR – DAMPER
MP3	PNEUMATIC MOTOR – DAMPER
MP4	PNEUMATIC MOTOR – DAMPER
MP5	PNEUMATIC MOTOR – DAMPER
MP6	PNEUMATIC MOTOR – DAMPER
EP1..EPn	PNEUMATIC MOTOR – DAMPER
TF	PNEUMATIC TRANSDUCTER
F1	TROPICAL FAN (6 FANS)
F2	FAN – UNIT A
F3	FAN – UNIT B
IV1	EXTRACTOR – EXHAUST AIR
IV2	INVERTER – FAN UNIT A
V1..V8	INVERTER – FAN UNIT B
V9	EXISTING VALVE
V10	3-WAY VALVE – FLOW TO AIR HANDLING UNITS
V11	3-WAY VALVE – FLOW TO FAN COILS
V12	2-WAY VALVE – DISTRICT HEATING
P1	3-WAY VALVE FROM STORAGES
P2	CIRCULATION PUMP – TO AIR HANDLING UNITS
P3	CIRCULATION PUMP – TO FAN COILS
P4	CIRCULATION PUMP – SECONDARY SOLAR COLLECTOR CIRCUI
P5	CIRCULATION PUMP – PRIMARY SOLAR COLLECTOR CIRCUIT
DFa	CIRCULATION PUMP – FROM BT2 TO BT1
DFb	DIFFUSER TYPE a (5 DIFFUSERS)
SP1	DIFFUSER TYPE b (3 DIFFUSERS)
SP2	DIFFERENTIAL PRESSURE SENSOR DAMPER D1
	DIFFERENTIAL PRESSURE SENSOR DAMPER D5

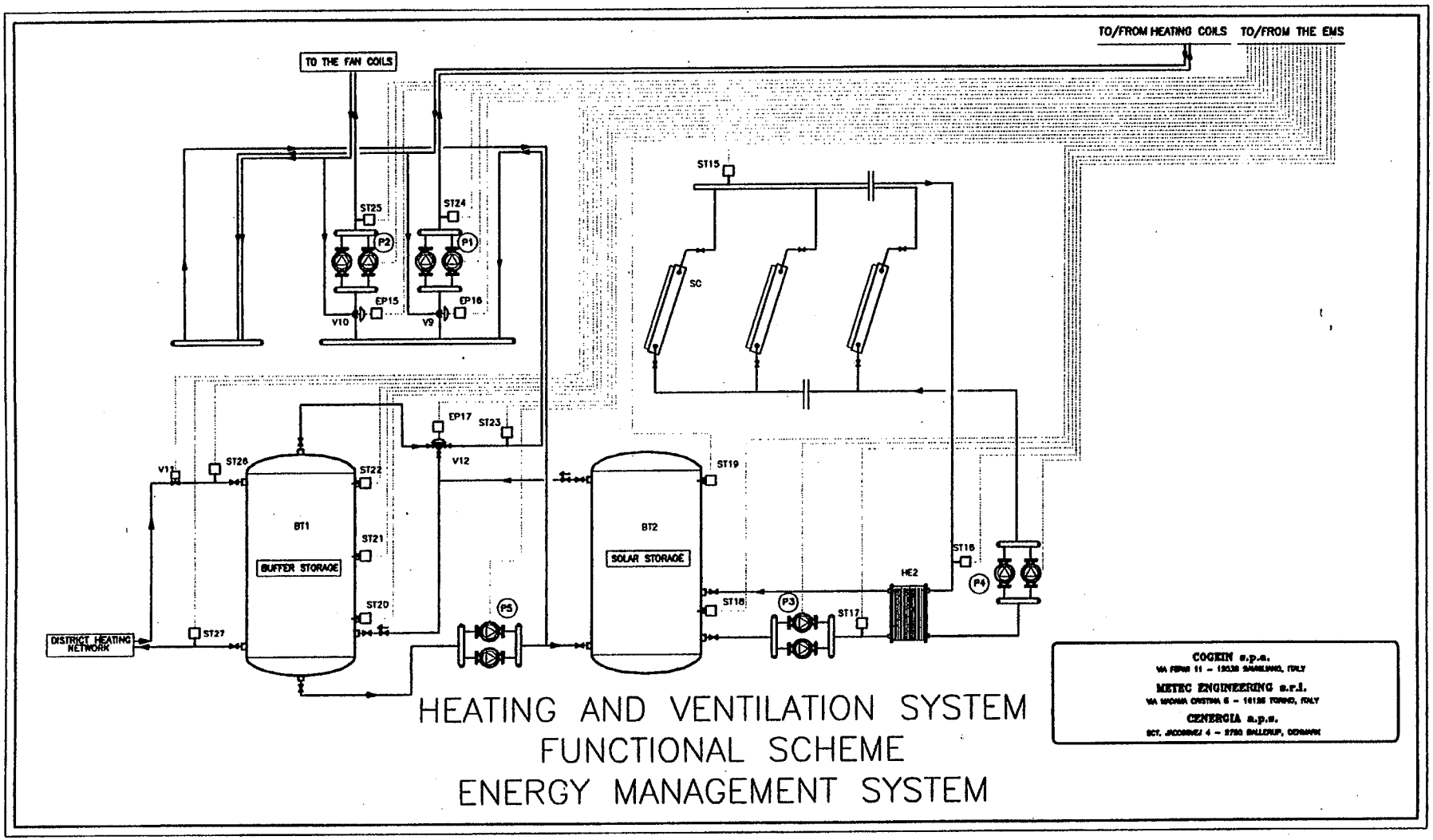
TO/FROM HEATING COILS
TO/FROM THE EMS
TO THE FAN COILS
ST25
ST24
P2
P1
EP15
EP16
V10
V9
ST15
SC
EP17
ST23
V12
V11
ST26
ST22
BT1
BUFFER STORAGE
ST21
ST20
ST27
DISTRICT HEATING NETWORK
P5
BT2
SOLAR STORAGE
ST19
ST18
P3
ST17
HE2
ST16
P4
HEATING AND VENTILATION SYSTEM
FUNCTIONAL SCHEME
ENERGY MANAGEMENT SYSTEM
COGEIN s.p.a.
METEC ENGINEERING s.r.l.
CENERGIA a.p.s.

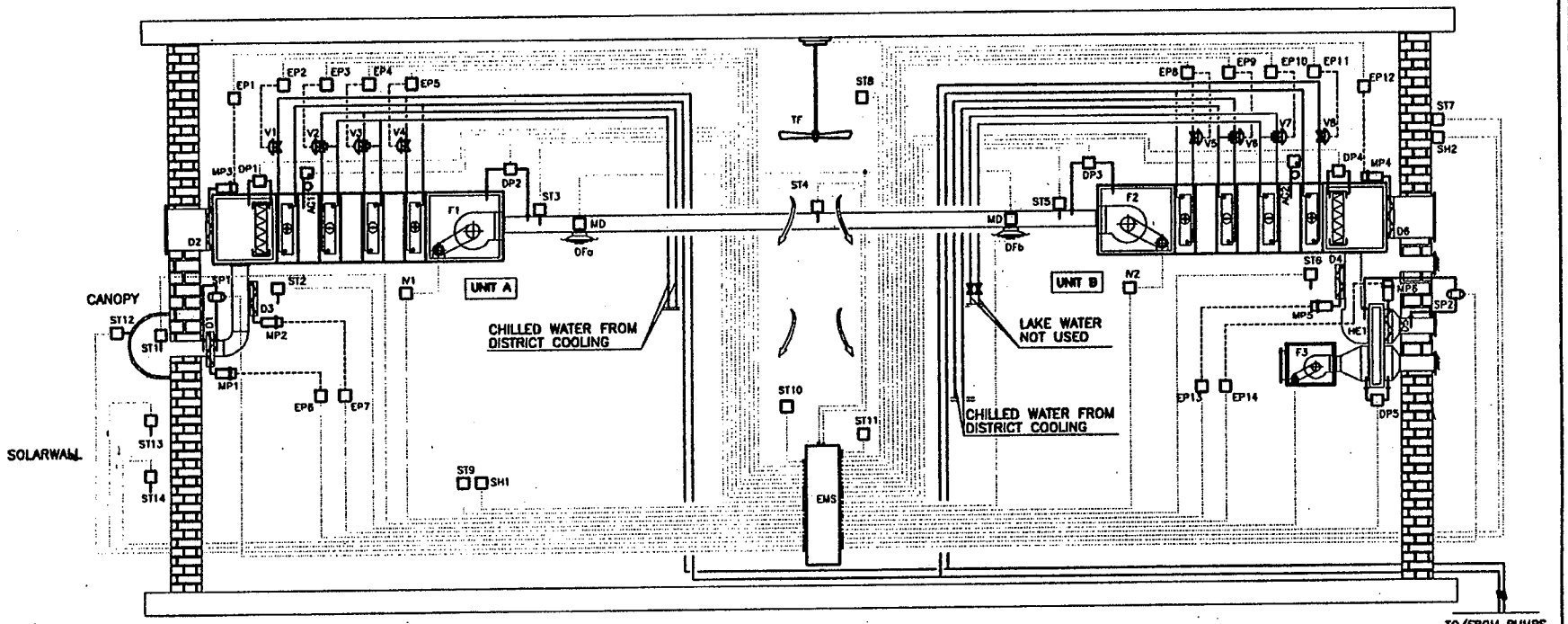

HEATING AND VENTILATION SYSTEM
FUNCTIONAL SCHEME
ENERGY MANAGEMENT SYSTEM

COGEIN s.p.a.
VIA FERMI 11 – 13030 SALUGGIA, ITALY
METEC ENGINEERING s.r.l.
VIA MADAMA CRISTINA 6 – 10125 TORINO, ITALY
CENERGIA a.p.s.
SCT. JACOBSMEJ 4 – 2700 BALLERUP, DENMARK

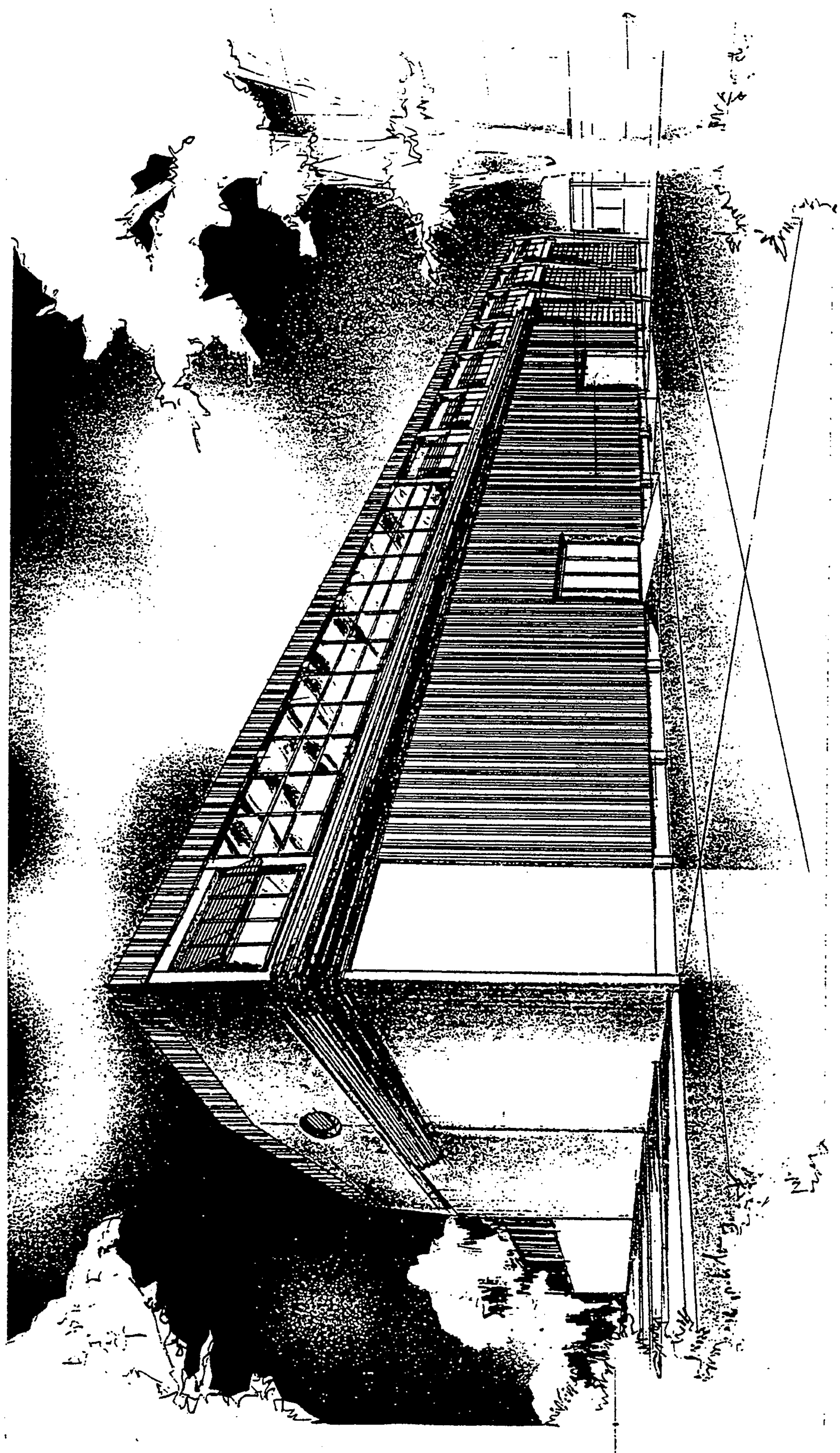

2.6 Tea Drying in Indonesia

General Project Information

The solar dryer for tea was constructed at a plantation at Malabar, West Java, Indonesia. The site is located at a latitude of approximately 7 degrees south, at a longitude between 105 and 110 E. The perforated collector system was constructed with the assistance of the R&D Centre for Applied Physics - LIPI. The purpose of the project was to determine the feasibility of using solar energy to displace oil as the heating system for the wilting of tea leaves.

System Description

System Operating Modes The system is designed to wilt tea leaves through a batch process using the existing drying troughs. The troughs are loaded manually from a trolley that moves through the wilting area. The fan system delivers solar heated air to a chamber under the trough, and the air then rises through the trough. The system operates year round. The fans operate only during the day when solar energy is available.

Key System Parameters A 600 m^2 perforated collector is mounted on the roof of the drying shed. The collector mounting system, the air handling system, and the duct-work were all obtained locally. The perforated-plate material was purchased from Canada.

The system is designed for a total flow of 86 400 m^3/h. The solar collectors supply heated air to three of the original twenty-two fan systems on the first floor of the drying shed.

Figure 2.6.1 shows a view of the south end of the drying shed. The solar collectors on the west facing roof are connected, by the shaded ducts, to three of the eleven fans at the south end of the drying shed.

Collector Description The collector is as described in Chapter 1.

Collector Parameters The collectors have a porosity of 1%. They are mounted on a 22 degree angle facing west. The collectors cover about one third of the total roof area.

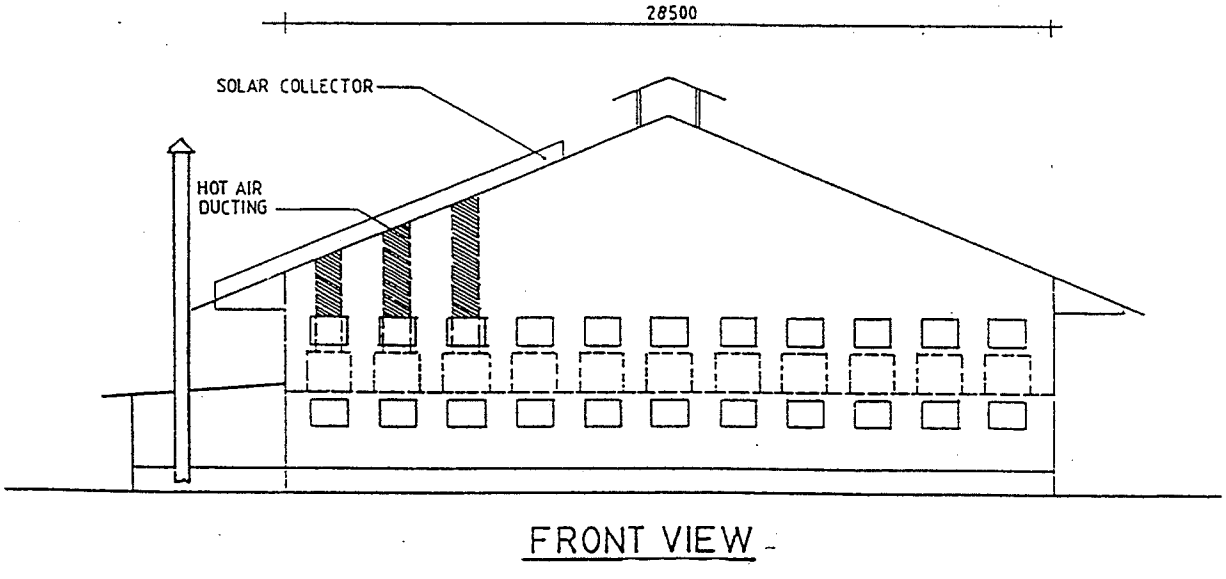

Figure 2.6.1 Front View of the Tea Drying Shed

System Components The system is quite simple in that there are no automated controls. An axial fan draws air from the collector, and an air damper is used to regulate the air flow. The on-off mechanism is a manually operated switch. Figure 2.6.2 shows the connection of the perforated collector to the fan system and the fan system to the plenum leading to the dryer bed.

Description of Advanced Features The perforated absorber removes the need for a glazing. Glass is costly, requires an extensive support system when close to horizontal and is prone to breakage (in S.E. Asia tempered glass is uneconomic). Moreover, the perforated absorber system performs better than the glazed one. The spacing of the perforated-plate above the roof increases nearer the fan intakes to balance air flow distribution along the collector surface.

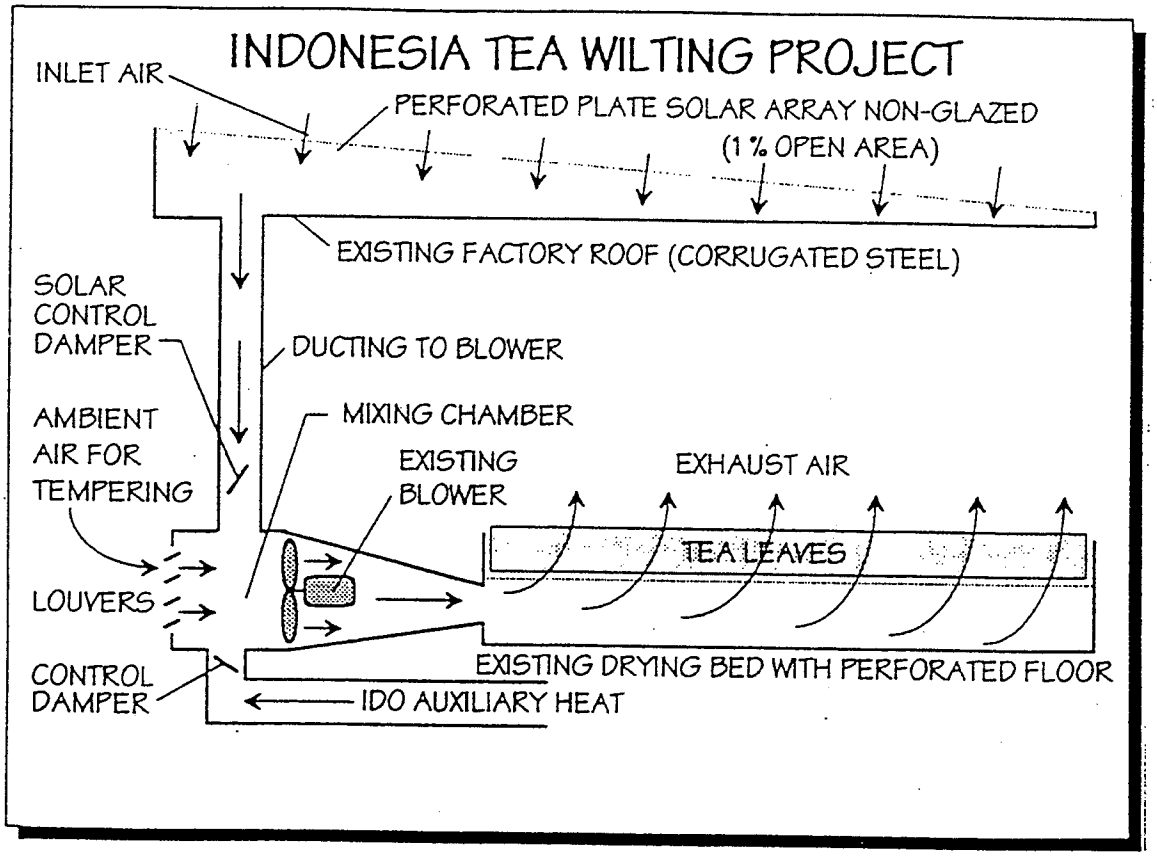

Figure 2.6.2 Indonesia Tea Wilting Project.

Justification of Advanced Features Laboratory testing has shown the perforated collector to have efficiencies up to 30% higher under no and low wind conditions while the glazed collector was 17% more efficient under high wind conditions. Table 2.1 under Justification of Advanced Features under Section 2.1 (page 10 of the report) summarizes efficiency test results for both glazed and perforated prototypes. Figure 2.2 in that same section shows the test results for the aluminum absorber with 2% void area at various collector flows, wind speeds and radiation levels. Efficiency is a function of wind speed and rate of air flow through the collector.

Description of Back-Up System/Auxiliary An oil-fired back-up system is available, but is not used.

Description of Load The drying of tea is a three-stage process. In stage one, wilting, the harvested tea leaves are put into drying troughs. Air at between 30 and 32 °C is blown through the crop for 18 hours. This process reduces the moisture content from 78% to 50% (wet basis). Solar heating is ideally suited to the first stage of the drying process. The average monthly ambient temperatures in Djakarta (Indonesia) is an almost constant 26 to 27 °C . Thus the solar system need only raise the air temperature 5 to 6 °C. The tea drying operation in Indonesia runs 7 days a week, 52 weeks a year.

Description of Controls Figure 2.6.2 shows the controls design. Each fan system has a solar control damper that is manually adjustable to balance the flows in the system. A second manually adjustable damper is used to admit ambient air for tempering. A dial thermometer is monitored by the operator, and tempering air is adjusted to maintain a maximum of 35 °C to the drying bed. Auxiliary heating from the oil boilers is available, but has not been used to date. A manual control damper is used to turn the auxiliary heating on and off if required. A simple manual switch controls the fans, turning them on in the morning and off in the evening.

Key Meteorological Information The weather data for the simulations was generated from monthly average weather data using the WATSUN Synthetic Radiation Data Generator, WATGEN. Table 2.6.1 gives the synthetic data for total monthly solar radiation on a horizontal surface and the mean monthly ambient temperature.

Table 2.6.1: Monthly Solar Radiation and Average Ambient Temperature for Djakarta

Month	Solar Radiation (MJ/m^2)	Air Temperature (°C)
Jan	468	26.1
Feb	445	26.1
Mar	518	26.7
Apr	498	27.2
May	484	27.2
Jun	453	27.0
Jul	502	26.7
Aug	552	26.7
Sep	528	27.2
Oct	549	27.0
Nov	498	26.7
Dec	481	26.4
Annual (Total , Avg.)	**5,971**	**26.8**

Performance Data

Computer simulations were made of the expected performance of glazed and perforated-plate solar tea drying systems using the SIMAIR computer program and Djakarta (6.2 °S, 106.8 °E) weather data. The simulations showed that the perforated-plate would perform 7% better than the glazed design. Over the year, the perforated system was expected to deliver 2.1 GJ/m² of solar heat. The solar heat delivered was restricted because, for many of the hours, the ambient temperature was equal to or greater than the maximum delivery temperature of 35 °C.

In 1993 and 1994, (prior to the solar installation), industrial diesel oil was used at an average rate of 1.18 kWh_e per kg of tea. After the conversion only fan energy was required. It is assumed that approximately the same amount of fan energy was required before and after the conversion. In September 1994 the three solar troughs produced 108,000 kg of good quality wilted tea for a total savings of 127,000 kWh_e (11,880 litres of oil).

Estimated Costs

The reported project costs are listed in Table 2.6.2

Table 2.6.2: Solar Tea Dryer Costs

Component	Cost (US$)	US$/m²
Absorber Plate (600 m²)	16,658	27.76
Additional Materials	2,268	3.78
Air Ducting + Fan	15,043	25.07
Electrical Work	6,289	10.48
Structure	9,430	15.72
Others	7,346	12.24
Total	57,034	95.05

Update on Monitored performance

The system was installed in August 1994, and was monitored from September 1994 through December 1995. The installed collector area was 560 m², instead of the 600 m² area of the original design. During the monitoring period from October through December 1994 the measured average collector efficiency was 65% when the air flow rate was 60 480 m³/h (70% of the design flow rate). Tarigan, Utomo, Halawa and Brojonegoro (Monitoring and Performance Evaluation of Malabar Solar Energy Tea Wilting, presented at the ASEAN-Canada Project on Solar Energy in Drying Processes Workshop on Monitoring, Evaluation and Adoption Strategy, Cebu, Philippines, 26-27 February 1996) reported that the utilization of the system was more than 264 days per year. They calculated that the energy cost (for diesel oil and electricity) to produce one kg of product before the installation of the solar system was Rp 84, compared to Rp 52 per kg after the installation of the solar system, representing a simple payback period for the solar system of about five years.

2.7 Cocoa Drying in Malaysia

General Project Information

A solar heating system for drying cocoa beans has been constructed in Tawau, Malaysia. The site is located at 4.3 °N, 118 °E, near the eastern end of Malaysia. A perforated collector system was chosen on the basis of high solar heat collection efficiency, low operating cost, ease of operation, high reliability, and no off-gassing of toxic gasses.

System Description

System Operating Modes The preliminary design called for the system to provide

- solar heated air,
- an ambient bypass to temper the solar heated air thereby limiting the temperature of air entering the drying bed, and
- auxiliary heating for the times when insufficient solar is available to dry the product.

Key System Parameters The system has 370 m² of perforated collector mounted on the roof of the drying shed. The array is 6.4 m high by 57.9 meters long. Figure 2.7.1 shows the system components with respect to the drying shed.

Collector Description The collector is as described in Chapter 1.

Collector Parameters The collectors have a porosity of 0.25%. The low porosity is due to the high temperature rise required. They are mounted on a 24 degree angle facing south. The collectors cover almost half of the total north and south roof area.

System Components The system is very simple and there are no controls. An axial fan draws air from the collector through two outlets. One outlet is located near each end of the array. A manually set air damper is used to balance the flows in two ducts. The fan on-off mechanism is a manual switch. Figure 2.7.2 schematically shows the original design of the system.

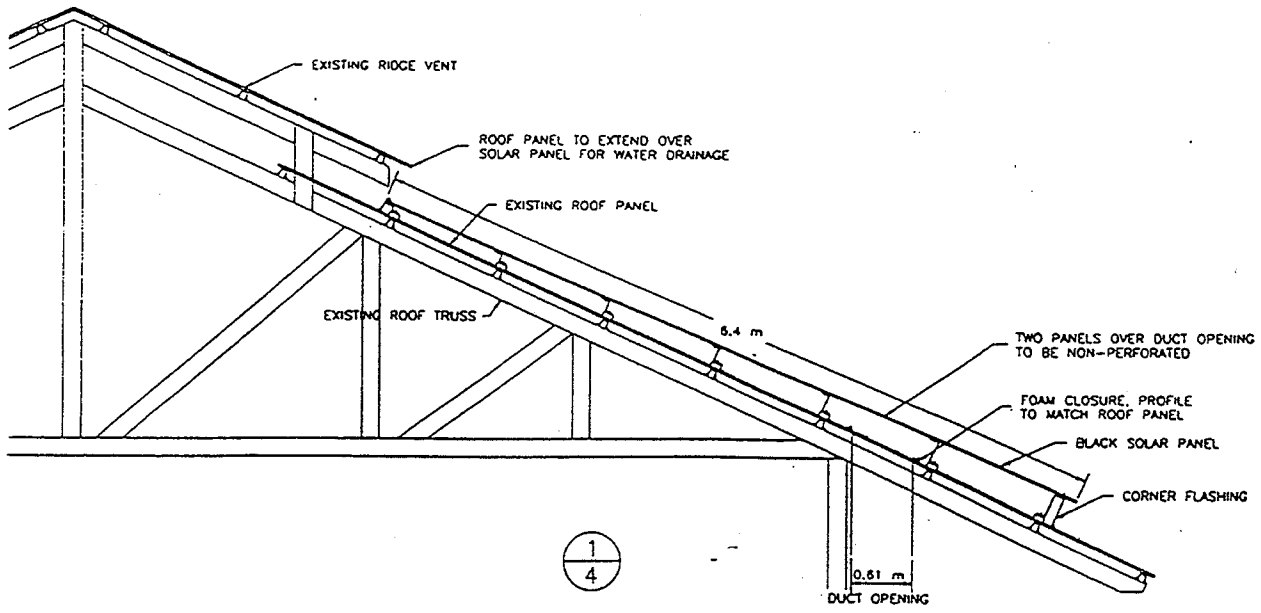

Figure 2.7.1 Cross Section of Perforated Collector on Roof

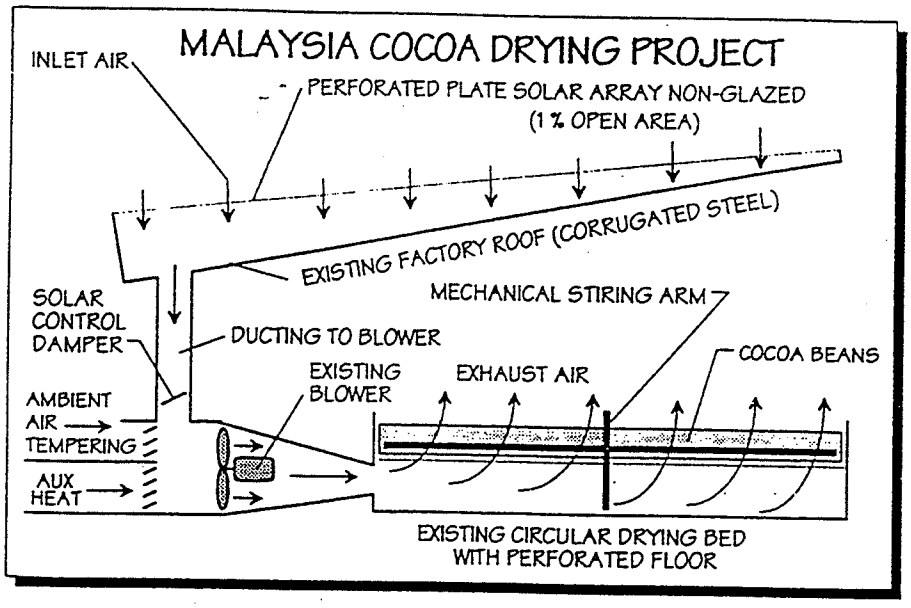

Figure 2.7.2 Malaysia Cocoa Drying Project

Description of Advanced Features The perforated absorber removes the need for a glazing. Glass is costly, requires an extensive support system at low angles, and is prone to breakage (in S.E. Asia tempered glass is uneconomic). Performance for the glazed and unglazed systems are expected to be similar. The panels are roof-mounted with a low porosity and have a tapered inlet to balance air flows.

Justification of Advanced Features Laboratory testing has shown the perforated collector to have efficiencies up to 30% higher than glazed collectors under no wind and low wind conditions while the glazed collector was 17% more efficient under high wind conditions. Table 2.1 in Justification of Advanced Features under Section 2.1 summarizes efficiency test results for both glazed and perforated prototypes. Figure 2.2 in the same section shows the test results for the aluminum absorber with 2% void area at various collector flows, wind speeds and radiation levels. Efficiency is a function of wind-speed and collector flow. The low flow higher temperature system will be compared with another glazed collector as part of the ASEAN-Canada project.

Description of Back-Up System/Auxiliary The back-up system is direct heating from a wood-fired oven.

Description of Load Cocoa in deep beds has been found to dry most effectively at moderate temperatures (60-66 °C) and low airflows (0.05 m/sec face velocity)[1]. Rapid drying can cause the beans to turn bitter.

For drying, the beans are placed in a circular drying bed with mechanical stirring arms. The drying process reduces moisture content from about 43-45% to 6-6.5%. Solar heating is ideally suited to the drying process. The average monthly ambient temperatures in Malaysia are an almost constant 26 to 27 °C. Thus the solar system needs to raise the air temperature less than 30°C. Cocoa bean processing operations run 7 days a week, 52 weeks a year.

Description of Controls Figure 2.7.2 also shows the controls design. The fan system has a solar control damper that is manually adjustable to balance the flows in the system. A second manually adjustable

[1] Shelton, B. (1967) Artificial Drying of Cocoa Beans. Tropical Agriculture. Trinidad. 44:125-32

damper is used to admit ambient air for tempering. A dial thermometer is monitored by the operator, and tempering air is adjusted to maintained a maximum of 65 °C to the drying bed. Auxiliary heating from the wood oven is piped to the fan. A manual control damper is used to turn the auxiliary heating on and off. A simple switch manually controls the fans, turning them on and off as each batch is dried.

Key Meteorological Information

Hourly weather data was synthetically generated from monthly average weather data using the WATSUN Synthetic Radiation Data Generator called WATGEN. Table 2.7.1 lists the total monthly solar radiation on a horizontal surface and the mean monthly ambient temperature.

Table 2.7.1: Monthly Solar Radiation and Mean Temperature for Kuala Lumpur

Month	Solar Radiation (MJ/m^2)	Air Temperature (°C)
Jan	485	26.0
Feb	485	27.0
Mar	600	27.0
Apr	611	27.0
May	604	27.0
Jun	528	27.0
Jul	558	27.0
Aug	596	27.0
Sep	564	26.0
Oct	579	26.0
Nov	507	26.0
Dec	476	26.0
Annual (Total , Avg.)	**6,592**	**26.7**

Performance Data

No monitored data are currently available.

Estimated Costs

The reported project costs are listed in Table 2.7.2.

Table 2.7.2 Malaysia Cocoa Dryer Costs

Component	Cost (US$)	US$/m²
Absorber Plate and Mounting Hardware (370 m²)	11 100	30.00
Engineering	3600	9.73
Air Ducting + Fan	13 320	36.00
Installation Labour	5540	14.98
Transportation (including collector)	2770	7.49
Other (including monitoring)	2160	5.84
Total	**38 490**	**104.03**

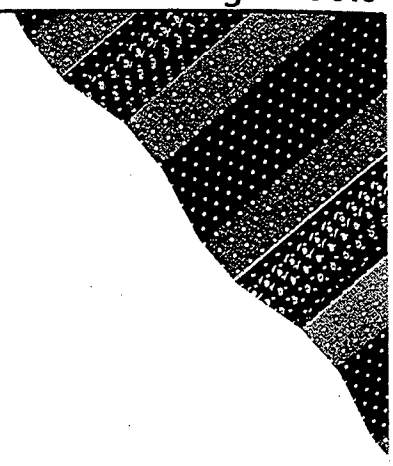

Chapter 3:

Design Tools

3.1 TCFLOW Computer Design Model

3.1.1 Introduction

The research at NREL on unglazed transpired collectors included the development of a computer model of the air flow and temperature profile of the collector under steady state conditions. The model employs a pipe network technique to model the flow through the collector and properly accounts for pressure drops that occur inside the collector. The program has been compiled to run on IBM-compatible, Macintosh, and Silicon Graphics machines. The program should prove useful to design engineers wishing to extract optimal performance from their collector designs. This work was done as part of a master's thesis (C. Dymond) at the University of Colorado, Boulder.

3.1.2 Technical Details

Pipe Network

The flow inside the collector is modeled as if it were constrained to flow in a network of fictitious connected pipes. The purpose for doing this is that the pipe network model is simple and can easily handle the correlations for the pressure drop across the absorber and heat exchange effectiveness.

A square grid of connected pipes is used to model the collector. Each interior node represents the intersection of five pipes: four pipes corresponding to the flow in the plenum from/to four adjacent nodes (left, right, top, bottom) and one pipe corresponding to the flow across the absorber from the outside. The flows in all of the pipes represent the unknowns. An equal number of equations is generated by applying the conservation of mass at each node and the conservation of pressure around closed pipe loops. These equations are linearized, and then solved in matrix form. At each iteration , the linearization coefficients are updated, and a new set of equations is defined.

One problem with modeling the flow as a pipe network is that the flow behavior at the junctions of the pipes is difficult to characterize. The challenge was to model the flow as a pipe network without applying any constraints on the air as it entered the junctions of the pipe network. After all, the model is of an open plenum, and the fluid is not actually constrained to flow in only horizontal and vertical pipes. The method we used to overcome this problem is briefly described in the following section.

Pressure Drops

The air passing through an unglazed transpired collector experiences four distinct pressure drops. The first pressure drop is a frictional pressure drop due to the fluid passing through the absorber. This is determined using an empirical correlation developed by Kutscher (1992). The second pressure drop is a frictional pressure drop inside the plenum as the air moves toward the exit or header. The third pressure drop is that of thermal buoyancy, or stack effect. The buoyancy has the effect of increasing the flow rate through the bottom of the collector and under extreme circumstances can cause out flow at the top of the collector. The fourth pressure drop is due to the fact that the air is undergoing acceleration toward the exit. This acceleration pressure drop is a Bernoulli effect caused by both the addition of mass into the collector plenum and the convergence of flow as it moves toward a single exit.

The acceleration pressure drop proved to be the most difficult pressure drop to model because it relied on knowledge of the behavior of the air at the junctions of the pipe network. Unfortunately in a pipe network, the only information available is the flow rate inside each pipe. To establish the acceleration pressure drop inside the collector, we employed the Bernoulli equation along a streamline that started at a junction, traveled along the pipe and ended at the junction at the opposite end of the pipe. The exact nature of the flow inside a junction was based on an assumed knowledge of the local flow direction in the plenum.

As a result of this assumption, and the complicating effect of the buoyancy on our assumed direction, the current version of the model is only able to find a solution for cases where the exit is in the upper left or upper right corner, or is equally distributed along the top of the collector (as in the case of a constant-velocity header). Fortunately these cases cover the most common installation situations (an exit at the top center is modeled by solving one-half of the symmetric problem and using a corner exit.)

Temperature

The temperature of the collector surface is determined by applying an energy balance on the front of the collector. Using the empirical relation developed by Kutscher (1992) for the effectiveness of the collector, we could relate the temperature of the air entering the plenum to the temperature of the surface of the collector. The temperature profile of the collector surface is intended to aid the designer in collector performance optimization.

3.1.3 Example Program Output

The computer program generates three absorber profiles. The first profile is the flow distribution of the air entering the absorber surface, the second profile is the temperature distribution of the collector surface, and the third profile is of the local collector efficiencies. The following section presents each of the three profiles for the default collector model.

The default collector is 5 meters tall by 10 meters wide with a single exit in the top center of the collector. It is modeled as if it were 5 meters tall by 5 meters wide with an exit in the top right corner of the collector. By applying a symmetry condition to the right side of the model a mirror image is generated and the model becomes essentially a 5 meter tall by 10 meter wide collector with an exit in the top center of the collector. The parameters used for the default collector are provided in Table 3.1.

Table 3.1: Parameters Used as the Default Settings of the Computer Model

COLLECTOR PARAMETER	VALUE UNITS
Height	5.0 m
Width	5.0 m
Plenum Depth	20 cm
Mass Flow Rate	1.50 kg/sec
Hole Diameter	1.0 mm
Porosity	2.0%
Absorptance	90.0%
Emissivity	80.0%
Exit	Single Top Right
Insolation	800 W/m^2
Ambient Temperature	20 °C
Ground Temperature	10 °C
Dew Point	10 °C
Wind Speed	2.0 m/sec
# of X direction Nodes	8
# of Y direction Nodes	8
Flow Iteration Limit cm/secTemperature	0.015 0.1 °C

Figure 3.1 is a plot of the face velocities data generated by running the model for the default collector. The x axis of the plot shows the horizontal position of the collector (Width) , the y axis of the plot shows the vertical position of the collector (Height) and the z axis shows the velocity of the air as it enters the absorber surface.

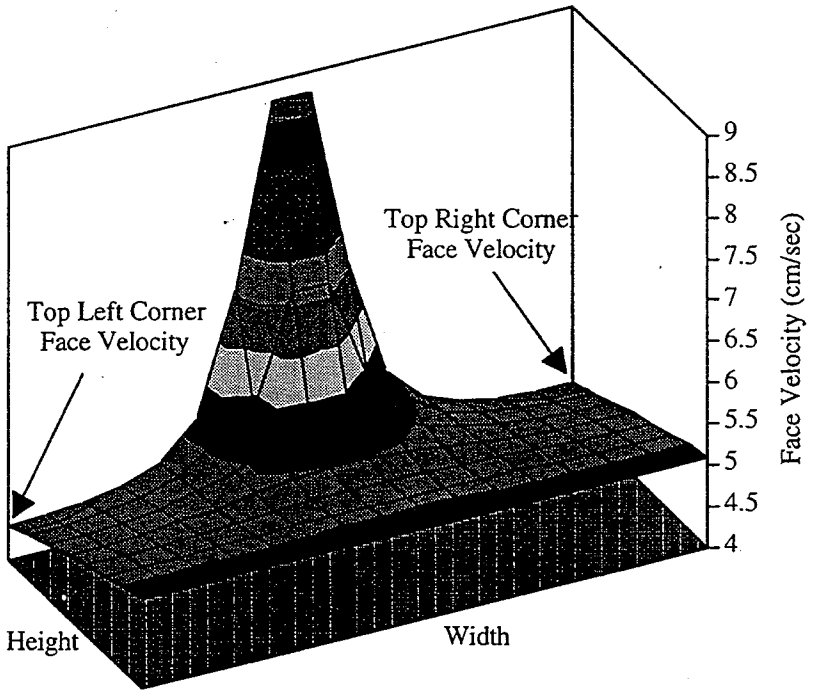

Figure 3.1 Face Velocity Profile for Default 5 m by 5 m Collector with the air outlet at the top centre of the collector.

The most obvious feature in Figure 3.1 is the large rise in face velocity near the top center of the collector. This large peak is immediately in front of the exit where the air flows directly into the interior of the building. At locations away from this top center of the collector the air must travel inside the collector plenum experiencing the three plenum pressure drops: acceleration, friction, and buoyancy. As a result the pressure drop across the absorber and therefore the face velocity, decreases dramatically the further away it is from the exit.

Along the left and right sides of the collector there is less flow through the top of the collector than through the bottom of the collector. This is because the buoyancy pressure drop is positive toward the bottom of the collector, unlike the acceleration and frictional pressure drops which are always positive in the direction of the fluid motion. Figure 3.1 shows the local flow starvation in the top left and top right hand corners of the collector which is characteristic of a collector with a single top center exit. In these corners the buoyancy force opposes the air being drawn in through the absorber surface.

Figure 3.2 shows the temperature profile generated by the model for the default collector. The temperature profile of the unglazed transpired collector is mirror image to the face velocity profile. The larger the air flow through the collector the better the heat is transferred away from the absorber which results in a lower absorber temperature. The top left and right corners of the collector are warmer than the rest of the collector because of flow starvation due to the buoyancy force.

Figure 3.3 shows the efficiency profile generated by the model for the default collector. The efficiency profile of the unglazed transpired collector has the same shape and form as the face velocity profile. The larger the air flow through the collector, the better the heat is transferred away from the absorber which results in a higher collector efficiency.

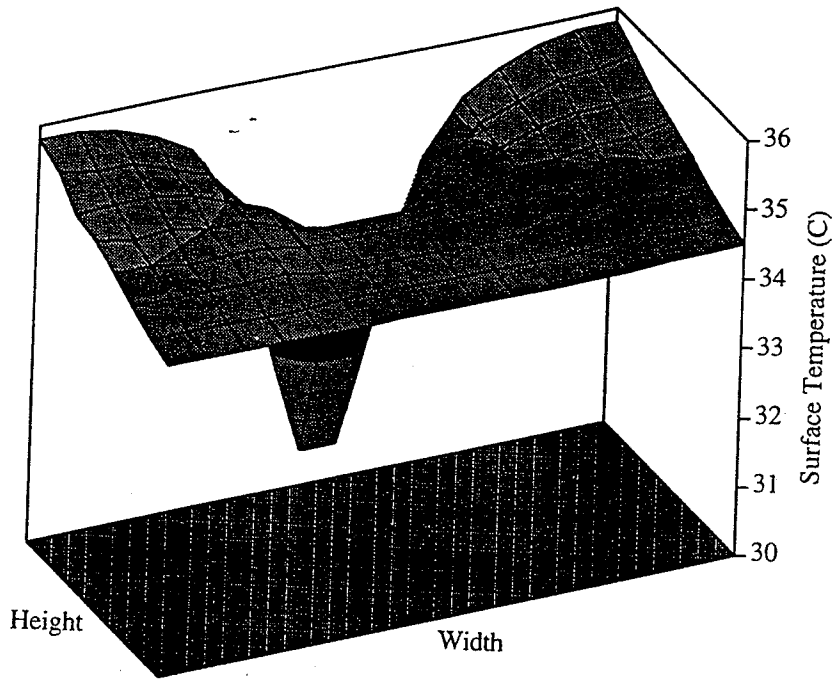

Figure 3.2 Surface Temperature Profile for the Default 5 m by 5 m Collector.

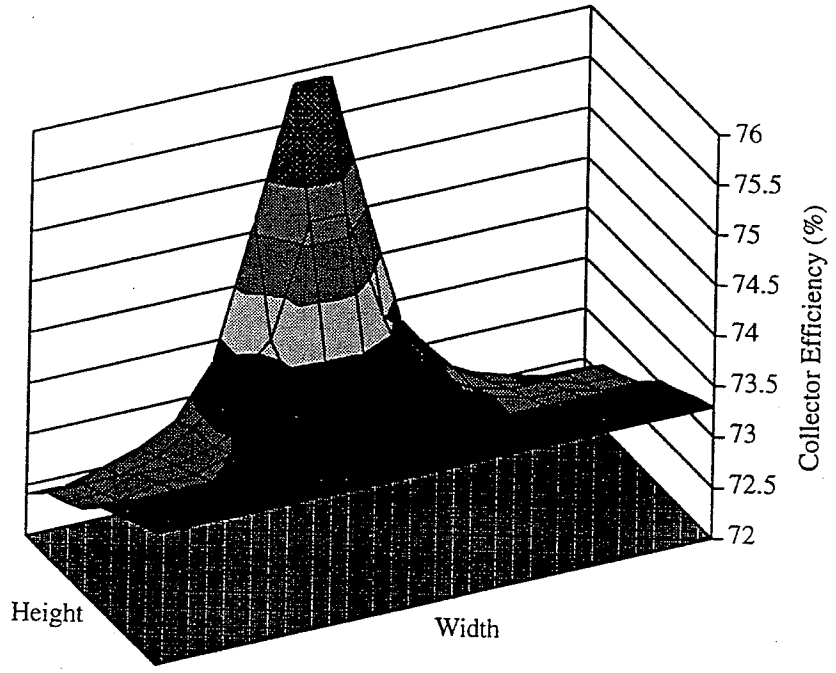

Figure 3.3 Efficiency Profile of the Default 5 m by 5 m Collector.

3.1.4 Validation of Model to Actual Data

Figures 3.4 and 3.5 show the temperature profile of the unglazed transpired collector located on NREL's Waste Handling Facility generated from an IR thermography image of the collector and the collector model respectively. Because the computer model can only handle a collector with a single exit in the upper left or upper right corner of the collector, only the right 64% of the collector was modeled. The collector was modeled as if it were a 2% porosity collector with an exit in the upper left hand corner. The collector had a 4% porosity section directly in front of the exit, and a section just below the exit with 1% porosity. The 4% porosity exit was used to simulate the leaky by-pass damper, and the 1% porosity section is part of the design of the collector.

Ignoring the temperature of the exit, the two temperature profiles shown in Figures 3.4 and 3.5 compare very well. The maximum and minimum temperatures along the right side of the collector only differ by 0.5 degrees C or less. The 1% porosity section below the exit is warmer in the model results which may be due to the rather arbitrary choice of 4% for the porosity of the leaky bypass damper. Because the energy balance used in the model assumes a porous metal surface it is not capable of accurately evaluating the temperature of the bypass vanes of a leaky bypass damper. The shape of the two curves are similar, although the model results are flatter than the IR thermography results. This is probably due to the fact that the frictional pressure drop terms were modeled as if the flow was traveling in smooth metal ducting and hence may have underestimated the frictional pressure drop experience in the WHF collector plenum that has a rough concrete back wall.

As with all comparisons of computer models to actual data, it is very important to have the input parameters given to the model be as close to reality as possible. Given the uncertainty of some of the input parameters (frictional pressure drop inside the plenum, leakiness of the bypass damper) the model compares very well to experimental data.

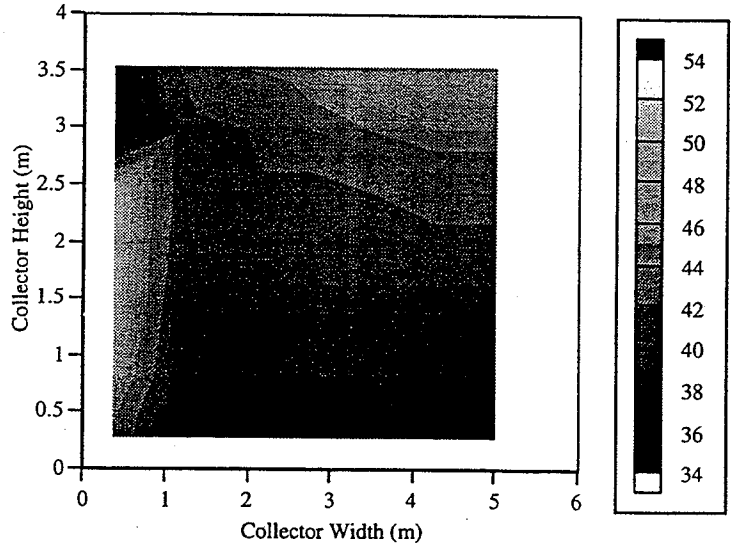

Figure 3.4 Temperature Profile Generated by IR Thermography of the Waste Handling Facility Perforated Collector. The temperature scale is degrees C.

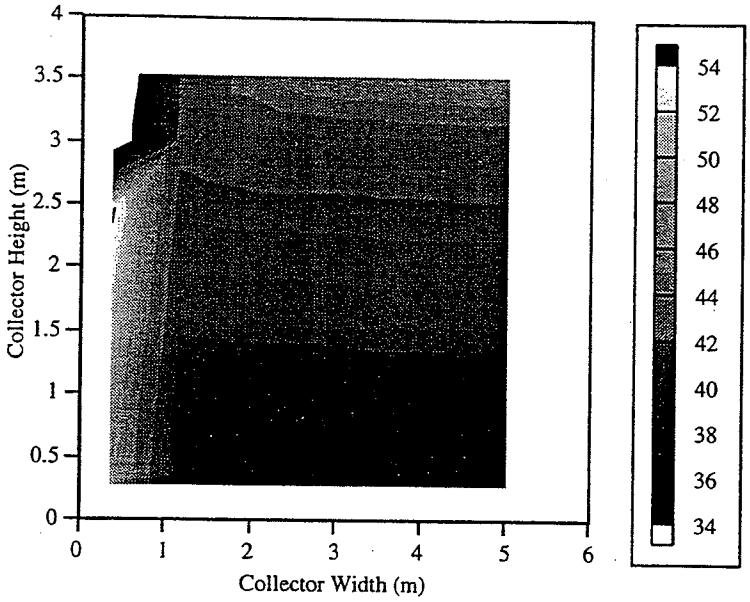

Figure 3.5 Temperature Profile Generated by Model for the Waste Handling Facility Perforated Collector. The temperature scale is in degrees C.

3.1.5 Computer Program "TCFlow" Information

Capabilities/Requirements

1.1 TCFLOW has successfully run on three different computer systems, IBM PC, Macintosh PC, and Silicon Graphics workstations. The hardware requirements are as follows:

- 386 or 486 CPU (preferably the latter)
- 4 MB of system memory
- 2 MB of hard disk space

1.1 TCFLOW is capable of determining the flow distribution and surface temperature for any collector configuration with the exit located at any of the following locations:

1. Single exit in the upper right corner
2. Single exit in the upper left corner
3. Continuously distributed exit along the top edge of the collector*
4. Single exit anywhere along the top edge of the collector*
5. Single exit located in the top center of the collector**

* These have some convergence problems with matrices larger than 8 by 8.

** This can be simulated by applying a symmetry condition to half a collector with an exit in the upper right or left corner.

Running the Program

The program currently has a text-based menu driven interface which allows the user to change various parameters, save parameter sets to file and load parameter sets previously saved. Upon typing "1.1 TCFLOW" to start the program, a main menu is displayed which looks like the following.

1.1 TCFLOW Main Menu

Change Collector	C
Change Air/Weather Parameters	A
Change Model Parameters	M
Display All Parameters	D
Save Input File	S
Load Input File	L
Run Program	R
Quit Program	Q

Change Collector Parameters

This menu choice allows the user to change one of the following parameters associated with the collector itself (default values shown):

H	Height	5.0 meters
W	Width	5.0 meters
D	Depth	0.1 meters
F	Exit Flow Rate	1.62 kg/sec
L	Exit Location	25
DIA	Hole Diameter	0.001 meters
P	Pitch	0.0067 meters
A	Absorptance	0.90
S	Slope	90
Z	Azimuth	0.0
T	Header Type	1

The two parameters which are not self-explanatory are exit location and header type. Exit location shows a grid of nodes (connection points in the pipe network) and asks the user to choose a location on the grid which best describes the exit location of the collector. Header type allows the user to choose either a single exit (1) or a collector with a constant velocity header (2) note that we have experienced some problems with the constant velocity header on large models (more than 8 by 8 nodes)

Change Air/Weather Parameters

This menu choice allows the user to change one of the following parameters associated with the collector environment:

S	Specific Heat	1006 J/KgC
D	Density	1.292 Kg/m3
V	Viscosity	0.1720E-04
I	Insolation	800 W/m^2
A	Ambient Temp	20 C
D	Dew Point	10 C
W	Wind Speed	0 m/sec

Change Model Parameters

This menu choice allows the user to change one of the following parameters associated with the collector model:

X	X Direction	5
Y	Y Direction	5
F	Flow Limit	0.015 cm/sec
T	Temp Limit	0.005
O	Over-relaxation	0.050

X direction nodes allows the user to define the number of x-directional nodes there are in a pipe network. Similarly Y direction nodes allows the user to define the number of y-directional nodes there are in a pipe network. Flow limit defines the flow convergence criterion. Temp limit defines the temperature convergence criterion. Over-relaxation lets the user apply an over-relaxation parameter other than 0.50 to aid in convergence.

Display all Parameters

This menu choice displays on screen all the parameters used by the model.

Save Input File

This menu choice allows the user to save the parameters for a particular collector to a file.

Load Input File

This menu choice allows the user to load the parameters for a particular collector that was previously saved.

Run Program

This menu choice runs the program. Although the menu only shows one choice, there are actually four choices which allow the user to start the program. These choices allow the user to run the program with or without one or more of the pressure drops accounted for. The following list describes these options:

R. Run the program with all pressure drops accounted for.

1. Run the program with all pressure drops accounted for except the buoyancy term.

2. Run the program with all pressure drops accounted for except the acceleration term.

3. Run the program with only the frictional pressure drops accounted for.

In general, the designer will only need to use the first option ('R').

Model Output

After the program converges to a solution, the user is prompted for the name of the file to which the output will be written.

Summary of Modeling Project

The modeling project has to date developed a computer program capable of modeling the temperature and flow distributions of an unglazed transpired collector. The model incorporates the previous work done at NREL to characterize the heat exchanger effectiveness of the absorber, the pressure drop across the absorber, and the wind-driven convective losses of the collector. The program is useful for conducting parametric analysis to determine affect of varying one or more design parameters on the collector's performance and/or flow distribution. The program can also be useful to engineers designing optimally performing collectors that still meet specific design requirements.

Future work on the computer model includes: improving the convergence stability of the code, and the program's user interface. Now that the bulk of the model development has been completed, further testing and parametric analysis will be conducted at NREL and other institutions.

3.2 SIMAIR

3.2.1 Introduction

The SIMAIR computer program was developed by Enermodal Engineering Limited to simulate the performance of air-based solar heating systems for preheating building ventilation or process air. SIMAIR is a general purpose program which performs calculations using a one hour time step to ensure maximum accuracy. The purpose of using the SIMAIR program is to predict the long-term (annual) performance of any configuration of the Solarwall using Typical Meteorological Year (TMY) or actual weather data.

3.2.2 Efficiency Inputs

The SIMAIR program requires information on collector efficiency as an input. To characterize collector performance, a number of laboratory tests have been done at the National Solar Test Facility (NSTF) in Mississauga, Ontario. Three parameters were varied during the tests:

- collector face velocity (volume air flow per unit collector area);
- solar radiation intensity; and
- wind speed across the face of the collector.

Over the course of Task 14, three different curve fits have been used to model the efficiency of the Solarwall based on these results.

First, a simple quadratic equation was used to fit a curve through the laboratory test data. The shortcoming of this approach was that the curves did not pass through zero and the efficiency began to drop off beyond the highest collector face velocity measured. Still, the results of the simulations appeared to fit with the field test results from Ford of Canada reasonably well within the limits of the collector face velocity tested.

A second set of curve fits were developed by the Solar Thermal Research Laboratory (STRL) at the University of Waterloo. (See Part II, Chapter 2.) The form of the equations was developed using basic heat transfer theory. NSTF test results were used to develop the coefficients for the equations. These equations did pass through zero and did level off at higher collector flow rates. The results were found to underestimate the GM field test results. Two reasons for this were proposed. First, convective losses due to wind effects were overestimated when the ratio of wall area to perimeter length was increased. Second, the canopy increased heat collection and efficiency and these effects were not accounted for in the model.

The third set of equations were developed by the STRL on the basis of evaluation and testing performed at the National Renewable Energy Laboratory (NREL) in Boulder, Colorado, U.S.A. That work suggested that the loss of efficiency due to wind across the Solarwall was smaller than the NSTF data suggested. The form of the efficiency equation was changed to reflect reduced convective losses at higher collector face velocities. The coefficients were based on basic solar collector theory and test results from the NREL. Figure 3.6 shows the high wind and low wind curves of the original STRL curve fits in dashed lines and the modified STRL curves for no, low and high wind conditions in solid lines.

The final version of the efficiency equation produces results closer to, but approximately 10 % below, the field results from GM. The higher-than-predicted field results are attributed to the addition of the canopy. Further testing of canopy walls is currently underway. Results from these tests will allow performance verification and development of new SIMAIR models. Using the non-canopy SIMAIR model will produce conservative results, and actual performance can reasonably be expected to be higher by about 10 %.

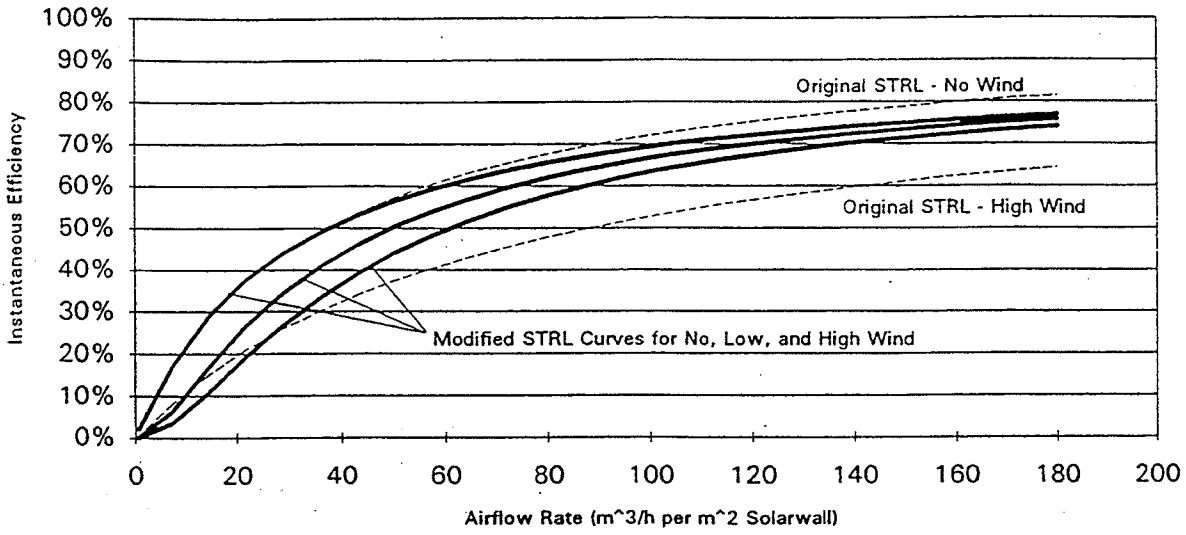

Figure 3.6 Original and Modified STRL Curve Fits

3.2.3 Other Inputs

Figures 3.7 and 3.8 show the SIMAIR input data sheet. Inputs are grouped into 5 sections which require parameters defining:

- collector size, orientation, and installation;
- collector efficiency;
- building heating load;
- building ventilation load; and
- stratification temperatures and fan locations.

Either TMY or monitored weather data can be used for the simulations. To use monitored solar radiation, air temperature, and wind speed are required and the data must be put into the same file format as the TMY data. The number of days to be analyzed can be defined. SIMAIR calculates the useful heating available from the Solarwall system based on the design of the system, the needs of the building, and the weather conditions.

```
*****************************************
*                                       *
*     SIMAIR  SIMULATION PROGRAM        *
*        -    VERSION 4.0               *
*                                       *
*****************************************

        OUTPUT DATA FILE : IEA-RPT.OUT
     DATE : 1994 12  1     TIME :  7:48
          IEA TASK 14 SAMPLE RUN

     SIMULATION PERIOD  - FIRST DAY :1
                        - LAST DAY  :365

****  SIMAIR - VERSION 4.0 INPUT DATA  ****
```

C. **COLLECTOR DATA**

C1	TOTAL COLLECTOR AREA (M^2)	197.00
C2	COLLECTOR SLOPE (DEGREES)	90.00
C3	COLLECTOR ORIENTATION (SOUTH=0,EAST=+, DEG.)	-5.00
C4	FAN POWER CONSUMPTION (W)	7500.00
C5	COLLECTOR BACK INSULATION (M^2-C/W)	1.20
C6	WIND SPEED AUGMENTATION FACTOR (0-5)	.30

T. **COLLECTOR TEST DATA**

T1	COLLECTOR NORMAL SOLAR ABSORPTIVITY	.95
T2	ABSORBER PLATE EMISSIVITY	.90
T3	FREE CONVECTION HEAT TRANSFER COEF.(W/M^2-C)	5.40
T4	FORCED CONVECTION HEAT TRANSFER COEF (J/M^3-C)	.03
T5	FACE VELOCITY HEAT TRANSFER COEF. (J/M^3-C)	.00
T6	PLATE EFFECTIVENESS MODIFIER (S/M)	.00
T7	INCIDENT ANGLE MODIFIER	

I	:	1	2	3	4	5
THETA	:	15.000	30.000	45.000	60.000	75.000
XKT	:	1.000	1.000	1.000	.980	.900

Figure 3.7: SIMAIR Input Data

Figure 3.8: SIMAIR Input Data (Continued)

B. BUILDING LOAD DATA

B1	BUILDING PERIMETER (M)	140.00
B2	THERMAL RESISTANCE OF WALLS (M^2-C/W)	2.25
B3	AREA OF ROOF (M^2)	1000.00
B4	THERMAL RESISTANCE OF ROOF (M^2-C/W)	5.25
B5	AVERAGE HEIGHT OF WALLS (M)	10.00
B6	DAILY INTERNAL HEAT GAIN (MJ/DAY)	2500.00
B7	HOURLY INTERNAL HEAT GAIN PROFILE (%)	100.00
	2.7780 2.7780 2.7780 2.7780 2.7780	2.7780
	5.5560 5.5560 5.5560 5.5560 5.5560	5.5560
	5.5560 5.5560 5.5560 5.5560 5.5560	5.5560
	2.7780 2.7780 2.7780 2.7780 2.7780	2.7780
B8	NATURAL INFILTRATION RATE (AIR CHANGES / HOUR)..	3.00
B9	MINIMUM DAYTIME BUILDING TEMPERATURE (C).....	21.00
B10	MINIMUM NIGHTIME BUILDING TEMPERATURE (C).....	21.00
B11	HOUR OF TEMPERATURE SETBACK (E.G. 23 = 11:00 PM)	23.00
B12	HOUR OF TEMPERATURE SET-UP (E.G. 7 = 7:00 AM)...	7.00
B13	BUILDING THERMAL CAPACITANCE (MJ/C).....	1500.00

V. VENTILATION LOAD DATA

V1	DESIRED DELIVERED AIR TEMPERATURE (C).....	-40.00
V2	OPERATING DAYS PER WEEK	6.00
V3	MAXIMUM COLLECTOR FLOW RATE (L/S).....	10380.00
V4	NORMAL EXHAUST AIR FLOW RATE (L/S).....	10380.00
V5	FRACTION OF FLOW RATE V3 EACH HOUR	.00
	1.000 1.000 1.000 1.000 1.000 1.000	
	1.000 1.000 1.000 1.000 1.000 1.000	
	1.000 1.000 1.000 1.000 1.000 1.000	
	1.000 1.000 1.000 1.000 1.000 1.000	
V6	FRACTION OF FLOW RATE V4 EACH HOUR	.00
	1.000 1.000 1.000 1.000 1.000 1.000	
	1.000 1.000 1.000 1.000 1.000 1.000	
	1.000 1.000 1.000 1.000 1.000 1.000	
	1.000 1.000 1.000 1.000 1.000 1.000	

S. STRATIFICATION DATA

S1	FLOOR-TO-CEILING TEMP. STRATIFICATION (C).....	4.00
S2	OUTDOOR TEMP. FOR COLLECTOR BYPASS (C).....	18.00
S3	% OF EXHAUST AIR INTAKES AT CEILING.....	100.00

3.2.4 SIMAIR Outputs

Figure 3.9 shows the general output available, and Figure 3.10 shows the detailed daily output available.

The general output provides:

- solar radiation incident on the collector surface;
- solar radiation available when the summer bypass damper is closed;
- total solar energy collected;
- useable solar energy delivered to the space i.e. the energy that does not exceed space heating requirements. Thermal storage in the building mass is included;
- savings attributable to insulation added with the installation of the Solarwall;
- savings attributable to destratification of building air;
- auxiliary energy required to meet the building heating load;
- total building heating load; and
- power required to operate the Solarwall fans.

Outputs are provided for each month or part thereof that is simulated. The values are then summed. An analysis can be made of the solar contribution provided in term of :

- the useable energy delivered;
- the percentage of the total heating requirement displaced;
- the percentage of the solar energy available with the bypass damper closed that is delivered to the space as useable heat; and
- the total solar energy delivered over the simulation period on a per square meter basis.

The detailed output provides information on a limited number of parameters on an hour-by-hour basis. The parameters include hourly average values of:

- ambient temperature;
- solar radiation available;
- useable solar energy delivered;
- auxiliary energy required to maintain space temperature at the set-point;
- total heating load of the building;
- the collector airflow; and
- the temperature of the delivered air.

The general and detailed outputs can be used to fine tune the design by determining the impact of various colours, orientations, temperature settings, airflow rates and so on.

****** SIMAIR - VERSION 4.0 ******

CITY DATA

LOCATION ..... TORONTO
LATITUDE OF LOCATION (DEG.)..... 43.9

COLLECTOR EFFICIENCY
AT FLOW V3 = .82
COLLECTOR AREA (M2) = 197.00

PERFORMANCE PREDICTION

FAN MONTH	SOLAR INCID. (GJ)	SOLAR AVAIL. (GJ)	SOLAR COLLECT (GJ)	SOLAR DELIVER (GJ)	INS. SAVING (GJ)	STRAT SAVING (GJ)	AUX. ENERGY (GJ)	SPACE HT LOAD (GJ)	POWER
JAN	55.65	55.65	37.47	37.47	2.35	188.18	1142.22	1370.23	20.09
FEB	63.97	63.97	42.35	42.35	2.20	169.76	1068.80	1283.12	18.14
MAR	85.43	85.43	60.38	60.38	2.06	192.65	972.30	1227.38	20.09
APR	63.61	61.81	45.16	45.16	1.36	186.08	619.25	851.84	19.44
MAY	54.72	41.09	30.34	30.34	.98	176.14	439.42	646.88	20.09
JUN	57.42	11.63	8.43	8.43	.45	91.57	196.83	297.28	19.44
JUL	57.95	.37	.23	.23	.22	37.75	96.53	134.73	20.09
AUG	74.67	2.41	1.64	1.64	.27	47.12	126.98	176.01	20.09
SEP	71.48	32.31	25.12	25.12	.62	113.41	274.42	413.56	19.44
OCT	70.25	64.33	49.82	49.82	1.19	186.12	532.07	769.19	20.09
NOV	45.07	41.92	31.12	31.12	1.60	186.02	749.87	968.60	19.44
DEC	36.18	36.18	23.87	23.87	2.20	188.37	1068.21	1282.64	20.09
YR	**736.4**	**497.1**	**355.9**	**355.9**	**15.5**	**1763.2**	**7286.9**	**9421.4**	**236.5**

ENERGY SAVINGS DUE TO SOLAR (GJ) :355.92

ENERGY SAVINGS DUE TO SOLAR (%) : 3.78

AVERAGE SOLAR SYSTEM COLLECTION EFFICIENCY (%) : 71.60

SOLAR CONTRIBUTION PER SQUARE METRE (GJ/M2) : 1.807

Figure 3.9 SIMAIR General Output

****** OUTPUT DATA FILE ******
: IEA-DTL.OUT

DATE : 1994 12 1 TIME : 7:58

SIMULATION PERIOD - FIRST DAY : 20 - LAST DAY : 20

SIMAIR - VERSION 4.0

CITY DATA

LOCATION ..... TORONTO
LATITUDE OF LOCATION (DEG.)..... 43.9

COLLECTOR EFFICIENCY
AT FLOW V3 = .82
COLLECTOR AREA (M2) = 197.00

DETAILED RESULTS FOR DAY 20

HOUR	AMB TEMP (C)	SOLAR RAD (W/M2)	SOLAR DEL (KJ)	SOLAR HEAT (KJ)	AUX. LOAD (KJ)	HEATING FLOW (L/S)	COLL TEMP (C)	DELIV
1	-9.0	0.	0.	789267.	2039941.	2270.6	15.0	
2	-10.0	0.	0.	1849651.	2100117.	2209.8	15.0	
3	-11.0	0.	0.	1909939.	2160207.	2149.0	15.0	
4	-11.0	0.	0.	1909939.	2160207.	2149.0	15.0	
5	-11.0	0.	0.	1909939.	2160207.	2149.0	15.0	
6	-9.0	0.	0.	1789267.	2039941.	2270.6	15.0	
7	-8.0	0.	0.	1660043.	1911035.	2351.7	15.0	
8	-8.0	8.	3167.	1658444.	1912820.	2392.3	15.0	
9	-7.0	245.	107374.	1528482	1892278.	3324.8	15.0	
10	-5.0	505	250031.	1326164.	1843017.	4865.6	15.0	
11	-1.0	666.	356040.	1051292.	1691746.	6852.4	15.0	
12	-1.0	882.	482826.	1010513.	1793389.	8190.5	15.0	
13	.0	869.	480947.	962328.	1748045.	8555.4	15.0	
14	.0	884.	494293.	960691.	1761987.	8717.6	15.0	
15	1.0	746.	407561.	932336.	1639206.	8149.9	15.0	
16	1.0	443.	227248.	998780.	1502566.	6082.0	15.0	
17	1.0	8.	3239.	1122843.	1382629.	3487.0	15.0	
18	.0	0.	0.	1182827.	1437987.	3243.8	15.0	
19	-1.0	0.	0.	1312486.	1567028.	3122.1	15.0	
20	-1.0	0.	0.	1312486.	1567028.	3122.1	15.0	
21	-1.0	0.	0.	1312486.	1567028.	3122.1	15.0	
22	-1.0	0.	0.	1312486.	1567028.	3122.1	15.0	
23	-1.0	0.	0.	1312486.	1567028.	3122.1	15.0	
24	-1.0	0.	0.	1312486.	1567028.	3122.1	15.0	

Figure 3.10 SIMAIR Detailed Daily Output

Chapter 1

Summary of Air-Preheating Collector Tests Made at the NSTF

1.1 Chronology of NSTF Tests of Air-Preheating Collectors.

The National Solar Test Facility (NSTF), operated by ORTECH International on behalf of the Canadian Government through Natural Resources Canada, played an important role in the development of the unglazed perforated-absorber collector. Thermal efficiency measurements of collectors having various absorber geometries have been performed at the NSTF starting in 1988. These measurements have provided quantitative evidence of the effect on thermal performance of suction air flow rate, wind speed, solar radiation intensity, absorber porosity, collector orientation, and absorber emissivity.

The tests that have been done at the NSTF are described in chronological order below, along with a brief description of the main physical characteristics of the collector and the purpose of the test. All of the different absorber types were mounted to the same test frame, and most were irradiated in the typical position shown in Figure 1.1. The collector box has a gross irradiated area of 4.65 m^2, and all efficiencies reported by the NSTF were based on this gross area. The net active area of perforated absorber was 4.25 m^2 for all tests except A0507. In early tests, the collector box was insulated with 76 mm of polystyrene and 25 mm of fibreglass. Before the 1993 tests—test report A0507—the collector box was reinsulated with 50 mm of polyisocyanurate insulation, and the box was well sealed against the higher pressure drop across the absorber plate expected for the tests on plates with porosities less than 1% of the absorber surface area. For the horizontal collector tests, air flow was extracted from a hole in the centre of the collector back. For all other tests, the air exited the collector at the top centre. The typical test configuration is shown in Figure 1.2. A wind deflector was used on most tests to direct the air parallel to the face of the collector from left to right.

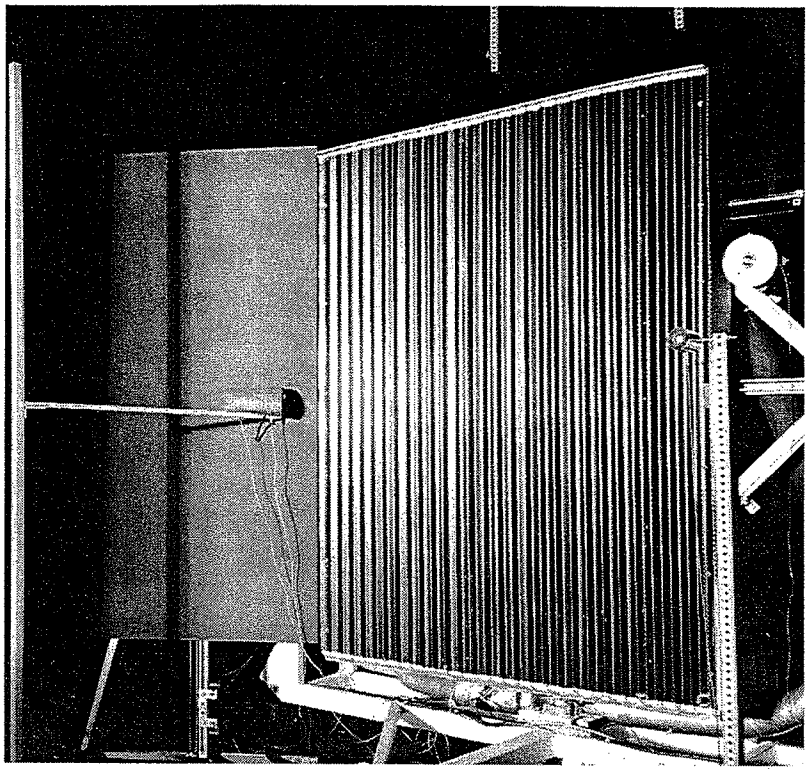

Figure 1.1 ***The perforated aluminum absorber set up for NSTF test A0402. The inlet air temperature sensor is inside the insulated cylinder at the left, in front of the black sheet that is positioned to direct wind flow across the face of the corrugated absorber. (Photo by P. Geisberger, NSTF)***

Initial Tests

Nine collector configurations were tested between December 20, 1988, and March 1990 to determine the relative performance of a fiberglass-glazed collector, a canopy collector, an unglazed collector with airflow behind the absorber, and a perforated-absorber collector. In these tests, the unglazed perforated absorber configuration performed better than all the other configurations. Subsequent tests focused on improvements to the perforated absorber design.

Report 90-29-A0398 (10-OCT-1990)

This test was carried out on corrugated, perforated aluminum sheet absorbers having perforations of 1% and 2% of the total absorber area. Efficiency was measured for irradiance levels from 300 to 900 w/m^2, suction flow rates from 0.03 kg to 0.19 kg/s, and no wind, low wind and high wind conditions. The average efficiency for the no-wind and low-wind cases for the 2% porosity absorber plate was 75%, and it was 70% for the 1% porosity absorber. The differences in efficiency between the 1% and 2% porosity plates were small for the no-wind tests, but the efficiency was up to 12 percentage points less for the 1% plate for the low wind cases. The absorber with 1% perforations was not tested at high-wind conditions. The average efficiency of the absorber with 2% perforations was 55% with high wind speeds.

Along with the NSTF tests reported in 90-29-A042 on January 16, 1991, these efficiency measurements became the basis for prediction of the perforated absorber collector systems on the Ford and General Motors buildings described in Part I, Sections 2.1 and 2.2.

Report 90-29-A0402 (16-JAN-1991)

A collector with a corrugated aluminum absorber with perforations covering 2% of its surface was tested in this series of tests. Collector efficiency was measured at nominal irradiance levels of 300, 600 and 900 W/m²; suction air flow rates of 0.035 kg/s (1.1 CFM/ft2), 0.11 kg/s (4 CFM/ft2) and 0.19 kg/s (7 CFM/ft2); and high, low and no wind speeds. The results were plotted along with data from test number A0398, and simple quadratic equations were fit to the data to represent the dependence of collector efficiency on suction air flow rate and wind speed. These simple correlations provided the basis for the simulations of the Ford, Oakville solar wall and for early simulations of the GM Oshawa solar wall. The summary of these tests is presented in Figure 1.2. A photograph of the test configuration is shown in Figure 1.1.

Report 92-E37-A0494 (26-NOV-1992)

This was a test of an aluminum absorber with a porosity of 1% and a horizontal orientation. The purpose of the test was to show how the horizontal collector performed compared to the vertical collector. The efficiency for both the horizontal collector (this test) and for a vertical collector (1% porosity absorber results for NSTF test No. A0398) are plotted together in Figure 1.3, from which one can conclude that collector orientation does not make a significant difference to collector efficiency. The efficiency is in some cases higher for the horizontal collector and in some cases higher for the vertical collector.

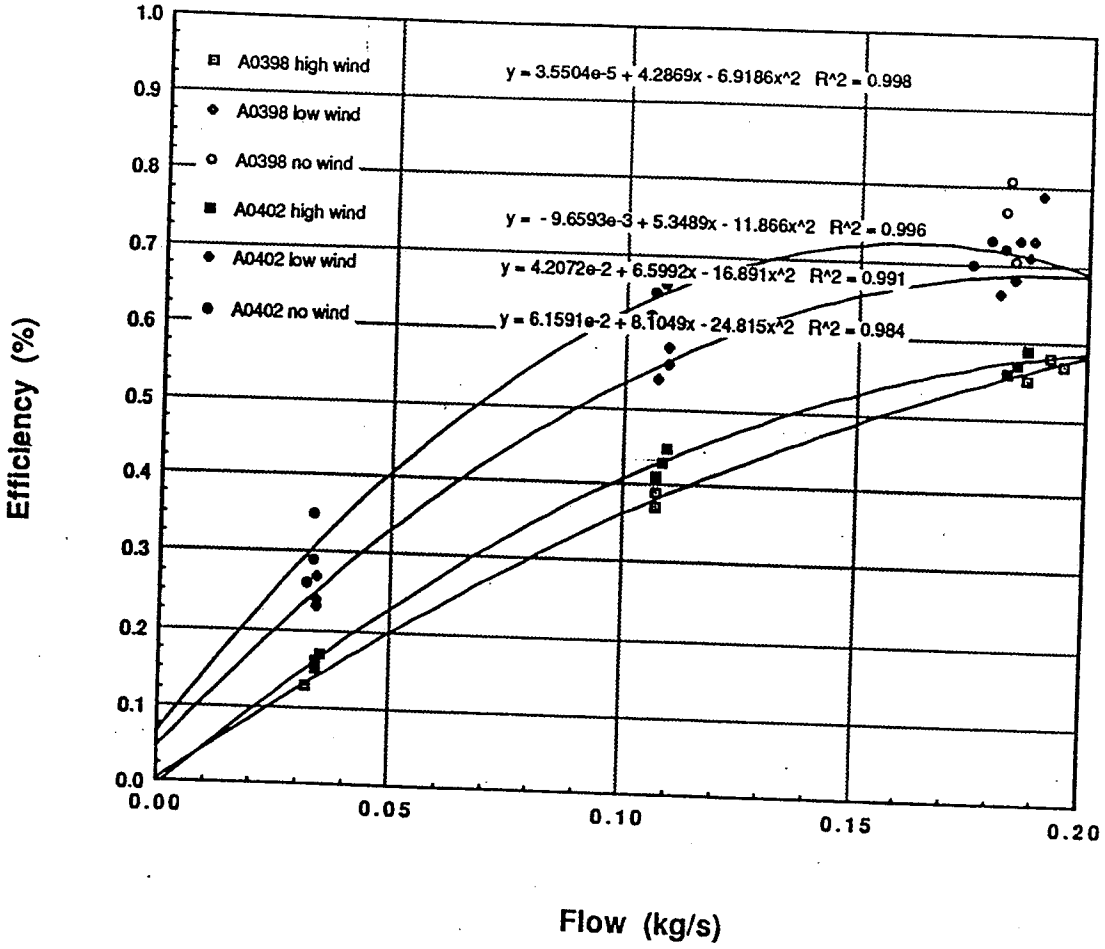

Figure 1.2 Measured Collector Efficiency from NSTF Test No. A0398 and A0402. (From NSTF test Report A0402)

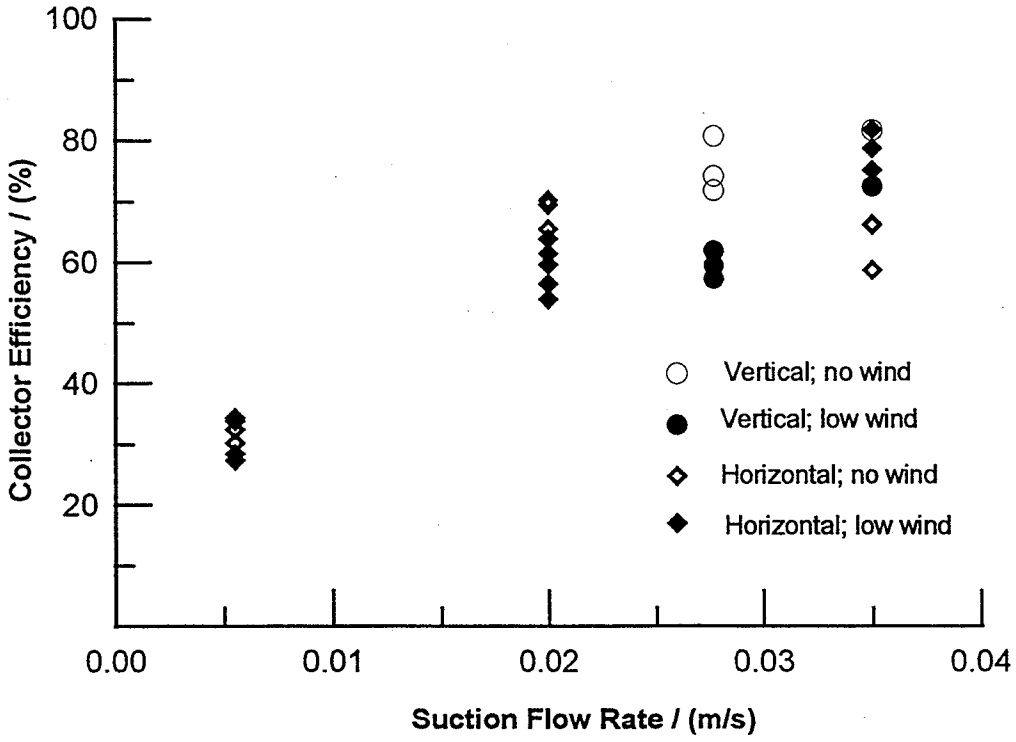

Figure 1.3 Comparison of 1% Porosity Absorber Efficiency for Vertical and Horizontal Collector Orientations

Reports 93-E37-B007801-A0507 (7-SEP-1993) and A0507B (22-DEC-1993)

These reports describe tests of perforated collectors with three different absorbers: one with a standard black paint coating with solar absorptivity of 0.95 and thermal emissivity of 0.87, one with Alcan "group#1" low emittance with absorber absorptivity of 0.94 and a thermal emissivity of 0.21, and one with an Alcan "group#3" low emittance coating with a solar absorptivity of 0.92 and a thermal emissivity of 0.42. Both absorbers had an active area of 2.45 m high by 1.625 m wide with perforation comprising 0.1% of the absorber area. The absorptivities and emissivities were measured at the NSTF by University of Waterloo personnel.

The performance of the two different paints are compared in Table 1.1. For all these test, the irradiance was 911 to 928 W/m^2, the collector was vertical, and the wind direction was parallel to the absorber.

Table 1.1: Comparison of Standard and Selective Paints

Air Flow Rate (m/s)	Wind Speed (m/s)	Collector Efficiency		
		Standard Absorber	Selective Surface	
			Group 1	Group 3
0.0052	0	0.32	0.42	0.39
	1.6	0.26	0.33	0.31
	3.1	0.21	0.26	0.25
0.0105	0	0.50	0.64	0.61
	1.6	0.41	0.51	0.48
	3.1	0.34	0.42	0.41
0.0209	0	0.65	0.80	0.79
	1.6	0.58	0.69	0.66
	3.1	0.52	0.60	0.59

Indoor/Outdoor Tests: Supplement to Report 93-E32-A0507 (SEP-1993)

These tests were carried out on September 24 and 30, 1993, to compare indoor NSTF test results with outdoor test results. The measured efficiency was a linear function of wind speed for the indoor tests, as shown in Table 1.1. The outdoor tests produced efficiencies from 0 to 6 percentage points below the corresponding efficiency for indoor conditions. On average, the outdoor efficiencies were 0.02 below the efficiencies given by equations in Table 1.2.

Table 1.2: Collector Efficiency for Indoor NSTF Tests

Test Condition	Collector Efficiency as a Function Wind Speed WS in m/s
Standard absorber, Medium flow (Vs = 0.009 m/s)	h = 0.49 - 0.045 WS
Standard absorber, Low flow (Vs = 0.0045 m/s)	h = 0.32 - 0.032 WS
Selective absorber, Medium flow (Vs = 0.009 m/s	h = 0.60 - 0.058 WS
Selective absorber, Low flow (Vs = 0.0045 m/s	h = 0.39 - 0.045 WS

Report 93-E37-B001802-A0507C (20-APR-1994)

The group#1 absorber tested in NSTF test number A0507B was retested at suction velocities of 0.0105 m/s and 0.0209 m/s, with no wind, but this time the steady state temperature of the absorber plate was measured at 12 locations. The measured efficiencies were within 0.006 of those measured in test A0507B. At the high flow rate (V_S = 0.021 m/s), the average plate temperature was 76.1 °C, the thermal effectiveness, ε_{HX}, was 0.615, and the collector efficiency was 80%. At the low flow rate (Vs = 0.0105 m/s), the average plate temperature was 92.0 °C, the thermal effectiveness was 76.1%, and the collector efficiency was 64.6%. In both tests, there was a general 3 °C rise in temperature from the bottom of the absorber plate to the top, and a general 6 to 7 °C temperature rise from the left side to the right side of the collector.

Chapter 2:

National Renewable Energy Laboratory (NREL) Studies

2.1 Introduction and Background

Unglazed transpired solar collectors offer a very low-cost, high-performance means for heating air on a once-through basis for applications such as ventilation preheat, crop drying, and desiccant regeneration. During the early workshop days of IEA Task 14, we spent a considerable amount of time thinking of new advanced heating ideas. By the summer of 1989 Craig Christensen had proposed an unglazed, transpired collector for preheating ventilation air. We first presented this concept at the summer ASES meeting in 1990 (Christensen, Hancock, Barker, and Kutscher). Some time in late 1989 we discovered that Conserval Systems Inc. of Toronto had also thought of this concept and had patented the idea (Hollick and Peter 1990). However, very little theoretical or experimental work had been done and, encouraged by Conserval's commitment to the concept, we embarked on a research program. We then developed the performance theory (Kutscher, Christensen, and Barker, 1991a) and then conducted tests on a small outdoor absorber (Kutscher, Christensen, and Barker, 1991b). Conserval has since installed a number of large outdoor systems (tradename "Solarwall") for preheating ventilation air and has reported good success. IEA Task 14 has provided an opportunity for the US to work with Conserval and Canadian researchers on the advancement of this concept.

2.2 Basic Theory

The overall heat balance on an unglazed transpired collector is:

$$\rho C_p V_s A_c \varepsilon_{HX} (T_s - T_{amb}) = I_c A_c \alpha_c - Q_{rad} - Q_{conv} \qquad (2.1)$$

where ρ is the air density in kg/m^3, C_p is the constant pressure specific heat in J/kg-K, V_s is the suction face velocity in m/s, A_c is the collector area in m^2, ε_{HX} is the heat exchange effectiveness (ratio of suction air temperature rise to maximum possible temperature rise), T_S is the surface temperature in K, T_{amb} is the ambient temperature in K, I_c is the solar radiation incident on the collector in W/m^2, α_c is the collector absorptance, Q_{rad} is the collector radiant heat loss in W, and Q_{conv} is the collector convective heat loss in W.

The left-hand side of this equation represents the useful energy collected. The first term on the right-hand side is the solar energy absorbed by the absorber, and is straightforward to calculate. Note that I_c is the total radiation striking the absorber including direct, diffuse, and reflected. The second and third terms are, respectively, the losses to the environment via radiation and convection.

The two most significant unknown terms are the convective heat loss term and the heat exchange effectiveness. The latter determines the surface temperature which, in turn, affects the radiative heat loss.

From the energy balance equation, the collector efficiency can be written as:

$$\eta = \dot{m} C_p \varepsilon_{HX} (T_s - T_{amb}) / I_c A_c$$

$$= \alpha_c / [1+(h_r + h_c) A_c / \dot{m} C_p \varepsilon_{HX}] \qquad (2.2)$$

where h_r is the linearized radiation heat loss coefficient in W/m^2K, and $\dot{m}$ is the suction mass flow rate in kg/s.

The radiation heat loss coefficient is straightforward to determine. It is as follows.

$$h_r = \varepsilon \sigma_{sb}(T_s^4 - F_{cs}T_{sky}^4 - F_{cg}T_{gnd}^4) / (T_s - T_{amb})$$

$$\approx 4\varepsilon \sigma_{sb} T_{avg}^3 (T_s - T_{sur}) / (T_s - T_{amb}) \qquad (2.3)$$

In this equation, ε is the surface emissivity, σ_{sb} is the Stefan-Boltzmann constant, F_{cs} and F_{cg} are view factors to the sky and ground, respectively, and T_{sur} is an average temperature of the surroundings in K.

In order to determine the performance of a transpired collector, we still must know the convective (wind) heat loss and the heat exchange effectiveness. The objectives of recent work at NREL were to determine the effectiveness as a function of hole size and spacing, suction flow rate, and wind speed, and to verify the previously developed theory of wind heat loss as given by Kutscher, Christensen, and Barker (1991a). Because pressure drop information is needed to estimate fan power and ensure wall flow uniformity, pressure drop data were also obtained for various plate geometries. The analytical, experimental, and numerical work done to obtain these results is covered in Kutscher (1992). The remainder of this section summarizes some key results from that document.

To experimentally determine the needed information under controlled conditions, a wind tunnel and small solar simulator were designed and constructed. The open circuit wind tunnel provides wind speeds of 0 to 10 m/s, and its design allows easy heat transfer visualization with an infrared camera. The solar simulator provides a flux of up to 1200 W/m^2 on test absorbers of dimensions 30 cm by 50 cm, with a spatial uniformity of better than ±2%. Suction face velocities of 0 to 0.1 m/s can be tested.

Kutscher, Christensen, and Barker (1991a) showed that the wind heat loss can be expressed as:

$$Q_{conv} = 0.82 (U_\infty \nu / V^2) W [\rho c_p V_s (T_s - T_{amb})] \qquad (2.4)$$

where U_∞ is the wind speed in m/s, ν is the kinematic viscosity in m^2/s, and W is collector width in m. For a large wall, this quantity is negligibly small relative to the energy collected. The convective heat transfer coefficient is just $h_c = Q_{conv}/A_c(T_s - T_{amb})$.

The theory used to develop this expression assumes a homogeneous suction surface. Laboratory wind tunnel tests showed that the measured wind heat loss for a black fabric absorber (which closely approximates the ideal surface) is well modeled by equation (2.4). Flat, perforated plates over a considerable range of hole spacings also exhibit quite good agreement with this equation. Although some deviations with the theory can be seen with larger hole pitches (where pitch is the distance between two closest holes), the theoretical

prediction that wind heat loss is negligible for a large collector operated at typical suction flow rates for vent preheat applications is quite reasonable.

With the wind heat loss known, the major remaining unknown for predicting thermal performance is heat exchange effectiveness. This was measured for a wide range of perforated plates tested in both horizontal and vertical orientations. The resulting correlation for Nusselt number for a vertical orientation is:

$$Nu_D = 2.75\,[(P/D)^{-1.21}\,Re_D^{.430} + 0.0110\sigma Re_D\,(U_\infty / V_s)^{.480}] \qquad (2.5)$$

where D is hole diameter in m, P is hole pitch in m, Re_D is hole Reynolds number (based on hole diameter and air velocity in the hole), and σ is the porosity.

The effectiveness can be written as:

$$\varepsilon_{HX} = 1 - e^{-NTU} \qquad (2.6)$$

where NTU is the number of heat transfer units and

$$NTU = UA / \rho V_s A_c C_p = (A / A_c)\,(U / \rho V_s C_p) \qquad (2.7)$$

where U is the overall heat transfer coefficient in W/m^2-K based on the log mean temperature difference, A is the plate surface area minus the hole area in m^2, and the ratio A/A_c can be expressed in terms of the porosity, $\sigma = .907\,(D/P)^2$, as:

$$A / A_c = 1 - \sigma \qquad (2.8)$$

Noting that the overall heat transfer coefficient, U, can be expressed in terms of the Nusselt number as:

$$U = Nu_D\,(k / D) \qquad (2.9)$$

where k is the thermal conductivity of the air (W/m-K), these can be combined to obtain the effectiveness as:

$$\varepsilon HX = 1 - \exp[(\sigma - 1)\,k\,Nu_D / (\rho V_s C_p D)] \qquad (2.10)$$

This effectiveness can be plugged directly into the collector efficiency equation (2.2), thus yielding the efficiency as a function of suction flow rate, surface optical properties, and hole geometry.

Numerical modeling of this problem was also done using the FLUENT computer code. An axisymmetric flow model was done to simulate zero-wind suction flow through a single hole. This model was run over a range of hole diameters and pitches, and the overall results showed good agreement with the zero-wind test results especially at higher plate porosities. Model results were used to generate individual heat transfer correlations for the front surface, hole, and back surface. In general, the great majority of the heat transfer occurs on the front surface. A three dimensional FLUENT model using boundary-fitted coordinates was also developed and has recently become operational on a work station. Preliminary results with this model clearly show that flow separation occurs in the holes in the presence of a crosswind.

2.3 Effect of Thermal Conductivity

All of the heat exchange effectiveness tests were done for flat, aluminum plates, such as those used by Conserval. Because we would like to have the flexibility to use non-metallic materials (e.g., a perforated, roll-out plastic sheet for crop drying), we have also investigated the effect of thermal conductivity. Numerical simulations showed that when geometrically identical plates are modeled under the same flow conditions, large changes in conductivity had a relatively small effect on heat collection. The two plates

modeled consisted of aluminum, with a conductivity of 216 W/m-K, and hard cardboard, with a conductivity of 0.14 W/m-K. For these plates, the pitch spacing of the holes is 13.5 mm, and the hole diameter is 3.2 mm. When the approach velocity is 0.02 m/s and there is no crosswind, the outlet temperature of a low conductivity plate is 322.2 K for an inlet temperature of 300 K. When the conductivity is changed to that of 6000 series aluminum, the outlet temperature rises to 325.0 K. The average plate surface temperatures for the high and low conductivity plates are 334.7 K and 340.2 K, respectively. The results show a 10% decrease in heat collection when the conductivity is changed by three orders of magnitude. When approach velocity is increased to 0.07 m/s, the aluminum plate's outlet temperature is 308.3 K and that of the cardboard plate, 307.4 K. This represents an 11% decrease in heat collection.

Experimental work showed that the difference in performance between actual plates with low and high thermal conductivities was low enough to be within the uncertainty of the apparatus. The experimental work used plates of aluminum and styrene, which has a conductivity of 1.2 to 1.9 W/m-K. Plates with a pitch spacing of 13.5 mm and hole diameter of 3.2 mm were used to match the geometry of the numerical model.

Another pair of plates was also tested which had a pitch spacing of 27.0 mm and a hole diameter of 1.6 mm; this latter pair had the same porosity as the former set. Over the range of approach velocities from 0.02 to 0.06 m/s, the outlet temperature differences between the plates of identical geometry but differing material was too small to measure accurately. One would have expected the temperature difference to be lower than predicted by the numerical work, since the conductivity values spanned only two orders of magnitude.

2.4 Pressure Drop Results

Because of a paucity of reliable data on pressure drop for flow through low-porosity perforated plates, a pressure drop correlation was also determined experimentally. The nondimensional pressure drop was found to be:

$$\zeta = 6.82\ Re_D^{-.236}[(1 - \sigma) / \sigma]^2 \qquad (2.11)$$

The designer can find the pressure drop as:

$$\Delta P = \rho V_s^2 \zeta / 2 \qquad (2.12)$$

As of this writing, a correlation for pressure drop in the presence of a cross-wind has not been completed. However, based on wind tunnel results to date, a wind speed of 3 m/s can be expected to increase the pressure drop on the order of about 10%.

2.5 Results for Corrugated Absorber

All of the above results are for flat perforated plates of .79 mm thickness. (Experimental tests showed that there is very little sensitivity to thickness.) In practice, the absorbers are often corrugated to improve structural rigidity. Preliminary laboratory tests with a Conserval corrugated plate of the type used in NREL's Waste Handling Facility, indicate that for zero-wind cases, heat exchange effectiveness is greater than and pressure drop is less than that of a flattened plate. However, the flat plate correlations are still fairly accurate provided one corrects the velocity according to the ratio of projected-to-actual area. For the Conserval plate, the ratio is only about 1.08, so the effect is fairly small. Tests in which wind is blowing perpendicular to the corrugations reveal that the low recirculation velocities that occur in the troughs reduce total heat transfer as compared with the noncorrugated case, although the effect is small.

While the effect of the corrugations on heat exchange effectiveness is relatively minor, the same cannot be said of wind heat loss. Preliminary wind heat loss tests show that the corrugations increase loss significantly as compared with a flat plate. Convective heat loss is the energy contained in the thermal boundary

layer which blows off the downstream edge of the collector in the presence of a cross wind. Most of the work to date has been experimental in which a corrugated, aluminum plate has been tested under a variety of approach and cross wind velocities.

Two means of measuring convective heat loss are used in the laboratory. One is to measure the incident short-wave radiation on the plate and subtract from that value the net long-wavelength radiation to the lab environment. The energy transferred to the outlet air stream is subtracted from the net radiation absorbed by the panel to determine the heat lost from the downstream edge of the collector. This method suffers a relatively high uncertainty in the result, mainly due to uncertainty in the measurement of radiation.

The other means of measuring heat loss is to make direct measurements of the velocity and temperature boundary layers using a traversing TSI hot wire anemometer. For velocity measurements, the system is used as an anemometer. For temperature measurements, the hot wire probe, which uses a 4 micron diameter tungsten wire, is used as a resistance thermometer. This method has been quite successful in making the heat loss measurement. The accompanying graph shows the velocity and temperature boundary layers for a Conserval corrugated perforated plate with a quasi-sinusoidal shape, with a mass flux through the plate of 0.03 kg/m^2-s and a cross wind speed of 2 m/s. Net radiation on the plate is approximately 750 W/m^2. The velocity and temperature boundary layers have been non-dimensionalized with respect to plate surface and free-stream velocities and temperatures. The heat loss from the subtractive method is 82 W per unit width of collector. The heat loss determined by integrating the measured velocity and temperature boundary layers is 83 W/m. A flat plate collector under similar conditions would have a convective heat loss of approximately 17 W/m. The agreement between the two heat loss measurements is good, but the uncertainty of the hot wire system is less than that of the subtractive method.

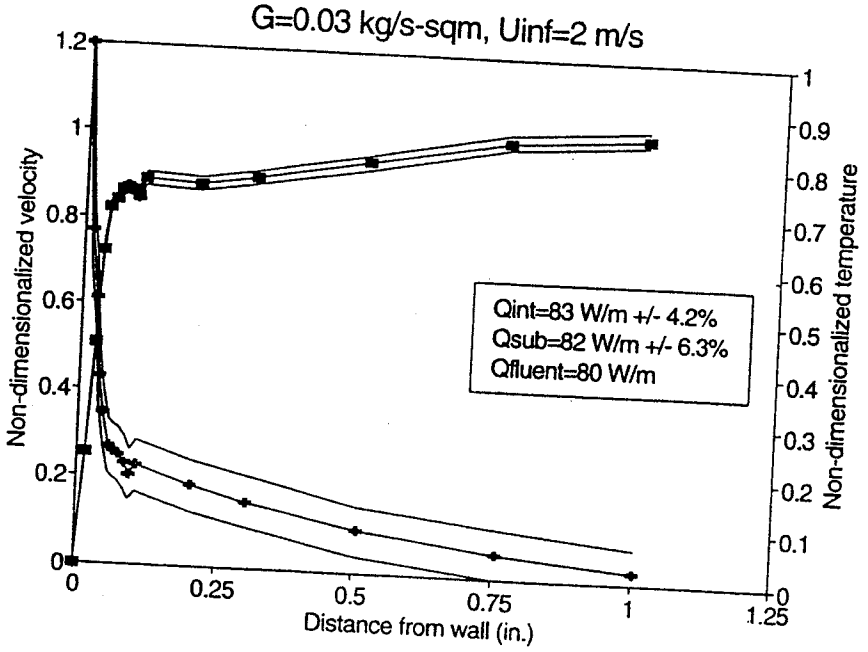

Figure 2.1 Velocity and temperature boundary layers for a Conserval Corrugated Plate

Numerical work is currently under way to model the corrugated plate in a cross wind.

Velocity and temperature profiles are being determined at the same locations as in the experimental work. Comparisons between the numerical and experimental studies will determine the usefulness and accuracy of a numerical model.

It should be pointed our that in a large collector wall, the wind heat loss is still expected to be very small relative to collected energy. The above results for wind heat loss are meant to be useful for small transpired collector applications

2.6 Adjustable Test Wall

Infrared thermography images of the adjustable test wall installed on NREL's Bulk Storage Facility show excellent flow uniformity. This is achieved through a combination of a 1% porosity absorber, a specially designed constant velocity header across the top of the wall, and an adjustable plenum depth. This wall is now completely instrumented for flow rate (Annubar flowmeter with MKS pressure transducer), delta T (thermopile array), incoming solar radiation (Eppley pyranometer), and long-wave radiation (Eppley pyrgeometer). Individual thermocouples were also installed on the absorber surface and at various depths in the plenum to measure heat exchange effectiveness as a function of height in the plenum. All data are read by an HP-3497 that is controlled by an IBM PC-AT programmed in Microsoft Quick Basic.

Installation of the instrumentation in this building was not encumbered by the space restrictions experienced in the Waste Handling Facility. Thus there is not a problem with radiation error on the thermocouples, and the flowmeter installation is a good one, with sufficient lengths of straight duct upstream and downstream (a honeycomb flow straightener is also used upstream). Unlike the Waste Handling Facility, however, this system only operates periodically to perform specific tests.

Overall efficiency measurements on this wall are consistently on the order of 75%. We believe this is the highest efficiency active solar air heating installation in existence. This improved performance relative to commercial installations (that have typical efficiencies on the order of 60%) can be attributed to the flow uniformity features described above as well as to the high heat exchange effectiveness resulting from the small holes (0.79 mm diameter) and small hole spacings.

The Bulk Storage Facility test wall was built for two purposes: 1) to demonstrate the high efficiencies that can be achieved with transpired collectors in actual outdoor conditions, and 2) to experimentally investigate flow uniformity issues.

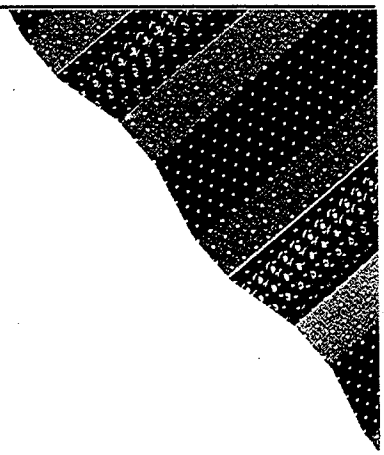

Chapter 3

Solar Thermal Research Laboratory (STRL) Studies

3.1 Overview of STRL Studies of Perforated-Absorber Collectors

The Solar Thermal Research Laboratory (STRL) at the University of Waterloo in Canada started work on unglazed perforated-absorber collectors (also called transpired collectors) in 1990 with the work of PhD student Ali Golneshan. Between 1990 and 1995, under the sponsorship of Natural Resources Canada (NRCan) and the Natural Sciences and Engineering Research Council (NSERC), we studied the modelling of unglazed transpired collectors by analyzing the measured performance of small and large collectors, by numerical simulations of the heat and air flow near perforated absorbers, and by direct experimental measurements of collector efficiency and absorber thermal effectiveness of slotted-plate absorbers. By mutual agreement stemming from discussions held in 1990, the work at NREL and the work at the STRL followed complementary paths during these earlier years. The work at NREL was focused on the theoretical behaviour of an absorber with continuous suction (infinitely small holes) and the experimental determination of the applicability of that theory to practical absorbers with discontinuous suction through absorbers with discrete circular holes spaced about 1 to 2 cm apart. The early work at the STRL was focused on the measurement and modelling of absorbers with slots rather than holes. (More recent work has included measuring and modeling of absorbers with circular holes, including thick and non-metal plates.) The flow over and through a slotted absorber is two-dimensional. The flow over and through an absorber with circular holes is three-dimensional, therefore resulting in somewhat different hydrodynamic and thermal behaviour. The theory of the hydrodynamic and thermal performance of the slotted absorbers, supported by experimental measurements and numerical simulations, is reported in the PhD thesis of Dr. Ali Golneshan (1995). From 1990 to early 1993, this STRL work was supported by NRCan-CANMET, and after that was supported by NSERC, Canada. A Strategic Grant from NSERC for the period 1991 to 1994 provided support for numerical modelling work in the STRL, carried out by MASc. students Shu Cao, Lowy Gunnewiek and Sarah Arulanandam. In August 1993 the STRL became an official part of IEA Task 14, and since then some work by Alfred Brunger on analyzing monitored data from the GM Perforated collector in Oshawa, Canada was supported by NRCan-CANMET.

A summary of the results of the STRL work on unglazed perforated absorbers during the period 1990-1995 is presented in this chapter. More details of the work can be found in reports prepared for NRCan and in the Theses of students who have worked in the STRL on this research. The development of simple collector efficiency equations, calibrated against measurements made at the Canadian NSTF, is described in Section 3.2. Those equations are used to quantify the effect of absorber thermal emittance and solar absorptance on collector efficiency. Section 3.3 contains the results of an analysis of measurements made on the Perforated collector on the General Motors (GM) battery manufacturing plant in Oshawa, Canada. The work that MASc. student Lowy Gunnewiek did on modelling the flow and heat transfer in the whole collector is summarized in Section 3.4, and a comparison with the calculations of TCFLOW is given in Section 3.5.

3.2 Effect of Absorptivity and Emissivity on Collector Efficiency

3.2.1 Introduction

In support of the research on selective surface development being done by Alcan for NRCan-CANMET, the STRL undertook an analysis 1995/6 of the potential for improving the efficiency of unglazed air-heating collector systems by using absorber plates having wavelength-selective optical properties. The results of this analysis have application to ventilation air pre-heating systems, crop-drying systems, and combustion air pre-heating systems.

There is current interest by the industrial users of active ventilation air pre-heating systems to use lighter colour absorber plates for perforated collectors. The lighter colours necessitate a lower absorptance of the visible wavelengths of the solar radiation, but the solar absorptance need not be small outside the visible range. Furthermore, a decrease in solar absorptance may be acceptable if it is accompanied by a decrease in thermal emittance.

In contrast to that of glazed flat plate collectors, the science of the thermal efficiency of the unglazed, perforated-plate collector is still in the development stage. The fact that the air pre-heating collector heats ambient air simplifies the analysis, since then the efficiency is not a function of $(T_{fi} - T_a)/G$ as it is in most other active solar heating systems. On the other hand, the efficiency of a perforated solar wall is a strong function of suction flow rate and (as indicated by NSTF tests (NSTF, 1990-1992)) ambient wind speed. Therefore, before we could quantify the effects of solar absorptance (α) and thermal emittance (ε) on Perforated collector efficiency, it was necessary to investigate the dependence of collector efficiency on other environmental and operational variables. This investigation is described in Section 3.2 of this report, in which the available measured collector efficiency data are used to calibrate an efficiency equation based on an overall heat balance on the Perforated collector.

The calibrated collector efficiency model is then used to produce plots of efficiency versus suction flow rate for a full range of absorber plate absorptance and emittance values.

3.2.2 Derivation of a Collector Efficiency Equation Satisfying Energy Conservation and Correlated to NSTF Measurements

Although a large perforated-plate collector wall is a complex (and under some operating conditions inhomogeneous) system, the application of conservation of energy to the entire collector can be used to derive a physically valid equation for the overall collector efficiency. An energy balance on the absorber plate leads to the efficiency equation (2.2) on page 101, which can be written in terms of the suction face velocity, V_s, as

$$\eta = Q_u / G = \alpha / [1 + (h_r+h_c) / (\rho C_p V \varepsilon_{HX})] \qquad (3.1)$$

The collector efficiency is roughly proportional to α, because h_r, h_c and ε_{HX} are only slightly influenced by α.

Since it derives from conservation of energy, equation (3.1) is the fundamental physically based efficiency equation for an unglazed transpired plate collector that is heating ambient air. This equation is valid for any part of a collector over which V_s, h_r, h_c, ε_{HX}, and T_p are constant. For a collector section over which these 5 parameters vary, (3.1) can still be used, with the understanding that all parameters on the right-hand side are appropriately averaged over the collector plate surface.

The model development starts from the general collector efficiency equation (3.1), but to simplify and make more exact the determination of the radiative heat transfer coefficient, it is convenient to deal, not with η, but rather with the collector efficiency for total (longwave plus shortwave) radiation (Saltau, 1992),

$$\eta' = Q_u / (A_c \alpha G') \quad (3.2)$$

where

$$G' = G + L \varepsilon / \alpha . \quad (3.3)$$

L is the net incoming longwave irradiance on a surface that is in the collector plane and is at the ambient air temperature. For the indoor test conditions at the NSTF, $G' = G$, and $\eta' = \eta$. For the outdoor operating conditions at the GM Battery Plant in Oshawa, L is measured by an Eppley PIR pyrogeometer, so it is possible to calculate G' from (3.3) and η' from (3.2). The relationship between η' and η is

$$\eta = \eta' [1 + \varepsilon L / \alpha G] \quad (3.4)$$

Because of the small amount of data available to fit the model efficiency equations to, simple linear equations were chosen to represent h_c and ε_{HX}. The linear equations were fitted to the set of efficiency measurements made in 1992 at the National Solar Test Facility[1]. The resulting equations for the efficiency of the collector are given below. The collector efficiency predicted by these equations is compared to the NSTF test data in Fig. 3.1.

$$\eta' = \alpha / [1 + (h_r' + h_c) / (\rho C_p V_s \varepsilon_{HX})] \quad (3.5)$$

$$h_r' = 4\varepsilon\sigma_s T_a^2 (T_a + 1.6\, t) \quad (3.6)$$

$$h_c = 6.0 + 4.0\, U_\infty - 76\, V_s \quad (3.7)$$

$$t = \alpha G' / [\rho C_p V_s \varepsilon_{HX} + 4\varepsilon\sigma_s T_a^3 + h_c] \quad (3.8)$$

$$\varepsilon_{HX} = 1.0 - 5.0\, V_s \quad (3.9)$$

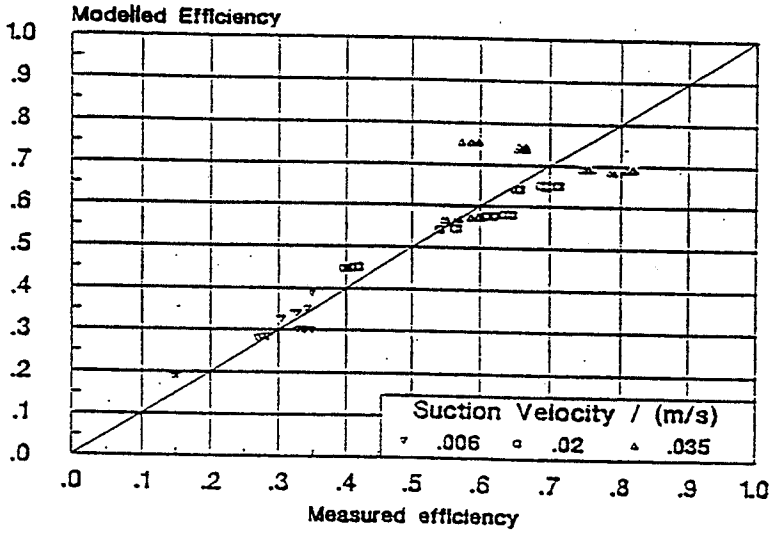

Figure 3.1: Comparison of predicted and measured collector efficiency.

[1] *National Solar Test Facility Report No. 92-E37-A0494, ORTECH Corporation. See Part II, Chapter 1 in this book for a description of the tests.*

3.2.3 Effect of α and ε on Collector Efficiency

Figures 3.2 and 3.3 show the effects of solar absorptance, α, and thermal emittance, ε, on collector efficiency as predicted by equations (3.5) to (3.9). The solar absorptance has the largest effect, since collector efficiency is roughly proportional to α. The absorber plate emittance affects the radiant heat loss from the plate, so its effect is similar to the effect of changing the overall collector heat loss coefficient.

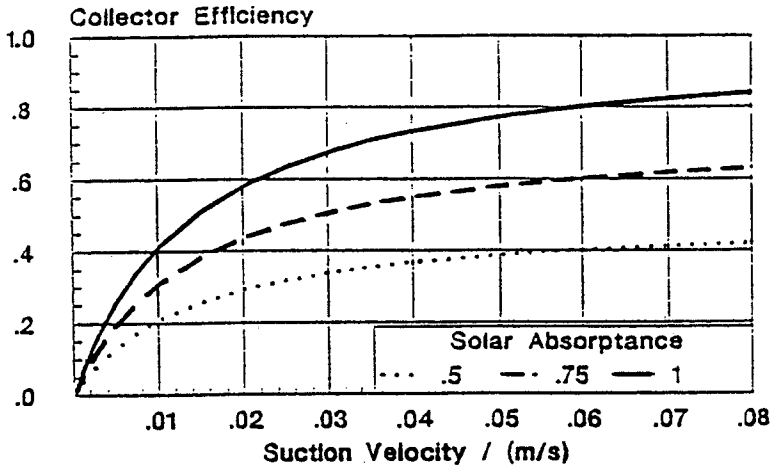

Figure 3.2: Effect of α on collector efficiency.

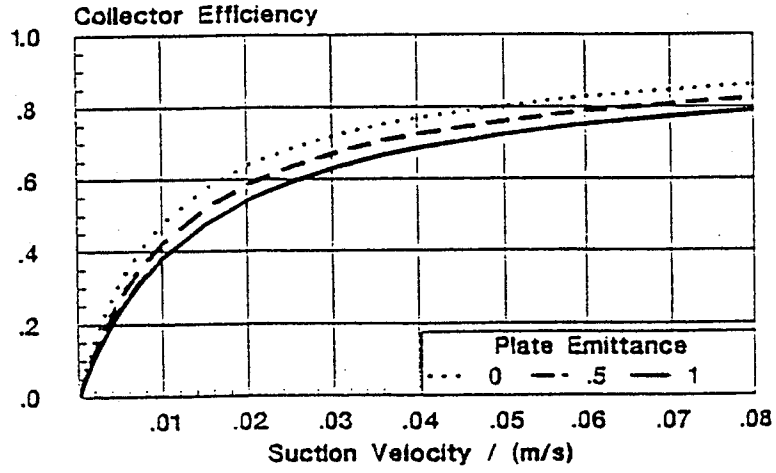

Figure 3.3: Effect of ε on collector efficiency at a = 0.95.

3.3 Analysis of GM Battery Plant Data

3.3.1 Introduction

An analysis was done on the monitoring data collected at the General Motors Canada Battery Plant in Oshawa, Ontario, during the spring of 1993. This ventilation air preheat system is described in Section 2.1 of Part I of this report. The emphasis of this analysis was to separately quantify the various heat flows making up the energy balance on the Perforated collector connected to the west fan unit of the collector. The ultimate goal of this work was to extract the most valid data from these measurements so that a comparison could be made against the theoretical transpired plate collector model.

3.3.2 Overall Heat Balance Equations

The calculation of any of the six components of the heat transfer to or from the Perforated collector must start with an overall heat balance equation for the collector. Since the GM Perforated collector required careful consideration of the different areas involved in the heat flows, the following heat balance was written in units of Watts rather than using an area-averaged equation.

$$Q_{sol} + Q_{IR} + Q_{wall} = Q_u + Q_r + Q_c\,, \tag{3.10}$$

where

$$Q_{sol} = \alpha G A_g \tag{3.11}$$

$$Q_{IR} = A_c\, F_{col\text{-}sur}\, \varepsilon \Phi \tag{3.12}$$

$$Q_{wall} = A_r\, U_{wall}\, (T_{room} - T_{cavity}) \tag{3.13}$$

$$Q_u = mC_p(T_{out} - T_a) \tag{3.14}$$

$$Q_r = A_c\, F_{col\text{-}sur}\, T_p^{\,4} \tag{3.15}$$

$$Q_c = A_{con} h_c (T_p - T_a) \tag{3.16}$$

In these equations, A_g is the equivalent area of the collector exposed to solar gain; $F_{col\text{-}sur}$ is the geometric configuration factor for radiation heat transfer from the collector to the surroundings ($F_{col\text{-}sur}$ = 0.909, since some of the radiation leaving the collector hits the collector rather than the surroundings); A_c is the area of collector surface corresponding to $F_{col\text{-}sur}$—that is, the total area of the canopy and perforated wall—$A_c = A_g(9.9)/(8.2)$; A_r is the wall area behind the collector on the indoor side of the building wall; G is the solar irradiance; m is the air mass flow rate through the collector; α = 0.95 is the solar absorptance of the collector's absorber plate; ε = 0.87 is its thermal emittance; Φ is the incoming longwave irradiance as measured by a pyrgeometer; U_{wall} is the thermal conductance of the building wall behind the collector; A_{con} is the area representative of thermal losses via convective heat transfer from the collector to its environment; h_c is the convective coefficient for heat loss to the environment. The heat capacity of air, C_p, is assumed to be constant at 1006 J/kg K.

In equation (3.10) the incoming longwave irradiance, Q_{IR}, is considered separately from the radiative losses, Q_r, since Q_{IR} varies with the temperature of the surroundings. The pyrgeometer measurements made at the GM Battery Plant were used to more accurately calculate the radiative heat losses from the wall for all of the 1993 data analyzed. (Note, however, that the pyrgeometer measurements are subject to uncertainties of up to ±15%.)

The calculation of the quantity Q_{wall} presents some difficulty because U_{wall} is unknown. From a plot of Q_{wall} versus $(T_{room}\text{-}T_{cavity})$ made from an energy balance on the absorber for nighttime periods when the absorber was at ambient temperature, the $(A_r\, U_{wall})$ was estimated to be 558 W/K.

3.3.3 Calculation of Q_C and Correlation with V_S and U_∞

Q_C was found for the daytime periods from

$$Q_c = Q_{sol} + Q_{IR} + Q_{wall} - Q_r - Q_u ,$$

or

$$Q_c = A_g\alpha G + A_c F_{col\text{-}sur}(\Phi - \sigma_s T_p^4) + (A_r U_{wall})(T_{room} - T_{cavity}) - mC_p(T_{out} - T_a) . \quad (3.17)$$

Figure 3.4 shows the values of Q_C calculated from (3.16) for all of the 1179 fifteen-minute periods in March 1993 when both fans were running. Both positive (heat losses) and negative (heat gains) values are present over a wide range of temperature differences, indicating a large uncertainty in the calculations of Q_C. Most of the points are for -10,000 W $\leq Q_C \leq$ 10,000 W and for -2 °C $\leq T \leq$ 5 C, with only about 10% of the cases showing a high correlation between Q_C and T. Seventy-five percent of the points are for temperature differences less than 4 °C, and for these the convective heat transfer is less than about 44 W/m², and fairly independent of ΔT.

The product $A_{con}h_C$ was calculated for each time period for which $\Delta T > 4$ °C from

$$A_{con}h_c = Q_c/(_p - T_a) ,$$

and the results are shown plotted as a function of wind speed in Figure 3.5. There is a definite correlation seen with wind speed, but the scatter is quite large.

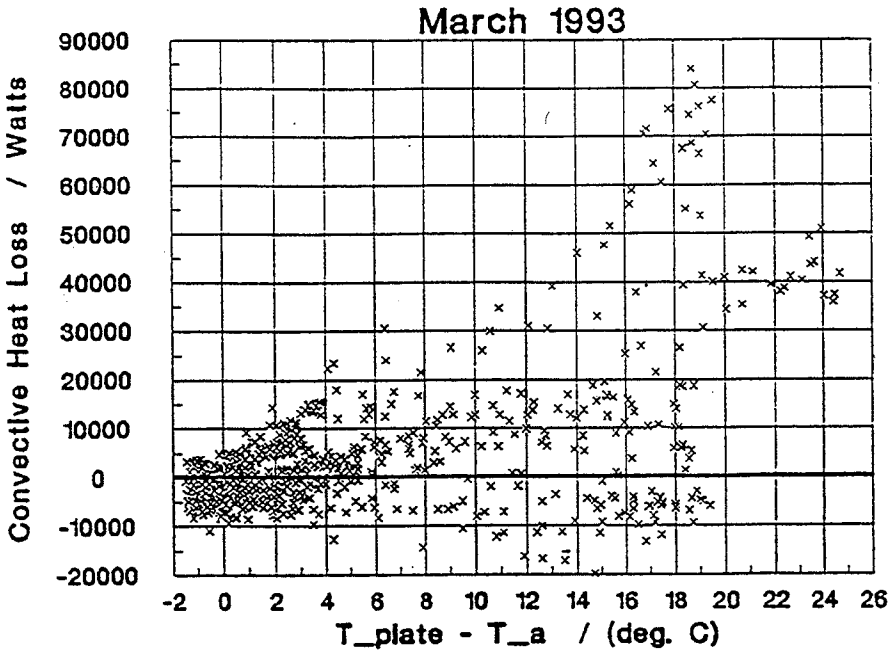

Figure 3.4: The convective heat loss from the Perforated collector plotted against the difference between the average absorber plate temperature and the south side air temperature. 1179 points are plotted for all day and night periods when both fans were operating.

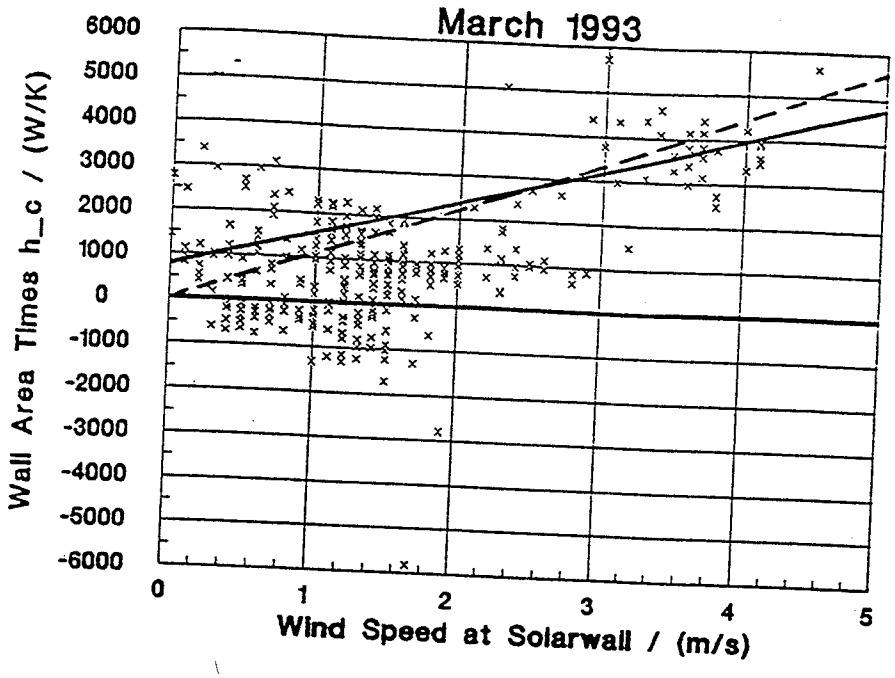

Figure 3.5: ***$A_{con}h_c$ plotted against wind speed, U_∞, for the 25% of the time that the wall was at least 4 °C warmer than the ambient air. The slope of the dashed line is 1100 (W/K)/(m/s). For A_{con} = 200 m², the equation for h_c given by the dashed line is $h_c = 5.5\ U_\infty$. The solid line corresponds to the fit of the NSTF data for this average V_s of 0.0257 m/s (9.2 (m³/hr)/m² of collector).***

A similar plot of $A_{con}h_c$ versus suction velocity, V_s, is shown in Figure 3.6. Again the scatter is large, but there is a definite trend toward lower h_c at higher suction velocities. Two important qualitative observations can be made from Figures 3.5 and 3.6:

(i) h_c appears to increase with U_∞, especially for $U_\infty > 2$ m/s,

(ii) h_c appears to decrease non-linearly with increasing V_s, with h_c approaching zero for $V_s > 0.04$ m/s (144 (m³/h)/m² of collector).

A visual inspection of Figures 3.5 and 3.6 reveals that the cases of highest $A_{con}h_c$ correspond to the combination of high wind speed and low suction velocity, and that all the cases of $A_{con}h_c < 0$ are for relatively low suction velocities. Since in the set of observations plotted in Figures 3.6 and 3.6, U_∞ and V_s are negatively correlated with each other, it is not possible to deduce the slopes of the $h_c\ (U_\infty)$ or $h_c\ (V_s)$ lines from these two plots alone.

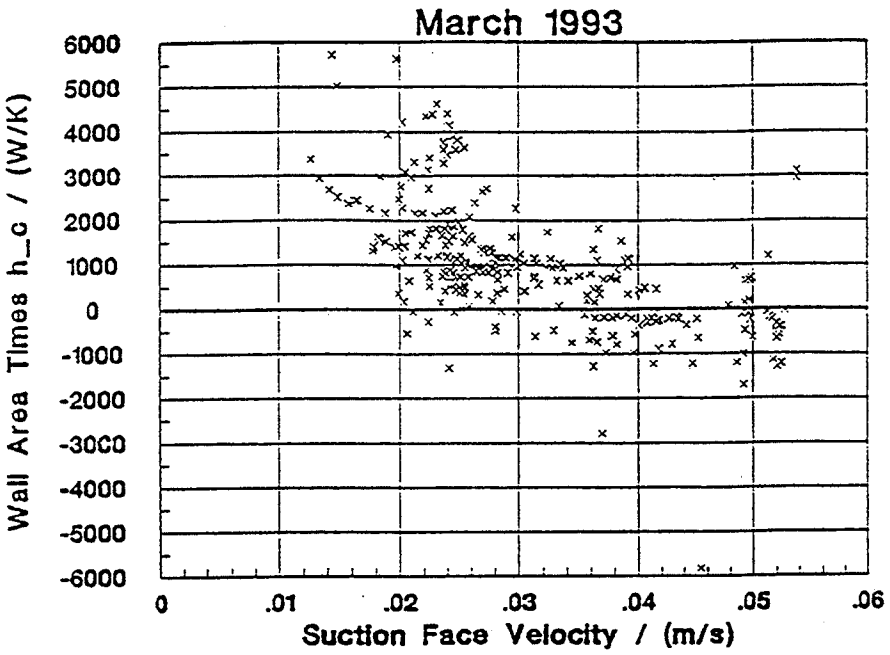

Figure 3.6: $A_{con}h_c$ plotted against the suction face velocity V_s for the daytime periods only.

3.3.4 Calculation of Absorber Plate Thermal Effectiveness

Thermal effectiveness of the absorber plate is more straightforward to calculate from the data than the efficiency is. The thermal effectiveness is a measure of the dimensionless temperature rise of the air heated by the collector:

$$\varepsilon_{HX} = (T_{out}' - T_a) / (T_p - T_a) \qquad (2.18)$$

To correct for the heating from the building wall, T_{out}' is used to calculate ε_{HX}, where T_{out}' is the temperature that the air would have reached if Q_{wall} was zero. The analysis of the recaptured building heat loss done by Enermodal Engineering (Interim Report on Performance of the Perforated Plate Collector at GM Canada, Oshawa, January 1994) showed that only half of Q_{wall} is recovered by the air delivered to the building. Thus $Q_{wall} / 2 = C_p(T_{out} - T_{out}')$. In relation to the measured quantities,

$$T_{out}' = T_{out} - (A_r / R_{wall}) (T_{room} - T_{cavity}) / (2mC_p) \qquad (2.19)$$

Then

$$\varepsilon_{HX} = (T'_{out} - T_a) / (T_p - T_a)$$
$$- (A_r / R_{wall}) (T_{room} - T_{cavity}) / ((T_p - T_a)2mC_p) \qquad (2.20)$$

The collector thermal effectiveness ε_{HX} was plotted versus V_s as shown in Figure 3.7. If one accepts the physical model that requires the effectiveness to approach 1.0 as suction velocity approaches zero, then these data suggest a reduction in effectiveness as suction velocity increases. However, the measured effectiveness is significantly above the range of values given by the NREL equation for this range of wind speeds and suction velocities. Figure 3.8 shows the same data plotted versus wind speed. The scatter in the data points obscures any dependence on wind speed.

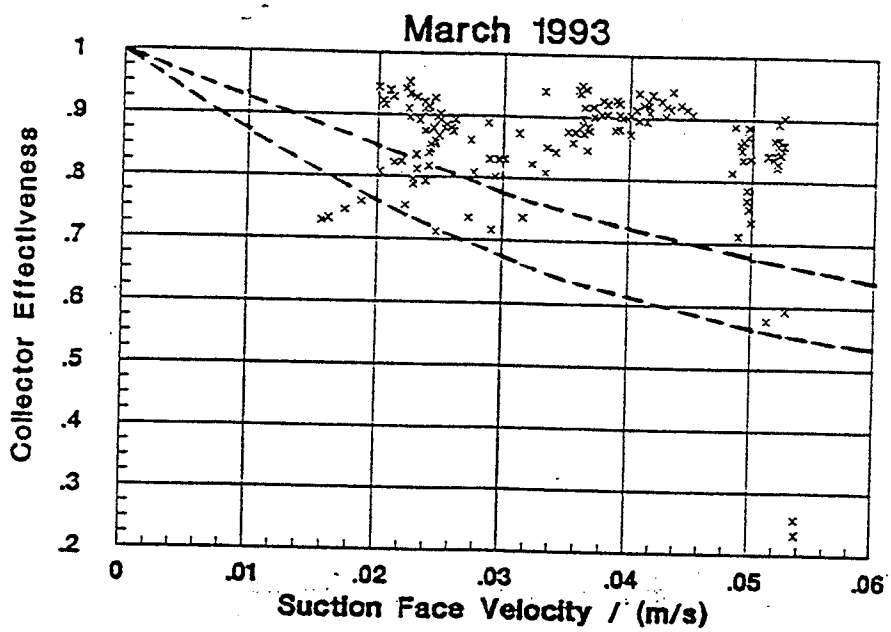

Figure 3.7: Thermal Effectiveness as a function of suction rate for 149 periods when G > 400 W/m². The dashed lines are from the equation of Kutscher (1994) for the range of wind speeds represented in this sample of points. The upper curve is for U_∞ = 4.1 m/s, and the lower curve is for U_∞ = 0.1 m/s.

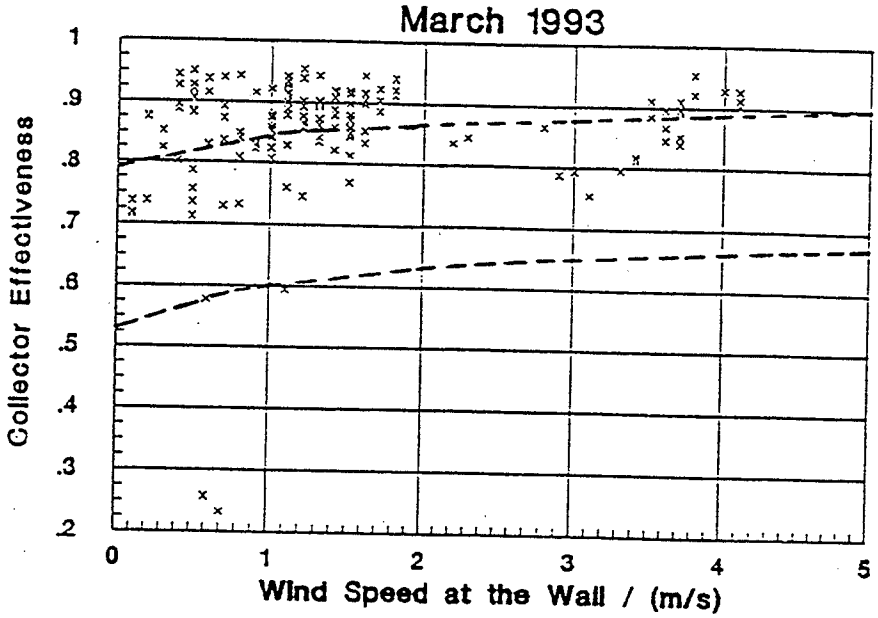

Figure 3.8: Collector effectiveness when G > 400 W/m² compared to calculated values given by the equation from C. Kutscher, January 1993. The upper curve is for V_s = 0.015 m/s, and the lower curve is for V_s - 0.054 m/s.

3.3.5 Measured Collector Efficiency

Figure 3.9 shows the gross collector efficiency plotted against suction velocity, and Figure 3.10 shows it plotted against wind speed. The two figures clearly show a general increase of collector efficiency with V_S, and a general decrease in efficiency with $U_\infty > 2$ *m/s*. The observed decrease in efficiency with wind speed is likely in part due to the lower suction rates for the cases of higher wind speeds as mentioned at the end of Section 3.3.3. Thus the wind acting alone may not have as detrimental an effect on collector efficiency as is suggested by Fig. 3.10.

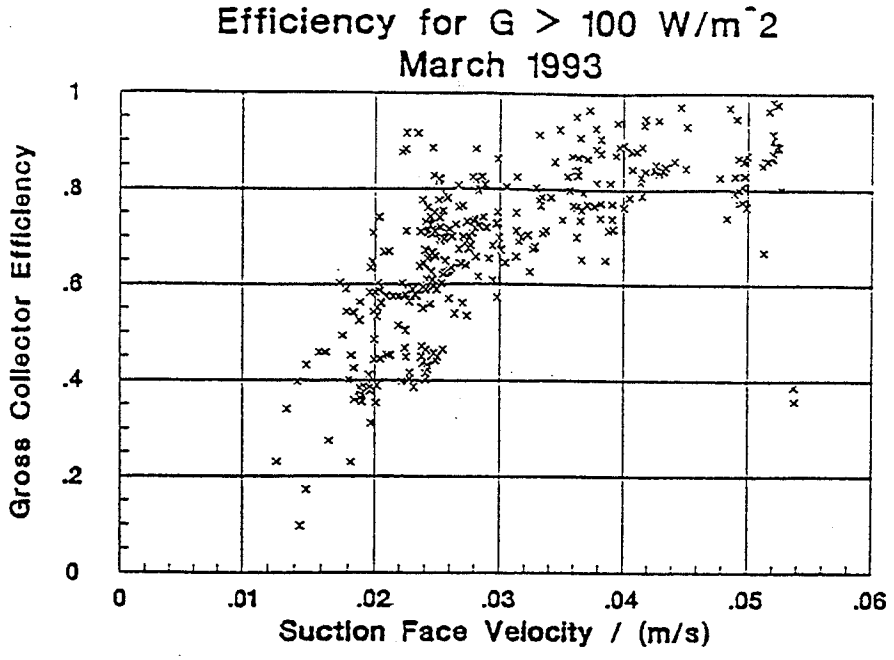

Figure 3.9: Collector efficiency versus suction velocity for periods when the solar radiation was above 100 W/m².

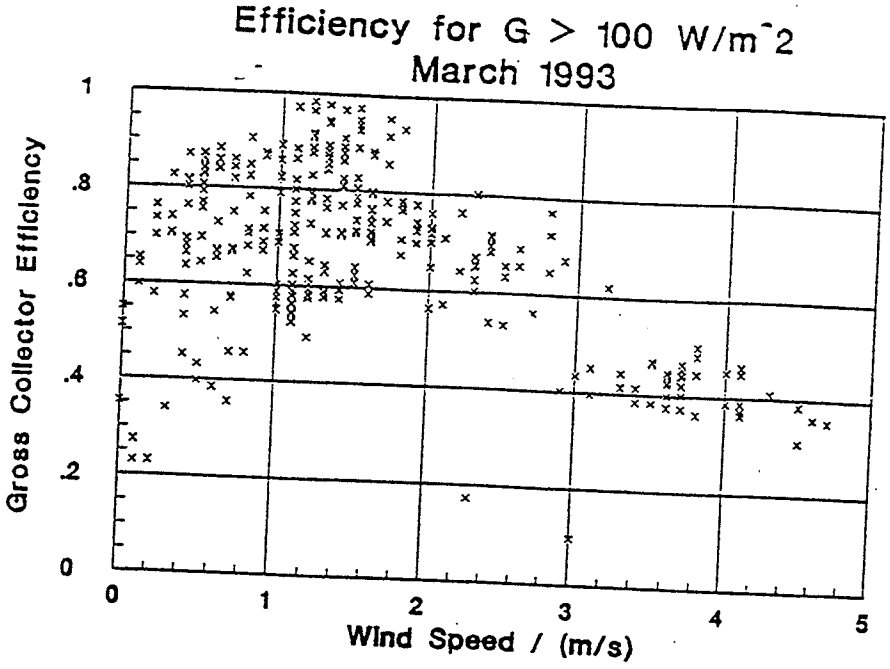

Figure 3.10: Collector efficiency versus wind speed for periods when the solar irradiance was above 100 W/m².

3.4 Results of STRL Flow Distribution Studies

3.4.1 Introduction

Lowy Gunnewiek completed his MASc thesis in the Solar Thermal Research Laboratory (STRL) at the University of Waterloo in 1994. In his work, Mr. Gunnewiek used a commercial computational fluid dynamics computer package called TASCflow (from Advanced Scientific Computing Limited, Waterloo, Canada, N2L 5Z4, 519-886-8435) to build a numerical model of an unglazed perforated-absorber collector to study how the local suction air flow rate through the absorber plate of the collector is affected by fan suction rates, thermal buoyancy inside the collector, and wind pressure distributions over the face of the collector. TASCflow solves the Reynolds-Stress averaged Navier-Stokes equations, satisfying the principles of conservation of mass, energy and momentum over the domain of simulation. Because of the level of detail of the calculations, this collector model requires a workstation computer with 48 Mb of RAM to run, and takes two to four hours to complete a single simulation.

3.4.2 Flow Results from Gunnewiek's Calculations

Lowy Gunnewiek used the TASCflow model to calculate the suction velocity distribution on the collector absorber plate for many different conditions. An example of some of his calculations are illustrated in Figures 3.11 and 3.12 in which are shown the local suction velocity and normalized temperature distributions with height on a 4.5 m high collector for average suction velocities ranging from 1.25 cm/s to 8 cm/s. The air space inside the collector was 15 cm deep (uniform from top to bottom of the collector), the absorbed solar irradiance was 650 W/m², and the collector heat loss coefficient $U_O=(h_r+h_c) / \varepsilon_{HX}$ was 5.0 W/m²K. A plate with a porosity of about 1.5% was assumed. In both figures, Z^* is the local height up the collector divided by the total collector height of 4.5 m. The normalized inlet temperature is defined as

$$\theta_{in} = (T_{in} - T_a) / (T_{ave} - T_a) \quad (3.21)$$

where $T_{in}=T_a+\alpha G/(\rho C_p V_S+U_0)$ is the temperature of the air after it goes through the absorber plate, and

$$T_{ave} = T_a + \alpha G/(\rho C_p U_{ave}+U_O) \quad (3.22)$$

The normalized suction velocity U^* is just the local suction velocity V_S divided by the average suction velocity U_{ave}.

The figures show that the plate temperature and the local suction velocity are constant within 8 percent for the high average suction velocity of 0.08 m/s. For the low average suction velocity, the effect of buoyancy forces inside the collector is apparent from the higher suction velocities and lower inlet air temperatures at the bottom of the collector.

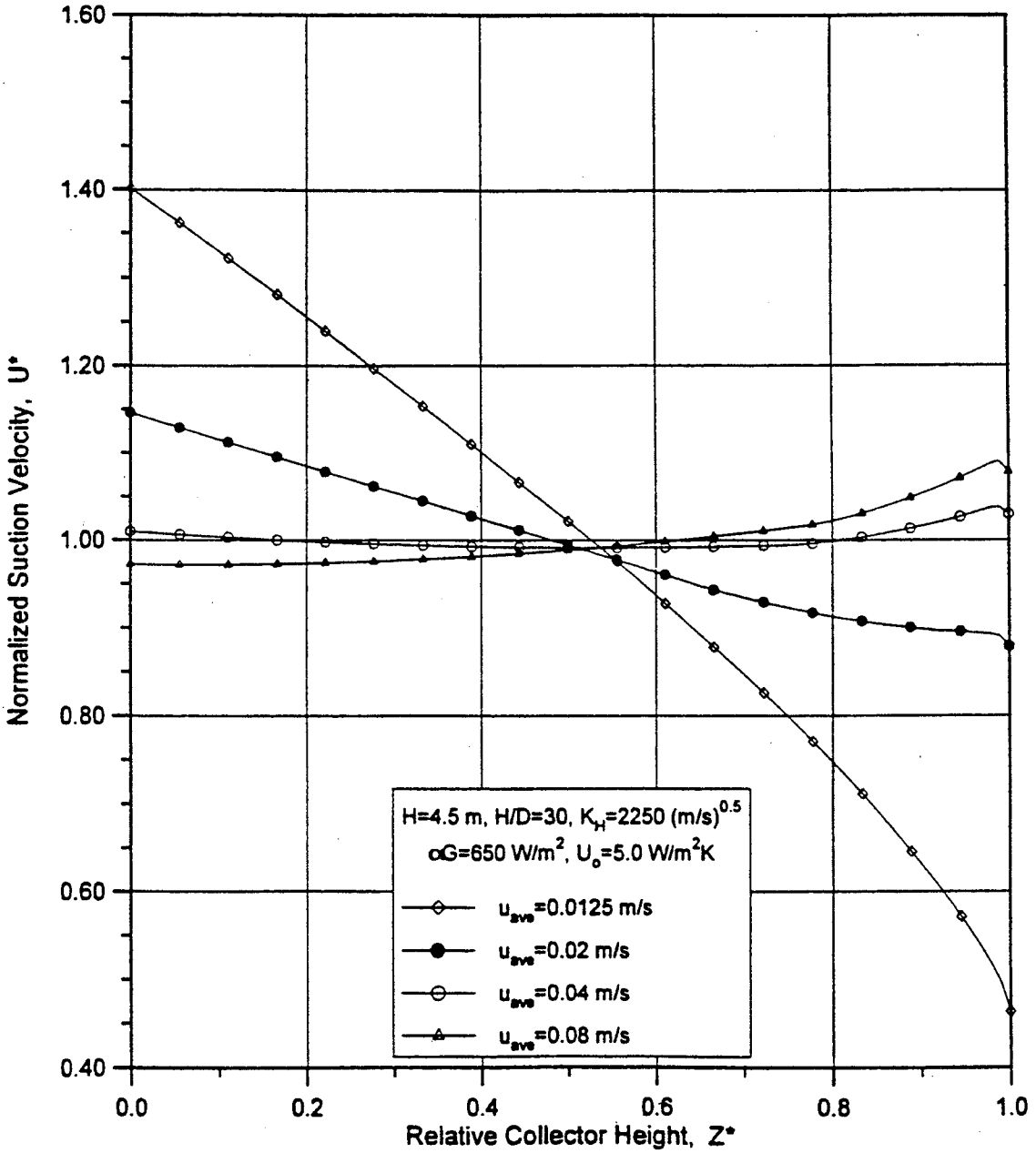

Figure 3.11: Local suction velocity as a function of height on the collector for a range of average suction velocities, U_{ave}.

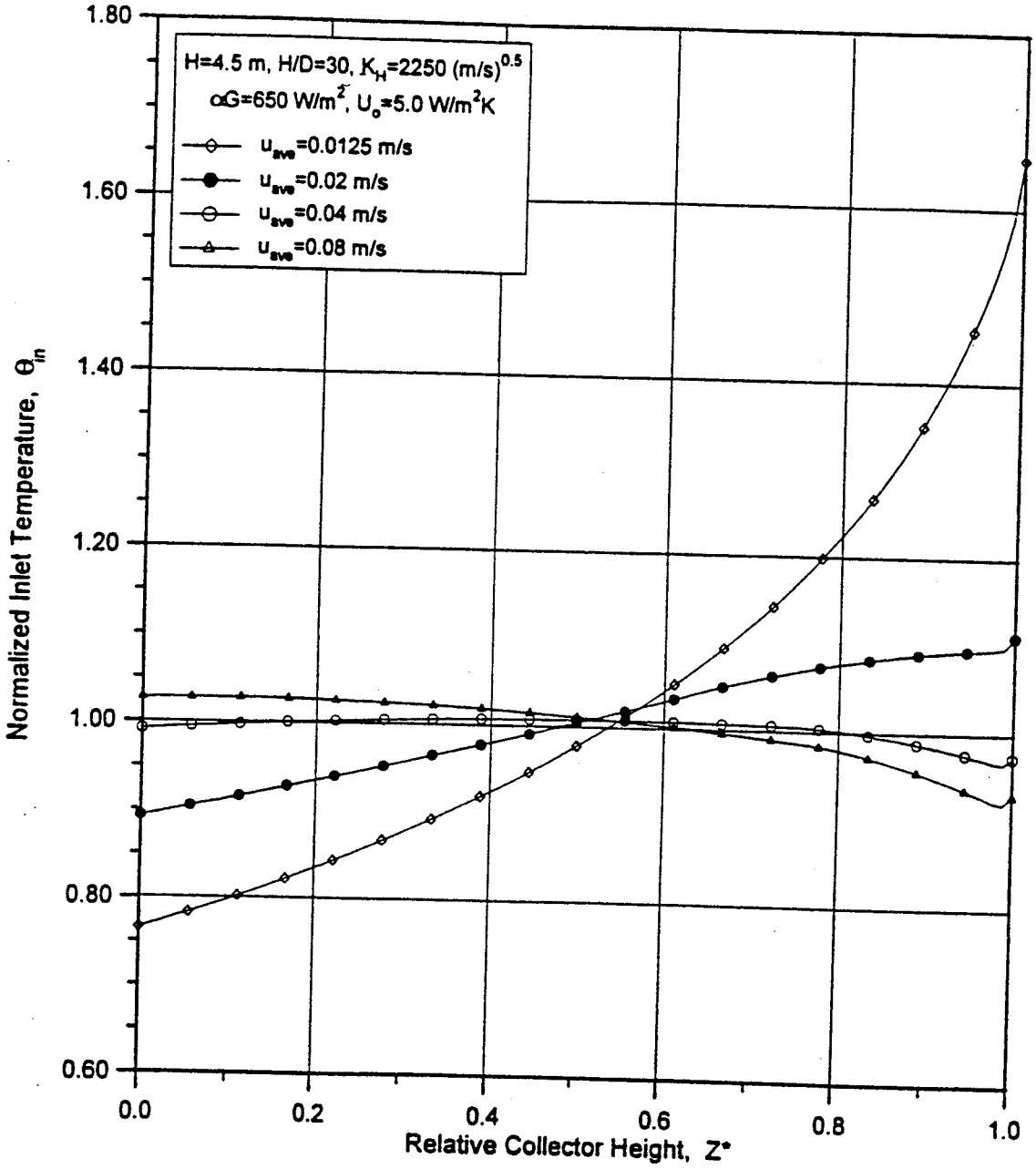

Figure 3.12: Local normalized temperature of the air entering the collector cavity as a function of height up the collector face for a range of average suction velocities, U_{ave}.

Lowy Gunnewiek included in his MASc. Thesis a parametric study of the effects of collector height (H between 3 m and 6 m), solar irradiance (αG between 400 and 900 W/m^2), collector heat loss (U_o between 1.0 and 9.0 W/m^{2}K), average suction velocity (U_{ave} between 0.0125 and 0.08 m/s), plenum aspect ratio (H/D between 10 and 50), and the absorber's hydraulic impedance (K_H between 750 and 3700 (m/s)$^{0.5}$).

A summary of the variations of local suction velocity for different values of the six main parameters is presented in Table 3.1. The variations, with position on the wall, of the local suction velocity and the local

plate temperature, for the base-case set of parameters, are included in Figures 3.11 and 3.12 as the values corresponding to the suction velocity U_{ave} = 0.02 m/s. Variation of U_{ave} , K_H , H/D, G, H or U_0 from the base-case values causes either a more-uniform or less-uniform suction velocity distribution over the absorber plate. The average velocity, U_{ave} , has the largest effect on the flow rate distribution over the absorber. The overall heat loss coefficient, U_0 , has the smallest effect on flow rate distribution. The parameters in Table 3.1 are listed in decreasing order of the size of the effect that each has on the air flow rate distribution over the absorber plate.

Table 3.1: Summary of Local Suction Flow Rate Distribution Resulting from Variations in the Simulation Parameters

Parameter ‡ Different from Base-Case	Parameter Value	Range of Local Suction Velocity	
		U^* at Z^*=0	U^* at Z^*=1
—	Base-Case †	1.15	0.88
U_{ave}	1.25 cm/s	1.40	0.46
	8 cm/s	0.97	1.09
KH	750 $(m/s)^{0.5}$	1.37	0.70
	3700 $(m/s)^{0.5}$	1.09	0.92
H/D	10	1.16	0.82
	50¶	1.03	1.30
G	400 W/m^2	1.08	0.96
	900 W/m^2	1.20	0.84
H	3 m	1.09	0.95
	6 m	1.19	0.81
U_0	1 W/m^2 K	1.17	0.86
	9 W/m^2 K	1.13	0.90

‡ Parameters are listed in order of decreasing effect on $U^*(z^*)$.

† Base-Case: U_{ave}=2 cm/s, K_H=2250 $(m/s)^{0.5}$ (porosity ≈ 1.5%), H/D=30, G=650 W/m_2, H=4.5 m, U_0=5.0 W/m_2 K.

¶ for H/D=50, U^* had a minimum value of 0.90 at Z^*=0.45.

3.4.4 Wind Pressure Effects

One of the main objectives of Lowy Gunnewiek's thesis work was to determine the influence of 3–D wind pressure effects on the distribution of local suction velocity over the face of a transpired plate collector. He ran CFD simulations for three cases for a frontal wind on a long collector perpendicular to the wind direction (so the wind pressure is a function of only height up the wall), for a frontal wind on a cubical building, and for a wind approaching a cubical building at a 45 degree angle to two of the building's walls. In the first case, acceleration of the wind flow over the top of the building causes a minimum wind pressure at the top edge of the vertical wall. In the latter two cases, the wind pressure varies in 2 dimensions across the face of the building. For these simulations, the wind far from the building was assumed to have an "urban" boundary layer profile, with a speed of 5.0 m/s at the height of the top of the collector. The wind pressure coefficients resulting from this wind were as measured by Brundrett (1993).

A summary of the effect that varying the simulation parameters has on the range of the suction velocities as a function of height up the absorber is given in Table 3.2 for a wide collector on which end-effects are not important. For this case, the low mean suction velocity of 0.02 m/s, combined with the high height-to-depth ratio of 50, results in 15% of the absorber area having local suction rates more than 20% different from the average suction rate of 0.02 m/s. A high average suction rate of 0.08 m/s has the expected effect of making the suction more uniform over the collector (in this case, within ±7% of $U^* = 1.0$) even in the presence of the wind.

Table 3.2: Summary of the effect of Variations in Simulation Parameters on Local Section Rates Through a Wide Absorber Subjected to a Frontal Wind.

Parameter Different from Base-Case	Parameter Value	Range of Normalized Suction Velocity (U*) (Near bottom-Near top)	Fraction of Absorb Area with $\lvert U^* - 1.0 \rvert \geq 0.2$
—	Base - Case	1.08 - 0.57	5%
U_{ave}	0.0164 m/s	1.14 - 0.35	7%
	8 cm/s	0.96 - 1.07	0%
KH	750 $(m/s)^{0.5}$	0.88 - ( )	4%
	3750 $(m/s)^{0.5}$	1.05 - 0.75	2%
H/D	10	1.10 - 0.50	7%
	50	0.85 - 1.28	15%

†The base-case parameters were the same as for Table 3.1.

3.5 Comparison of TCFLOW to TASCflow (CFD) Calculations

This section describes the comparison of the flow distributions predicted by the STRL model described in Section 3.4 and by TCFLOW described in Section 4.1 of Part I of this report. The model developed by Mr. Gunnewiek using TASCflow simulates a transpired collector with a constant velocity header all along its top edge. To be able to compare results with TCFLOW, example STRL results were chosen that assume no external wind pressure is applied. In this case the air flow inside the collector will be in a vertical plane perpendicular to the absorber plate, and the resulting local suction velocities will be a function of only vertical height up the collector.

The two codes TCFLOW and TASCflow were compared for two different average suction velocities. For the particular collector geometry chosen, the high average suction velocity of 0.08 m/s results in a very uniform suction rate over the whole collector. For the low average suction rate of 0.02 m/s, the local suction rate varies from 0.023 m/s at the bottom of the collector to 0.016 m/s at the top of the collector.

To do a fair comparison between the predictions of TCFLOW and those of Lowy Gunnewiek's model, it was necessary that the pressure drop across the absorber plate and the temperature rise of the air going through the absorber have the same dependencies on V_S in both simulations. To compensate for the different ways that TCFLOW and Lowy's code calculate the pressure drop across the absorber plate, it was necessary to specify a different hole pitch and diameter for each average flow rate.

A similar strategy was used to ensure that the temperature rise of the air as it passed through the absorber plate would be the same in both computer models. TCFLOW calculates an effectiveness that varies with local suction velocity. Since Lowy Gunnewiek used a constant effectiveness (actually a constant value of $U_0=(h_r+h_c) / \varepsilon_{HX}$), it was necessary to change the product ρC_p input to TCFLOW to get the same temperature rise from both codes. This was achieved while keeping the wind velocity zero (so that TCFLOW calculates $h_c=0$), calculating the value h_r / ε_{HX} from Kutscher's equations, and then reducing C_p so that the air temperature rise at the mean suction velocity was the same for both computer code methods.

The results from TCFLOW are superimposed on the TASCflow results in Figures 3.13 and 3.14. For the low suction velocity case, both codes predict that the local suction velocity near the bottom of the collector absorber is about 33% higher than near the top of the absorber. TCFLOW predicts a slightly lower variation in local suction velocity over the face of the collector than TASCflow does. For the high suction velocity case, both codes predict a uniform flow rate to with ±1%, with TCFLOW predicting a slightly larger variation of suction velocity from top to bottom of the collector.

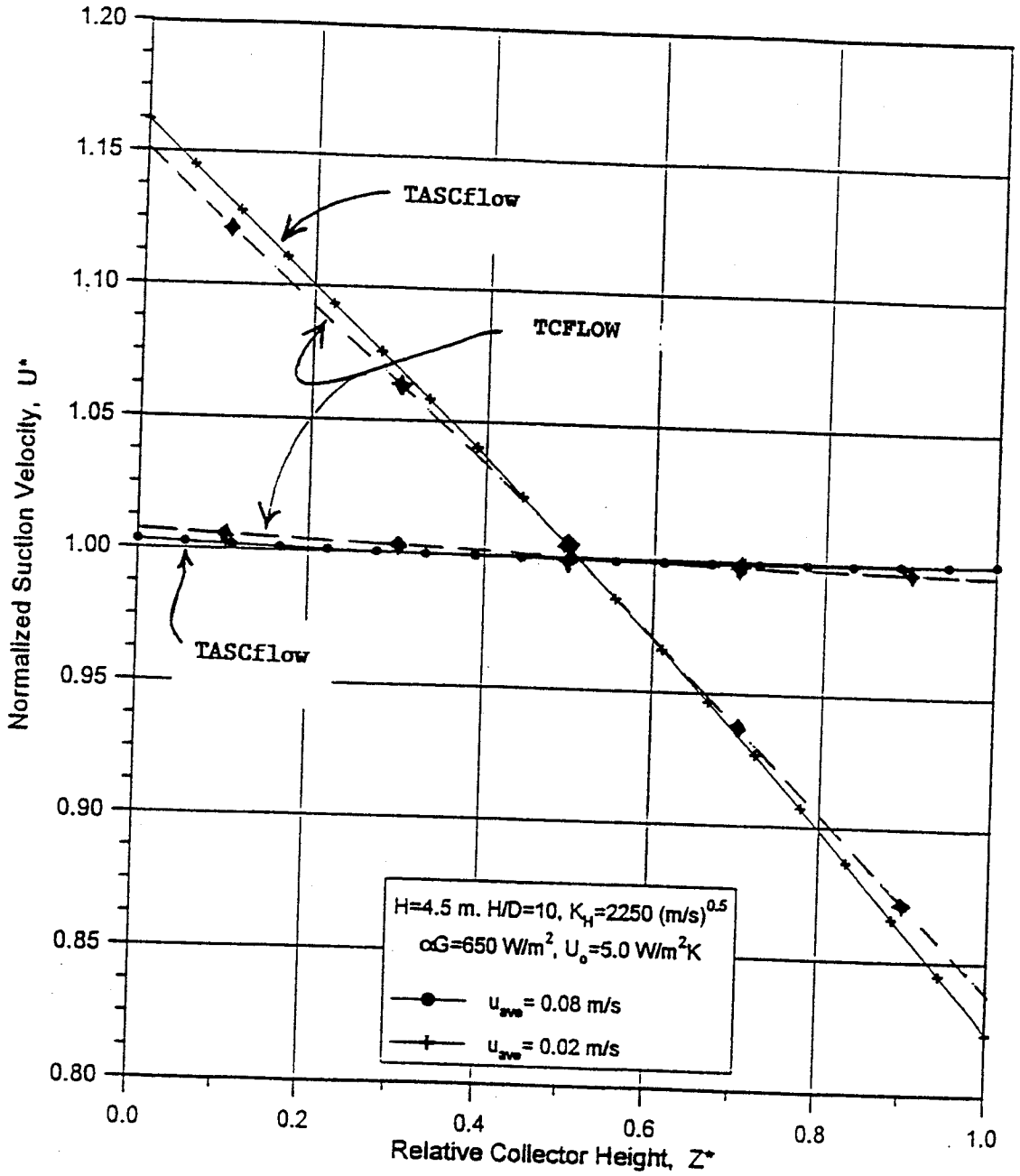

Figure 3.13: Comparison of the normalized suction velocity predicted by TCFLOW with those produced by Lowy Gunnewiek using TASCflow.

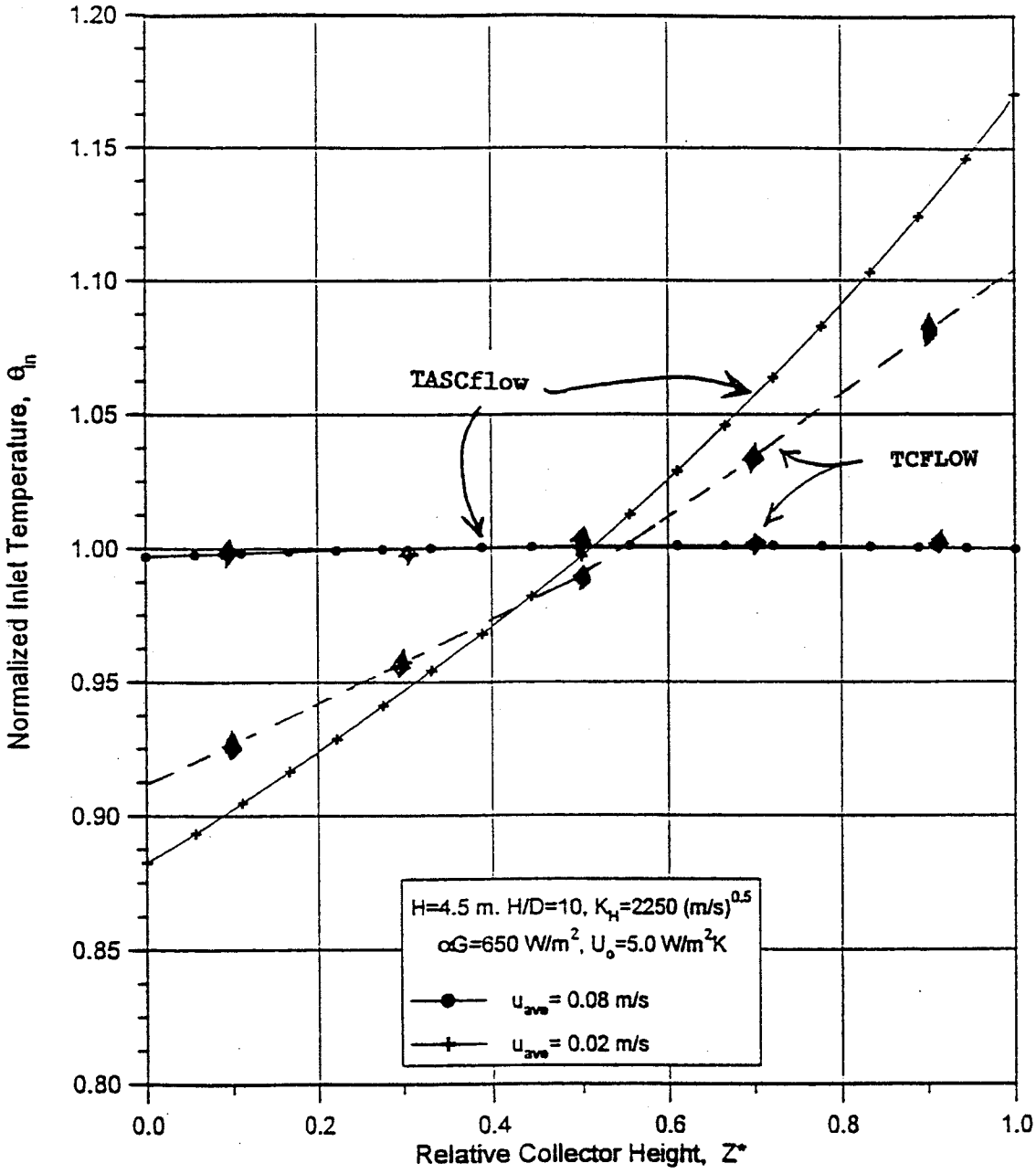

Figure 3.14: Comparison of the normalized inlet temperature predicted by TCFLOW with those produced by Lowy Gunnewiek using TASCflow.

References for Chapter 3

Brundrett, Ewart (1993): A brief survey of the influence of wind induced building pressures upon the operation of ungalzed solar walls. Personal communication, February 22, 1993. University of Waterloo, Dept. of Mechanical Engineering, Canada.

Cao, Shu (1993): *Numerical Investigation on Unglazed Transpired Plate Solar Collector*, MASc, thesis, Department of Mechanical Engineering, University of Waterloo, Waterloo, Ontario, Canada.

Enermodal Engineering Ltd. (1992): *Performance of the Perforated-Plate SolarWall at Ford of Canada, Oakville.* Final Report to EMR, August 1992.

Golneshan, Ali (1995): PhD. Thesis, Department of Mechanical Engineering, University of Waterloo, Waterloo, Ontario, Canada.

Gunnewiek, L. (1994): *An Investigation of the Flow Distribution Through Unglazed Transpired-Plate Solar Air Heaters*. MASc, thesis, Department of Mechanical Engineering, University of Waterloo, Waterloo, Ontario, Canada.

Kokko, John and Shaun Marshall (1992): Performance of the next generation of Solar Walls. *Proceedings of the 18th Annual Conference of SESCI, Edmonton*, pp. 201-205.

Kutscher, C.F. (1994): Heat exchange effectiveness and pressure drop for air flow through perforated plates with and without crosswind. *J. of Heat Trans.*, Vol. 116, pp. 391–399.

Kutscher, C.F, C.B. Christensen, and G.M. Barker (1991a): Unglazed transpired solar collectors: heat loss theory. In *Solar Engineering 1991, 12th Annual ASME Int. Solar Energy Conference*, AM. Soc. of Mech. Eng.

Kutscher, C., C. Christensen, and G. Barker (1991b): Unglazed transpired solar collector: an analytical model and test results. *Proceedings of ISES, 1991*, pp. 1245-1250.

Licharowicz, A., R.K. Duggins and E. Markland (1965): Discharge coefficients for incompressible non-cavitating flow through long orifices, *J. Mech. Eng. Sc.*, Vol. 7, pp. 210-219.

NSTF (1990-1992): Solar Collector Test Reports: Reference Nos. 90-29-A0398 and 90-29-A0402 prepared for Conserval Eng. Inc. October 10, 1990 and Jan. 16, 1991 by Larry West and Vern Nielson; and No. 92-E37-A0494 prepared for Energy, Mines and Resources Canada (Doug McClenahan) by Larry West and Paul Geisberger Nov. 26, 1992.

Soltau, H. (1992): Testing the Thermal Performance of Uncovered Solar Collectors, *Solar Energy*, Vol. 49, pp. 263-272.